



MSU Graduate Theses

Summer 2024


Thermochronology and Exhumation Dynamics of Metamorphic Units in the Salmon River Suture Zone

Jonathan J. Cone

Missouri State University, jjc730@live.missouristate.edu

As with any intellectual project, the content and views expressed in this thesis may be considered objectionable by some readers. However, this student-scholar's work has been judged to have academic value by the student's thesis committee members trained in the discipline. The content and views expressed in this thesis are those of the student-scholar and are not endorsed by Missouri State University, its Graduate College, or its employees.

Follow this and additional works at: <https://bearworks.missouristate.edu/theses>

 Part of the [Geology Commons](#), [Geophysics and Seismology Commons](#), and the [Tectonics and Structure Commons](#)

Recommended Citation

Cone, Jonathan J., "Thermochronology and Exhumation Dynamics of Metamorphic Units in the Salmon River Suture Zone" (2024). *MSU Graduate Theses*. 3963.

<https://bearworks.missouristate.edu/theses/3963>

This article or document was made available through BearWorks, the institutional repository of Missouri State University. The work contained in it may be protected by copyright and require permission of the copyright holder for reuse or redistribution.

For more information, please contact bearworks@missouristate.edu.

**THERMOCHRONOLOGY AND EXHUMATION DYNAMICS OF METAMORPHIC
UNITS IN THE SALMON RIVER SUTURE ZONE**

A Master's Thesis

Presented to

The Graduate College of

Missouri State University

In Partial Fulfillment

Of the Requirements for the Degree

Master of Science, Geography and Geology

By

Jonathan Cone

August 2024

Copyright 2024 by Jonathan Cone

THERMOCHRONOLOGY AND EXHUMATION DYNAMICS OF METAMORPHIC UNITS IN THE SALMON RIVER SUTURE ZONE

Earth, Environment, and Sustainability

Missouri State University, August 2024

Master of Science

Jonathan Cone

ABSTRACT

The Salmon River suture zone in western Idaho records the Jurassic-Cretaceous (160-90 Ma) accretion of amalgamated volcanic arc terranes onto the North American continent. Rocks exposed at the surface record burial to depths of more than 20 kilometers, with unclear drivers for uplift and exhumation. Two competing hypotheses have been proposed to explain the transport of deep crustal rocks to the surface: (1) delamination of a dense lithospheric root resulted in rapid isostatic uplift of the crust and (2) exhumation of crustal blocks along thrust faults. To test these models, I present temperature-time (T-t) paths for mid-crustal metamorphic rocks constructed using U-Pb ages of zircon, apatite, and rutile, accompanied by closure temperature estimates for apatite and rutile presented in context with local structural relationships. Samples from higher-grade metamorphic rocks were found to have higher closure temperatures and older ages than juxtaposed lower grade rocks, suggesting initial exhumation in higher grade crustal blocks before juxtaposition and transport to the surface. These findings align with the hypothesis indicating that exhumation occurred as a series of thrust faults.

KEYWORDS: zircon, apatite, rutile, closure temperature, metamorphic rocks, salmon river suture zone, U-Pb geochronology, thermochronometry, accreted terrane

**THERMOCHRONOLOGY AND EXHUMATION DYNAMICS OF HIGH
TEMPERATURE METAMORPHIC UNITS IN THE
SALMON RIVER SUTURE ZONE**

By

Jonathan Cone

A Master's Thesis
Submitted to the Graduate College
Of Missouri State University
In Partial Fulfillment of the Requirements
For the Degree of Master of Science, Geography and Geology

August 2024

Approved:

Matthew P. McKay, Ph.D., Thesis Committee Chair

Gary Michelfelder, Ph.D., Committee Member

Kevin Mickus, Ph.D., Committee Member

Julie Masterson, Ph.D., Dean of the Graduate College

In the interest of academic freedom and the principle of free speech, approval of this thesis indicates the format is acceptable and meets the academic criteria for the discipline as determined by the faculty that constitute the thesis committee. The content and views expressed in this thesis are those of the student-scholar and are not endorsed by Missouri State University, its Graduate College, or its employees.

ACKNOWLEDGEMENTS

Getting this thesis done has not quite been the journey I envisioned when I started out. I wouldn't have made it anywhere near this far if it weren't for the incredible support of my friends and fellow grad students JZ, Loren, Kelly, Thomas, Birch, Drew, Colleen, César, Sarah Prost, Sarah Rasor, Sarah Sommer, Chris, Anna, Logan, James, Ethan, and Kagan just to name a few (I apologize if I left anyone out). I would also like to thank my advisor, Dr. Matt McKay and my awesome committee members Dr. Kevin Mickus and Dr. Gary Michelfelder for helping me with my innumerable questions I've had along this journey. I also want to thank Dr. Tim Flood, Dr. Nelson Ham, and Dr. Rebecca McKean from the St. Norbert geology department for encouraging me to pursue a master's degree. Thank you to my loving parents, and partner Amy for believing in me. Special thanks also go to the cheesy corn at the Whole Hog café for being one of the only great things about Springfield, MO.

I dedicate this thesis to Ziggy. Miss you, buddy.

TABLE OF CONTENTS

Introduction	Page 1
Geologic Background	Page 3
Structure of the Blue Mountain Province	Page 3
The Salmon River Suture Zone	Page 6
Western Idaho Shear Zone	Page 9
Previous Investigations	Page 10
Study Area	Page 13
Methods	Page 15
Closure Temperature	Page 16
U-Pb Zircon	Page 17
U-Pb Rutile	Page 17
U-Pb Apatite	Page 19
Results	Page 21
Sample Descriptions	Page 21
U-Pb Zircon	Page 22
U-Pb Rutile	Page 25
U-Pb Apatite	Page 25
Discussion	Page 43
Igneous and Metamorphic Zircon History	Page 43
Zr-in-Rutile Thermometry	Page 46
Apatite Thermochronology	Page 46
Multi-Mineral Cooling Paths	Page 47
Exhumation Model of the Salmon River Suture Zone	Page 51
Lithospheric Delamination Hypothesis	Page 53
Thrust Propagation Hypothesis	Page 55
Conclusion	Page 59
References	Page 61
Appendices	Page 72
Appendix A. UTM Coordinates of Samples	Page 72
Appendix B. U-Pb Zircon Ages	Page 74
Appendix C. U-Pb Rutile Ages	Page 90
Appendix D. U-Pb Apatite Ages and Closure Temperatures	Page 92

LIST OF TABLES

Table 1. Mean zircon ages, MSWD, and grain counts	Page 29
Table 2. Mean apatite ages, MSWD, and grain counts	Page 30
Table 3. Mean rutile ages, MSWD, and grain counts	Page 30

LIST OF FIGURES

Figure 1. Map of the Blue Mountains Province	Page 12
Figure 2. Geologic map of study area	Page 14
Figure 3. Sample location photos	Page 31
Figure 4. Weighted mean plots for zircon samples from the Hazard Creek and Little Goose Creek complexes	Page 32
Figure 5. Weighted mean plots for zircon samples from the Pollock Mountain and Rapid River plates	Page 33
Figure 6. Zircon crystallization age vs. U/Th ratio with kernel density estimate (KDE) for U-Pb zircon samples from the Hazard Creek and Little Goose Creek complexes	Page 34
Figure 7. Zircon crystallization age vs. U/Th ratio with kernel density estimate (KDE) for U-Pb zircon samples from the Pollock Mountain and Rapid River plates	Page 35
Figure 8. Weighted mean plots for apatite samples from the Hazard Creek and Little Goose Creek complexes	Page 36
Figure 9. Weighted mean plots for apatite samples from the Pollock Mountain and Rapid River plates	Page 37
Figure 10. Apatite closure temperatures vs. U-Pb age with kernel density estimate (KDE) for age of apatite grains from the Hazard Creek and Little Goose Creek complexes	Page 38
Figure 11. Apatite closure temperatures vs. U-Pb age with kernel density estimate (KDE) for age of apatite grains from the Pollock Mountain and Rapid River plates	Page 39
Figure 12. C (long)/a ₂ (short) axis values vs. U-Pb age for apatite grains from the Hazard Creek and Little Goose Creek complexes	Page 40
Figure 13. C (long)/a ₂ (short) axis values vs. U-Pb age for apatite grains from the Pollock Mountain and Rapid River plates	Page 41
Figure 14. Grain size and U content versus age of apatite grains	Page 42
Figure 15. Temperature-time paths of units in the Salmon River Suture Zone	Page 57
Figure 16. Generalized exhumation model of the Salmon River Suture Zone	Page 58

INTRODUCTION

The growth of western North America is the result of Mesozoic to Cenozoic accretion of paleo-Pacific Ocean crustal fragments (Davis et al., 1978; Fleck and Criss, 1985; Dickinson, 2004). The Salmon River suture zone in western Idaho lies within the boundary between the accreted terranes of the western United States and North American cratonic rocks. Numerous studies have focused on the orogenic and metamorphic history of the area (Vallier, 1977; Selversone et al., 1992; Getty et al., 1993; Manduca et al., 1993; Goldstrand, 1994; Fleck and Criss, 2004; Lund, 2004; Kuntz and Snee, 2007; McKay, 2011; McKay et al., 2017, Long et al., 2023), but the exhumation history of the area is still debated.

Exhumation in the Salmon River suture zone was initially proposed to be the result of lithospheric delamination, where the crustal root detached from the overlying crust, resulting in rapid uplift of up to 3km/m.y. in the overlying block (Selverstone et al., 1992). More recent studies (Gray et al., 2009; McKay, 2011; Gray et al., 2012; Kurz et al., 2012) suggest that uplift in the region is a result of thrust faulting, as opposed to delamination (McKay et al., 2017), with estimated exhumation rates of less than 0.2 km/m.y. Although research has been performed on the prograde metamorphic history of the Salmon River suture zone, there is still uncertainty as to the area's exhumation scheme (Selverstone et al., 1992; Getty et al., 1993; Giorgis et al., 2005; Giorgis et al., 2008; McKay et al., 2011; McKay et al., 2017). One of the main questions regards the driving forces for uplift in the area, as ~20 km of material needed to be eroded to expose the metamorphic rocks present (Selverstone et al., 1992).

Identifying the exhumation scheme of the Salmon River suture zone would provide valuable insight into how terrain is uplifted in accretionary orogenic terranes. If the suture zone

was exhumed through lithospheric delamination, it would provide evidence that delamination can happen on a smaller scale than previously believed (Kay and Mahlburg Kay, 1993). If the suture zone was exhumed through propagating thrust faults, it would agree with evidence from other orogens (Westin et al., 2021), which suggest that progressive nappe stacking may provide an escape mechanism for mid-crustal level rocks.

I present geochronology and thermochronology estimates from mid-crustal metamorphic rocks exposed in the Salmon River suture zone and western Idaho shear zone to test the hypotheses of different mechanisms of exhumation. U-Pb ages of zircon are used for geochronologic control of igneous and metamorphic units to provide crystallization dates. Ratios of U/Th in zircon are used to determine if zircon grains have an igneous or metamorphic history. Uranium-lead (U-Pb) age of rutile and apatite grains and associated closure temperature estimates provide data on high to medium temperature (~650-420 °C) conditions to constrain cooling rates of rock units. Temperature-time data from this study was compiled with previous studies of different minerals in the region to create a multi-mineral cooling path from peak metamorphism through the closure temperature of biotite (~675-300 °C). This data was used to interpret burial depth over time and allow for the creation of an exhumation model of thrust sheets in the Salmon River suture zone, as well as intrusive suites in the western Idaho shear zone.

GEOLOGIC BACKGROUND

Structure of the Blue Mountains Province

The North American Cordillera is a mountain chain that parallels the Pacific coast from Alaska to southern Mexico (Press and Sevier, 1998). The cordillera forms part of the circum-Pacific orogenic belt which arcs on a great circle path for 25,000 km from the Antarctic peninsula to Taiwan (Dickinson, 2004). The Salmon River suture zone exists in a region of the North American Cordillera known as the Blue Mountains Province (Fig. 1) located in the northwestern United States. The eastern edge of the Blue Mountains Province records its accretion onto the Laurentian continent (Avé Lallemant et al., 1980; Dickinson 2004; Blake et al., 2009; Schwartz et al., 2021).

The geologic history of the Blue Mountains Province spans from the late Paleozoic to the late Mesozoic eras (Dickinson 2004). After the rifting of the supercontinent Rodinia in the late Proterozoic, the edge of the Laurentian continent formed a passive margin with passive margin sedimentation occurring until the late Devonian. From the Devonian to the early Triassic, oceanic allochthons were accreted onto the Laurentian miogeocline, eventually creating a subduction complex (Soreghan et al., 2000.). In the late Jurassic, exotic volcanic arcs including the Blue Mountains Province were accreted, accompanied by a major orogenic event (Avé Lallemant et al., 1980). After accretion, the west-vergent Salmon River thrust belt was formed along with a continental magmatic arc in the early Cretaceous (Blake et al., 2009). Contraction of the magmatic arc along with the subduction of an oceanic spreading center resulted in the onset of transpressional faulting in the late Cretaceous (McLelland et al., 2000; Dickinson 2004; Blake et al., 2009). Transpression was aided by a change in relative motion between the subducting

paleo-Pacific plate and the Laurentian continent from roughly orthogonal to left-lateral oblique motion, oriented SW-NE (Yonkee and Weil, 2015; Schwartz et al., 2021). This motion created the western Idaho shear zone that overprints the Salmon River suture zone. (Lund and Snee, 1988; Manduca et al., 1993).

The boundary between accreted terranes and the pre-collisional continental margin is marked by an abrupt change in crustal $^{87}\text{Sr}/^{86}\text{Sr}$ ratios from <0.7043 to the west to <0.7055 to the east (Armstrong et al. 1977). The difference in ratios is a result of strontium concentrations being depleted in oceanic and arc-derived magma in comparison to continental magma (Fleck and Criss, 2004). The strontium ratio break occurs in an area ranging from 5-15km in width, a feature unique to the North American Cordillera (Tikoff et al. 2001; Fleck and Criss, 2004; Kuntz and Snee, 2007) Giorgis et al. (2005) propose that the transition between accreted terranes and the Laurentian continent spanned >100 km along an active magmatic arc, but transpressional movement resulted in significant east-west shortening, resulting in the abrupt change in the isotopic ratios.

The isotopic boundary can be traced from eastern Washington initially in an east-west orientation. Near Orofino, Idaho, it turns 110° to the south where it continues until ~ 25 km northwest of Boise, where it is overlain by the Columbia River basalt (Fleck and Criss, 2004). The Blue Mountains Province itself is split into four separate terranes: Wallowa, Olds Ferry, Baker, and Izee. These assemblages record the history of the amalgamation of two volcanic arc systems (Wallowa and Olds Ferry) with an oceanic accretionary complex (Baker) and sedimentary basin rock (Izee) before accretion onto the Laurentian continent (Vallier and Brooks, 1986; Goldstrand, 1994; Dorsey and LaMaskin, 2007; Schwartz et al., 2009; Northrup et al., 2011).

The Wallowa terrane (Fig. 1) consists of Permian-Jurassic metavolcanic and metasedimentary rock recrystallized under zeolite to lower greenschist conditions (Vallier and Batiza, 1978; Gray and Oldow, 2005). Various plutons intruded this terrane in the Triassic between 226-219 Ma (Goldstrand, 1994). Paleomagnetic data suggests this volcanic arc was exotic, correlating with Wrangellian terrane in Canada and Alaska (Hillhouse et al., 1982). The Wallowa terrane is directly juxtaposed with Laurentian cratonic rocks near Riggins, Idaho, forming the Salmon River suture zone (Selverstone et al., 1992).

The Olds Ferry terrane (Fig. 1) consists of interbedded sedimentary, mafic, and felsic volcanic rocks, and is believed to be a segment of a fringing-arc system that bordered the North American Cordillera in the Mesozoic (Brooks and Vallier, 1978; Northrup et al., 2011; Ware et al., 2022). Fossil evidence places the rocks of the Olds Ferry terrane in the late Triassic between 237-208 Ma (Brooks and Vallier, 1978), and geochronology of the terrane dates it similarly (Ware et al., 2022). As a result of the transpressional western Idaho shear zone, Olds Ferry rocks stretched and transported north towards the Wallowa terrane and Salmon River suture zone. The Olds Ferry terrane extends into the Salmon River suture zone, where it was subsequently metamorphosed during terrain accretion (Vallier, 1998; Schwartz et al., 2011).

The Baker terrane (Fig. 1) is an oceanic *mélange* complex consisting of Devonian-Triassic metavolcanic and metasedimentary rocks (Cowan, 1985; Bishop, 1995; Northrup et al., 2011). Structures in the area including shear complexes, serpentinized oceanic crustal fragments, ultramafic igneous rocks, and small-scale blueschist metamorphism suggest that this terrane represents an oceanic subduction accretionary belt (Gray and Oldow, 2005; Dorsey and LaMaskin, 2007; Schwartz et al., 2009; LaMaskin et al., 2011; Northrup et al., 2011). Uplift and deformation occurred in the area during the collision of the Wallowa and Olds Ferry terranes in

the late Triassic-early Jurassic, creating a doubly-vergent thrust belt (Dorsey and LaMaskin, 2007).

The Izee terrane (Fig. 1) consists of thick layers of Triassic-Jurassic sedimentary rock that depositionally overlie the three other terranes (Dickinson et al., 1979; Dorsey and LaMaskin, 2007; Northrup et al., 2011). Once a forearc basin, the Izee terrane was filled in by sediment eroded from the uplifted Baker complex (LaMaskin et al., 2011). The presence of these sedimentary assemblages unconformably overlying the arc terranes suggests that amalgamation of the Blue Mountains Province had occurred by the middle Jurassic (Dorsey and LaMaskin, 2007; Northrup et al., 2011).

The Salmon River Suture Zone

The Salmon River suture zone is a belt of deformed rocks that lies within the boundary between rocks of Laurentian continental affinity to the east and accreted island arc terranes to the west (Gray and Oldow, 2005; Blake et al., 2009). Suture zones form in scenarios where interpolate collision causes material from one plate to be welded onto another. Suture zones are subjected to temperature and pressure conditions that can produce amphibolite-grade metamorphism, significant folding, and transport to depths up to 100 km (Selverstone et al., 1992; Burke et al., 2003). Over time, isostatic or tectonic uplift and erosion may expose deep-lithospheric metamorphic facies, allowing them to be researched (Trop et al., 2019).

The boundary between the Salmon River suture zone and continental terrane is noted by the sharp change in $^{87}\text{Sr}/^{86}\text{Sr}$ ratios. Near the $^{87}\text{Sr}/^{86}\text{Sr}$ isopleth line, the Salmon River suture zone is steeply-dipping to sub vertical along its eastern boundary with the Cretaceous Idaho batholith, (Criss and Fleck, 1987; Manduca et al., 1993; Gray and Oldow, 2005). The suture zone

encompasses multiple units of Permian-Jurassic arc-derived terranes thrust upon one another along three major faults; the Pollock Mountain fault, Rapid River fault, and Heavens Gate fault, decreasing in metamorphic grade towards its western boundary with the sub-greenschist Wallowa terrane (Selverstone et al., 1992; Getty et al., 1993; Lund, 2004; Blake et al., 2009; Schmidt et al., 2013). The faults are interpreted to be thrust faults due to metamorphic grade being higher in the hanging walls than in the footwalls (Blake et al., 2009). Three main thrust sheets make up the Salmon River suture zone, separated by the major thrust faults: the Heavens Gate plate, Rapid River plate, and Pollock Mountain plate (Selverstone et al., 1992, Lund, 2004, McKay et al., 2017).

The Heavens Gate plate is the lowest structurally and is juxtaposed above the Wallowa terrane rocks to the west (Gray and Oldow, 2005; McKay et al., 2017). Rocks in the Heavens Gate plate experienced lower greenschist facies conditions and are more ductilely deformed than the volcanoclastic rocks of the Wallowa terrane (Gray and Oldow, 2005). Units in this terrane include the volcanoclastics and plagioclase-rich greenstones of the Wild Sheep Creek Formation (Vallier, 1977). The eastern part of the Heavens Gate plate is overridden by the Morrison Ridge fault, exposing layers of undifferentiated marble (Lund, 2004; Gray et al., 2013; Nandi, 2018; DeYoung, 2019). Within the Heavens Gate plate is the Morrison Ridge thrust fault, which represents the boundary between the Blue Mountains Province and Salmon River suture zone exposed at the surface (Nandi, 2018).

The Rapid River plate is transported above the Heavens Gate plate along the Rapid River thrust fault (Hamilton, 1969; Selverstone et al., 1992; Lund, 2004). Rocks in this plate experienced upper greenschist to lower amphibolite facies metamorphism and are, therefore, higher grade than rocks in the footwall (Hamilton, 1963a; Gray and Oldow, 2005). The Rapid

River thrust sheet contains rocks of the Riggins Group that include the mafic-felsic Fiddle Creek schist, the mafic Lightning Creek schist, the graphic calc-phyllite and mica schists of the Squaw Creek schist that are intruded by tonalite and trondhjemite suites that range from undeformed to weakly foliated (Schmidt et al., 2016). Metavolcanic and sedimentary rocks from the Rapid River plate can be correlated with various assemblages within the adjacent Blue Mountains Province (Vallier, 1977; Brooks and Vallier, 1978; Vallier, 1995, Dorsey and LaMaskin, 2007; McKay et al., 2017).

The Pollock Mountain plate overrides the Rapid River plate and is the highest structural unit in the Salmon River suture zone (Selverstone et al., 1992; Vallier, 1995; Kuntz and Snee, 2007; Schmidt et al., 2016; McKay et al., 2017). The Pollock Mountain fault is presented at the surface as a low angle thrust but steepens along with the Rapid River fault to subvertical reverse faults at depth (Selverstone et al., 1992; DeYoung, 2019). The Pollock Mountain amphibolite is the main unit of the plate, consisting of hornblende orthogneiss, marble, calc-silicate quartzite, migmatites, and tonalitic intrusives (Getty et al., 1993). This unit is interpreted as the higher-grade metamorphic equivalent of rocks in the Rapid River plate (Selverstone et al., 1992; Gray and Oldow, 2005).

On the eastern side of the Pollock Mountain plate is the intrusive Hazard Creek complex, consisting of variably deformed Cretaceous epidote-bearing quartz diorite and trondhjemite plutons (Kuntz, 2004). Magmatic intrusion of the Pollock Mountain plate occurred in the mid Cretaceous after peak metamorphism had occurred (Manduca et al., 1993; Fleck and Criss, 2004). Age dating for the Hazard Creek complex produces an age of 118 ± 5 Ma (Giorgis et al., 2008). Due to epidote-bearing plutons typically crystallizing at pressures of >8 kbar, it is proposed that the pluton intruded the Pollock Mountain plate around the time of peak

metamorphism (Zen and Hammarstrom, 1984; Zen, 1985; McKay et al., 2017). Synmetamorphic foliation present in both the Pollock Mountain plate and Hazard Creek complex indicates ductile deformation in the Pollock Mountain plate and Hazard Creek complex post ~118 Ma (Gray, 2013; McKay et al., 2017). A hornblende Ar/Ar age of 119 Ma in the Pollock Mountain amphibolite suggests that the plate cooled past the closure temperature of Ar in hornblende of ~525 °C (Getty et al., 1993). Subsequent transpressional movement from the western Idaho shear zone resulted in penetrative deformation of these plutons, altering them into orthogneisses with minor mylonites (Gray and Oldow, 2005).

Western Idaho Shear Zone

The western Idaho shear zone records the late Cretaceous change in crustal movement from orthogonal to transpressional (Manduca et al., 1993; Tikoff et al., 2001; Giorgis et al., 2005; Giorgis et al., 2008). To the north and south of the Salmon River suture zone, various terranes exist between arc-derived and continental rocks, including preserved sections of continental slope and blueschist facies associated with subduction (Manduca et al., 1993; Tikoff et al., 2001). These terranes are missing in the Salmon River suture zone, as the western Idaho shear zone provided an escape mechanism which allowed for the juxtaposition of arc material next to the Laurentian continent (Selverstone et al., 1992; Giorgis et al., 2005; Giorgis et al., 2008).

The Little Goose Creek complex is situated on the $^{87}\text{Sr}/^{86}\text{Sr}$ boundary east of the town of Pollock and intrudes the eastern margin of the Hazard Creek complex (Manduca et al., 1993). Rock types are calc-alkaline granitoids, ranging from hornblende tonalite to porphyritic granodiorite orthogneiss (Blake et al., 2009). Formation Dates for the Little Goose Creek

complex are variable, with an interpreted age of 110 ± 5 Ma (Giorgis et al., 2008). The Little Goose Creek Complex was completely overprinted by western Idaho shear zone deformation, characterized by intense deformation and mylonitization (Gray and Oldow, 2005).

Previous Investigations

Numerous studies over the past half century have worked on determining timing constraints for metamorphic events in the Salmon River suture zone, especially in the higher metamorphic grade Rapid River and Pollock Mountain plates (Selverstone et al., 1992; Getty et al., 1993, McKay et al., 2017). Early studies of the Riggins area were inconclusive as to if metamorphism was regional or contact metamorphism from igneous intrusions (Hamilton, 1963b; Harrison and Jobin, 1963; Hamilton, 1969).

Metamorphism was underway by 144 Ma (Getty et al., 1993) and continued through ~ 112 Ma (McKay, 2011; Wilford and Vervoort, 2012; McKay et al., 2017). Undisturbed plutons 5-10 km from the suture zone emplaced before collision are used as an upper constraint for suturing. These indicate that suturing began no earlier than 135 Ma (Fleck and Criss, 2004). The presence of supracrustal island-arc material and cratonic quartzose metamorphic rock in 110 ± 5 Ma Little Goose Creek orthogneiss and 128 ± 3 Ma $^{40}\text{Ar}/^{39}\text{Ar}$ age dating of garnet amphibolite in accreted terrane provide a lower constraint for collision of 125 Ma (Getty et al., 1993; Manduca et al., 1993). This constrains the timing of collision to between 135-125 Ma (Getty et al., 1993; Manduca et al., 1993; Fleck and Criss, 2004). The preservation of two-stage garnets in the Pollock Mountain plate prompted early studies to propose two distinct metamorphic events in the suture zone, with the first event pre-144 Ma and the second around 128 Ma (Selverstone et al., 1992; Getty et al., 1993). Later studies, however, propose these features could also have been

created through one period of prolonged metamorphism, with conditions increasing to ~8.5 kbar at ~675 °C from 141-124 Ma in the Pollock Mountain plate, and 9 kbar at 650 °C between 124-113 Ma in the Rapid River plate (McKay, 2011; Bollen, 2015; McKay et al., 2017). Rankin (2022) used U-Pb zircon data to expand the range of metamorphism to 171-100 Ma. Garnet from within the Pollock Mountain amphibolite is interpreted to represent peak metamorphism in the Pollock Mountain Plate (Getty et al., 1993).

In the western Idaho shear zone, plutons on the Laurentian side of the $^{87}\text{Sr}/^{86}\text{Sr}$ boundary yielded ages of 105.3 ± 3 Ma and 103.9 ± 2.7 Ma, indicating the possibility of the Little Goose Creek complex extending through the assumed border of the western Idaho shear zone (Gray et al., 2012). Cessation of movement in the shear zone occurred by 90 Ma, evidenced by tonalitic dikes cutting through the Little Goose Creek complex (Giorgis et al., 2008). Cooling to closure point temperatures of hornblende and biotite occurred between 85-70 Ma (Giorgis et al., 2008).

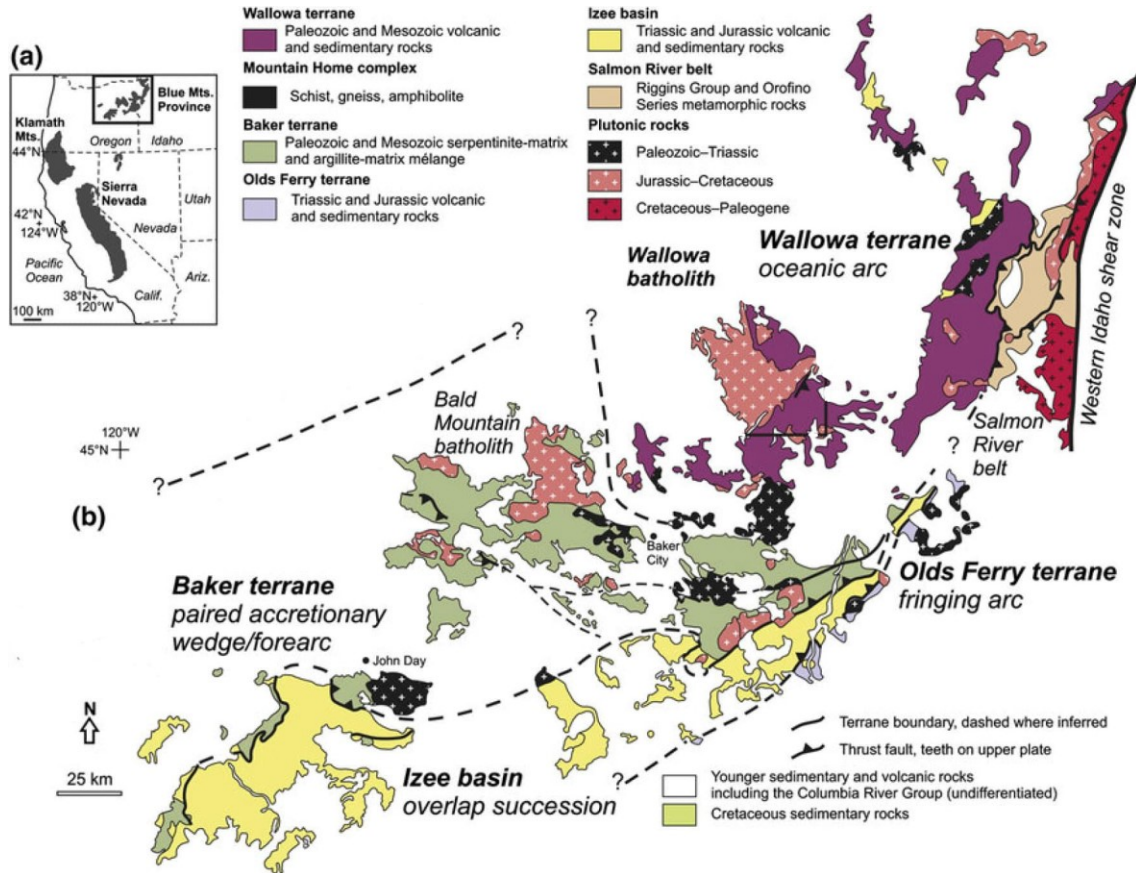


Figure 1. Simplified geologic map of the Blue Mountains Province showing rock types and relative ages. Modified from Schwartz et al., (2011) by Zak et al., (2012).

STUDY AREA

The section of the Salmon River suture zone being studied is an east-west span from near White Bird Ridge to the Goose Lake area (Fig. 2). The region is mountainous, with some peaks having over 600 m of relief. U.S. highway 95 runs roughly parallel to the suture zone, following the Little Salmon River. Numerous forest roads provide access to the western Idaho shear zone. Samples were collected over a wide area ranging from the banks of the Salmon River east of Riggins, ID to Goose Lake north of McCall, ID. Geologic mapping used for section identification was performed at 1:24,000 scale by Blake et al. (2016) and at 1:100,000 scale by Lund (2004). Samples of the Pollock Mountain plate were collected along US-95 south of Riggins as well as on Forrest Road 624 near the community of Pollock. Samples from the Rapid River plate were found on Forrest Road 624 as well. Samples of the Hazard Creek complex were from along Hazard Creek near its confluence with the Little Salmon River. Samples of the Little Goose Creek complex were collected along Goose Lake Road/Forrest Road 50257 north of the Brundage Mountain Resort (Fig. 2). Sample location coordinates are presented in Appendix A

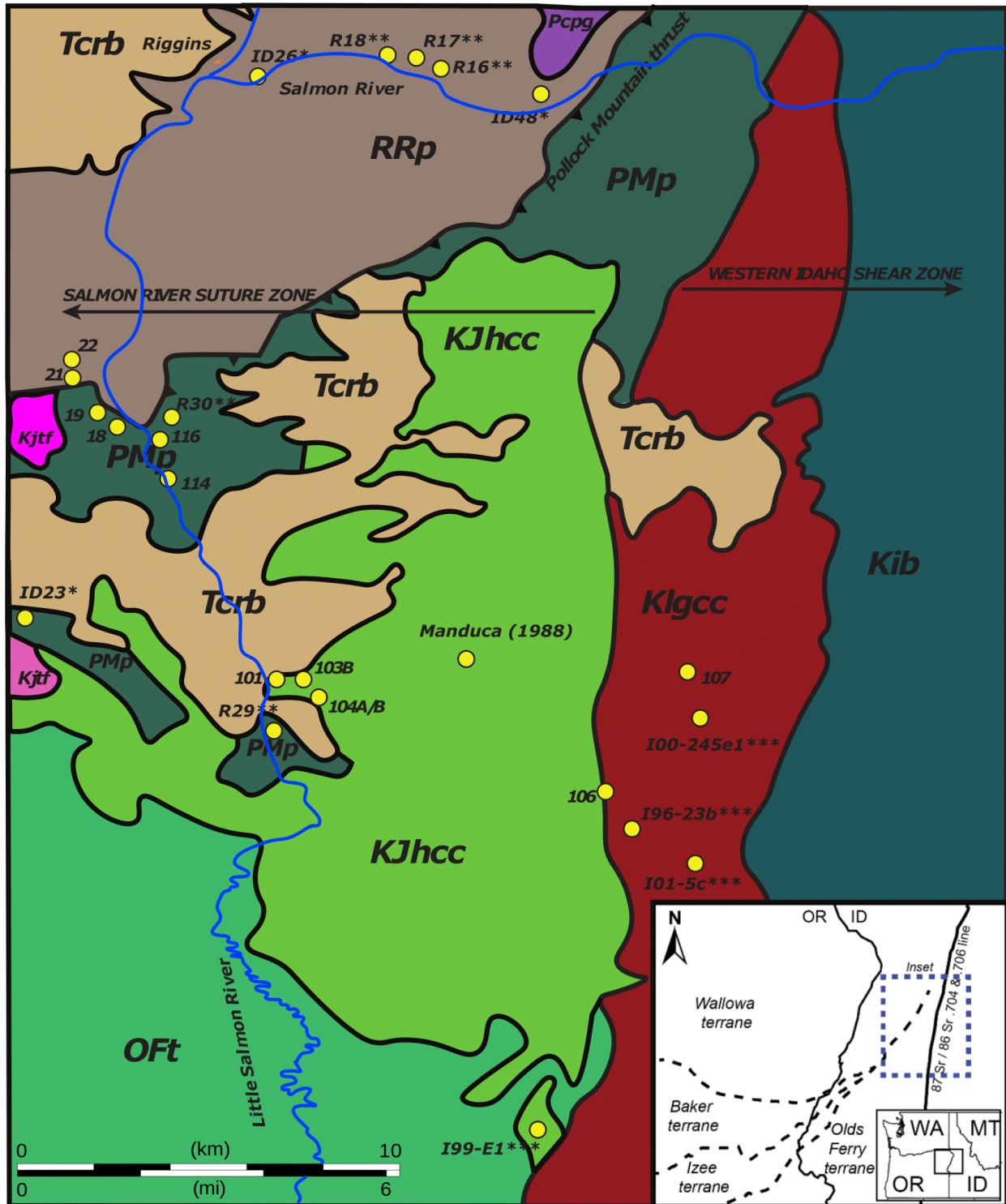


Figure 2. Geologic map of the Salmon River suture zone with sample locations from this study and previous geochronology results (*McKay et al. 2011; ** Lund and Snee, 1988; *** Giorgis et al. 2008). Tcrb – Columbia River Basalt Group; Pcp – Chair Point Pluton; Kjtf – Jurassic-Cretaceous plutons; RRp – Rapid River plate; Pmp – Pollock Mountain plate; KJhcc – Hazard Creek complex; Klgcc – Little Goose Creek complex; Kib; Idaho Batholith; Oft – Olds Ferry Terrane. Modified from Lund, (2004).

METHODS

To quantify post-peak metamorphic conditions in the Pollock Mountain plate and timing of intrusion from plutons associated with the western Idaho shear zone, U-Pb ages were collected from zircon, apatite, and rutile to create temperature-time paths. Fourteen samples were processed following methods described in Strong and Driscoll (2016) to separate grains of zircon, rutile, and apatite based on magnetic properties and density. Samples were first crushed using a Gilson LC-28 jaw crusher, then processed in a Gilson LC-53 bico pulverizer until grains are approximately <1mm in diameter. Grains were then run through a Gemeni GT-60 separation table which separates and collects dense minerals. Dried grains were run through a Frantz L-1 isodynamic magnetic separator twice, first at 5° and 0.5A then at 10° and 1.5A to separate out non-magnetic grains for further processing. The remaining grains are then further separated by density through use of the heavy liquid lithium sodium tungstate (LST), which has a density value of 2.85g/cc. Grains of zircon, rutile, and apatite sink in LST, while lighter grains such as quartz float on top. Zircon, rutile, and apatite samples were hand-picked and placed onto double-sided tape. Grains were analyzed using the University of Arkansas' laser ablation inductively coupled plasma mass spectrometer (LA-ICP-MS) laboratory. Ablation was performed using an ESI New Wave Research 193 nm Excimer laser. Spot sizes were 25µm in diameter and 5µm in depth, rep rates were 10Hz, power levels were 3 J/cm³, and burst time was 20 seconds.

Samples of apatite and zircon can be difficult to distinguish from one another based on morphology alone. The morphology of zircon prisms can vary considerably, with some resembling hexagonal apatite grains (Gärtner et al., 2015; Rankin, 2022). To address this, zirconium and calcium counts per second were collected during isotopic analyses to allow for

chemical-based discrimination of calcium-rich apatite from zirconium-rich zircon (methodology described in Rankin, 2022). Sample reduction was performed with Iolite4 using the VizualAge UComPbine program (Paton et al., 2010; Paton et al., 2011; Petrus et al., 2012; Chew et al., 2014).

Closure Temperature

The closure temperature of a mineral refers to the temperature below which significant diffusion of certain parent or daughter isotopes out of the system ceases (Dodson, 1973; Cherniak et al., 1991; Braun et al., 2012). Closure temperature varies between minerals and isotopic systems being studied. The radiometric dates retrieved from samples record the time at which the mineral passed below its respective isotopic closure temperature (DiPietro, 2013). This study examines the U-Pb isotopic system for zircon, rutile, and apatite. When introducing the concept of closure temperature, Dodson (1973) defined the closure temperature of a mineral using equation (1)

$$T_c = \frac{E/R}{\ln (ART_c^2 D_0/a^2)/E(dT/dt)} \quad (1)$$

Where T_c represents the closure temperature in Kelvin, R is the gas constant of 0.00199 kcal/Kmol. E is the activation energy, experimentally listed as 54.6 kcal/mol (Cherniak et al., 1991). A is a constant for describing volume diffusion, being 55 for a sphere and 27 for a cylinder. D_0 is the diffusion coefficient, with $1.27 \cdot 10^{-4} \text{ cm}^2 \text{ s}^{-1}$ used for this study. τ is a time constant representing the rate the diffusion coefficient diminishes, and a represents the effective sphere radius (μm) of the mineral grain.

U-Pb Zircon

Zircon has a U-Pb closure temperature of greater than 900 °C, which will provide constraints on crystallization ages of intrusive igneous suites (DiPietro, 2013). Zircon was found in 12 samples with an overall total of 182 grains. Elemental concentrations in the Plešovice standard zircons with an age of 334 ± 5.6 Ma were used as a control for zircon samples (Sláma et al., 2008). Analytical results were filtered in IsoplotR to eliminate outliers (Vermeesch, 2018). Reported ages are $^{206}\text{Pb}/^{238}\text{U}$ mean ages. Summary of all zircon data is found in Appendix B.

U/Th Ratios. The ratio of uranium to thorium (U/Th) in zircon is a reliable method to determine if grains have been altered by metamorphism. Igneous zircons have ratios <10 , with typical values ranging between 1-2. U/Th ratios of $>5-10$ are likely to be metamorphic, but ratios can vary depending on the degree of metamorphism (Kirkland et al., 2015; Yakymchuk et al., 2018). Zircon formed from compressional magmatism and accretionary orogenesis have a wider range of U/Th ratios (McKay et al., 2018). U/Th ratios also vary temporally in metamorphic systems, with low ratios occurring near times of peak metamorphism and decreasing during cooling towards the solidus (Yakymchuk et al., 2018). By analyzing U/Th ratios spatially across the Salmon River suture zone and western Idaho shear zone, we can determine the timings of compressional magmatism as well as peak metamorphism and early cooling.

U-Pb Rutile

Rutile occurs as an accessory mineral in igneous as well as metamorphic rocks ranging from greenschist to granulite facies (Meinhold, 2010). Rutile can crystallize over a wide range of temperatures (450-1000°C), making it a useful mineral to record conditions in ultra-high

temperature metamorphic rocks (Zack et al., 2004). The U-Pb closure temperature can vary between 400 °C in rims and 640 °C in cores (Kooijman et al., 2010). Uranium concentration can vary significantly in rutile, however U-Pb dating can be accurate with concentrations as low as 1 ppm (parts per million) (Li et al., 2011). In low to medium-grade metamorphic rocks, rutile occurs as small (~20-100µm) scattered grains and elongated crystals (Meinhold, 2010). Rutile was found in one sample totaling 20 grains. This sample was reduced using the final $^{206}\text{Pb}/^{238}\text{U}$ age mean with a correction for ^{207}Pb . Elemental concentrations in the R632 standard with an age of 495 ± 10.5 Ma were used as a control for rutile samples (Bracciali et al., 2013; Axelsson et al., 2018).

Zr-in-Rutile Thermometry. Along with U-Pb geochronology, Zr-in-rutile thermometry was performed to determine detailed P-T constraints on mineral formation. Zr in rutile has a high resistance to resetting under high-temperature conditions (Zack et al., 2004; Usuki et al., 2017). Rutile grains can also potentially preserve the equilibrium conditions from their formation, which is useful for determining post-peak metamorphic P-T paths (Zack et al., 2004). Since rutile is stable over a wide range of temperatures and pressures, the Zr content of the mineral can be used as a single-phase thermometer (Kooijman et al., 2010), however, Zr-in-rutile thermometry can only be performed if the SiO_2 - ZrO_2 - TiO_2 system is in equilibrium with quartz, zircon, and rutile (Zack et al., 2004; Watson et al., 2006; Tomkins et al., 2007; Kotowski et al., 2021). If rutile forms in the presence of zircon and quartz, Zr is buffered in the rutile structure (Kotowski et al., 2021). Rutile grains used in this study were collected in rocks containing both quartz and zircon. Zr content varies logarithmically with temperature (Watson et al., 2006; Kotowski et al., 2021), with concentration in rutile widely varying depending on metamorphic grade, ranging from 30 ppm in low metamorphic grades to >8400 ppm in high grades (Tomkins

et al., 2007; Meinhold et al., 2008). There are multiple calibration equations to find the crystallization of temperature of rutile. The calibration used in this study is defined in equation (2) from Watson et al. (2006):

$$T(^{\circ}\text{C})_{\text{rutile}} = \frac{4470 \pm 120}{(7.36 \pm 0.10) - (\text{Zr ppm})} - 273 \quad (2)$$

In conjunction with uncertainty addressed in this equation, Watson et al. (2006) defines a thermometer calibration uncertainty in amphibolite facies T-P conditions as ± 20 °C. The summary of all rutile data used is found in Appendix C.

U-Pb Apatite

Apatite was found in 10 samples totaling 131 grains. The U-Pb system in apatite becomes highly sensitive at temperatures above 350°C, making it a valuable accessory mineral for recording change in mid-crustal igneous and metamorphic facies (Cochrane et al., 2014). Apatite typically accumulates large amounts of common lead in its system, which can be problematic especially in Phanerozoic rocks with low U concentrations that have not had time to incorporate significant radiogenic lead (Chew and Spikings, 2021). To address this, Pb^{207} correction was performed on all apatite $\text{Pb}^{206}/\text{U}^{238}$ mean ages. Elemental concentrations from the Durango (28 ± 2 Ma) standard were used as a control on apatite ages (Chew et al., 2016).

The closure temperature of apatite spans from ~350-700 °C, making it highly adept at recording conditions of mid to high-grade metamorphism (Kirkland et al., 2018; Chew et al., 2021). The closure temperature of apatite can be refined by measuring the sizes of individual mineral grains (Cochrane et al., 2014). Long (c) and short (a2) crystallographic axes were measured to a precision of 0.01 μm using a Leica Dms1000 digital microscope to determine

effective sphere radii of grains. Published cooling rates in the Salmon River suture zone of 7 °C/m.y. (± 1 °C/m.y.) were used for calculations (McKay et al., 2017), and reported closure temperatures are recorded with an uncertainty of ± 3 °C. Average closure temperature was calculated for each sample. Summary of all apatite data can be found in Appendix D.

RESULTS

Sample Descriptions

Twelve locations were sampled in the study area. Samples 101, 103B, 104A, and 104B were collected from the Hazard Creek complex, samples 106, and 107 were collected from the Little Goose Creek complex, samples 21 and 22 were collected in the Squaw Creek Schist below the Pollock Mountain fault, and samples 18, 19, 114, and 116 were collected in the Pollock Mountain Amphibolite above the Pollock Mountain fault. Sample 101 was from a competent, moderately foliated orthogneiss along Hazard Creek. Sample 103B was from a similar orthogneiss with foliations oriented 055/41 NW. Sample 104A was collected south of Hazard Creek from a highly incompetent orthogneiss with possible shear structures and foliation oriented 026/43 NW. Sample 104B was collected ~100 ft to the south of 104A, and was much more competent, with strong foliation oriented 034/14 NW. Sample 106 was found in the Little Goose Creek complex from a strongly banded gneiss with foliation oriented 010/78 E. Sample 107 was collected from a highly-deformed gneiss displaying boudinage and mylonitic structures. Sample 21 was collected from a quartzose micaceous schist to the immediate north of the Pollock Mountain fault as drawn by Lund (2004). Sample 22 was found in a sequence consisting of micaceous schists and quartzose units. Sample 18 was collected from a foliated micaceous outcrop. Sample 19 was collected from a foliated mixed clastic sequence of micaceous schists immediately above the Pollock Mountain fault as drawn by Lund (2004). Sample 114 was selected from a well-foliated schist with mica and quartz banding. Sample 116 was collected from a sheared garnet-bearing micaceous schist. Sample photos are shown in figure 3. Mean age data from this study is tabulated for zircon in Table 1, apatite in Table 2, and rutile in Table 3.

U-Pb Zircon

Plutonic Rocks. Zircons from metamorphosed plutonic rocks were collected from the Hazard Creek and Little Goose Creek complexes. In total, 117 zircon grains were collected from six samples: 101, 103B, 104A, 104B, 106, and 107.

Sample 101 (Fig. 4A, 6A) contained three zircon grains with a weighted mean age of 141.90 ± 10.4 Ma (MSWD=1.4). All grains had U/Th ratios below 10, with values between 0.35 ± 0.01 and 5.88 ± 0.53 .

Sample 103B (Fig. 4B, 4B) contained 12 zircon grains with four outliers. Eight grains yielded a weighted mean age of 144.74 ± 2.14 Ma (MSWD=1.7). All grains had U/Th ratios below 10 ranging from 1.95 ± 0.28 and 5.86 ± 0.42 .

Sample 104A (Fig. 4C, 6C) contained 39 grains with two outliers. 37 zircon grains yielded a weighted mean age of 121.19 ± 1.25 Ma (MSWD=6.1). This sample contained three different age populations with population one consisting of 15 grains at 118.41 ± 2.19 Ma (MSWD=1.5), population two consisting of 10 grains at 128.87 ± 1.98 Ma (MSWD=1.1), and population three consisting of 12 grains at 140.22 ± 2.53 Ma (MSWD=1.8). Four grains in population one have high U/Th ratios between 13.29 ± 1.14 and 23.77 ± 3.71 . One grain in population two has a U/Th ratio >10 with a value of 11.21 ± 1.94 . U/Th ratios in population three ranged between 2.22 ± 0.21 and 6.78 ± 0.87 .

Sample 104B (Fig. 4D, 6D) contained 24 zircon grains with five outliers. Nineteen grains yielded a weighted mean age of 131.78 ± 2.20 Ma (MSWD=1.3). Two grains had U/Th ratios above 10, with values of 12.09 ± 2.09 and 15.68 ± 6.74 . The other 17 grains have U/Th values ranging between $\sim 1.75 - 7.50$.

Sample 106 (Fig. 4E, 6E) contained six zircon grains with three outliers. Three grains yielded a weighted mean age of 105.52 ± 1.27 Ma (MSWD=0.88). All grains had U/Th ratios greater than 10, with values spanning from 66.62 ± 13.02 to 156.64 ± 23.81

Sample 107 (Fig. 4F, 6F) contained 34 zircon grains with six outliers. A population of 26 grains yielded a weighted mean age of 104.47 ± 0.59 Ma (MSWD=14). This sample was split into three age populations, with population one consisting of nine grains at 97.68 ± 1.06 Ma (MSWD=1.1), population two consisting of seven grains at 103.85 ± 1.11 Ma (MSWD=1), and population three consisting of 10 grains at 110.15 ± 0.93 Ma (MSWD=1.6). Three grains in population one have U/Th ratios above 10, ranging from 10.54 ± 1.21 and 15.01 ± 1.07 . Two grains in population two have U/Th ratios above 10, with values of 26.35 ± 4.35 and 29.75 ± 2.48 . Five grains in population three have U/Th ratios above 10, with values ranging from 10.80 ± 0.73 to 48.29 ± 2.77 .

Below Pollock Mountain Fault. Nine zircon grains were collected from two samples: 21 and 22.

Sample 21 (Fig. 5E, 7E) contained six zircon grains with three outliers. Three grains yielded an age of 121.71 ± 4.01 Ma (MSWD=7.9). This sample was split into two age populations, with population one consisting of one grain at 110.27 ± 7.04 Ma and population two consisting of two grains at 127.04 ± 4.79 Ma. All three grains have U/Th ratios below 10, with values ranging from 0.72 ± 0.03 to 5.99 ± 1.10

Sample 22 (Fig. 5F, 7F) contained three zircon grains with a ^{207}Pb corrected weighted mean age of 115.19 ± 7.10 Ma (MSWD=0.2). Two grains have elevated U/Th ratios, with values of 8.92 ± 0.83 and 20.96 ± 4.05 .

Above Pollock Mountain Thrust Fault. A total of 54 Zircons were collected from five samples: 18, 19, 114, and 116.

Sample 18 (Fig. 5A, 7A) contained 10 zircons. Five grains yielded a weighted mean age of 138.07 ± 3.29 (MSWD=0.71). Three grains from this population have U/Th ratios above 10, with values ranging from 12.47 ± 1.10 to 141.14 ± 12.67 .

Sample 19 (Fig. 5B, 7B) contained three zircon grains with a ^{207}Pb corrected weighted mean age of 114.91 ± 3.70 (MSWD=0.29). All three grains have U/Th ratios below 10, with values ranging from 1.03 ± 0.16 to 4.95 ± 1.16

Sample 114 (Fig. 5C, 7C) contained 15 zircon grains with five outliers. Ten grains yielded a weighted mean age of 120.69 ± 1.41 Ma (MSWD=3). Six grains have U/Th ratios above 10, with values ranging from 11.20 ± 1.00 to 28.58 ± 1.32 .

Sample 116 (Fig. 5D, 7D) contained 26 zircon grains, with 23 grains yielding a ^{207}Pb corrected weighted mean age of 114.15 ± 1.13 Ma (MSWD=7). This sample was split into three age populations with population one consisting of 11 grains at 105.79 ± 2.46 Ma (MSWD=0.81), population two consisting of four grains at 112.16 ± 1.59 Ma (MSWD=0.94), and population three consisting of eight grains at 123.87 ± 2.12 Ma (MSWD=0.84). Five grains have U/Th ratios near or above 10, with values ranging from 9.71 ± 1.21 to 22.72 ± 3.39 . Seven grains in population two have U/Th ratios above 10, with values from 12.71 ± 1.40 to 140.69 ± 35.73 . Five grains from population three have U/Th ratios above 10, with values ranging from 14.61 ± 1.34 to 74.00 ± 14.92 .

U-Pb Rutile

Sample 104B in the Hazard Creek complex was the only sample containing significant rutile grains. Zr concentrations were an average of 258.6 ppm. 20 rutile grains were collected from this sample with six outliers. Fourteen grains yielded a ^{207}Pb corrected weighted mean age of 116.44 ± 7.23 Ma (MSWD=1). Using equation (1), closure temperature was determined to be 627.5 ± 6 °C.

U-Pb Apatite

Apatite U-Pb ages in the Salmon River suture zone and western Idaho shear zone reflect the cooling of rocks through their closure temperature window of 350-500 °C, providing temporal data for the thermal history of these units after peak metamorphic conditions at roughly 650 °C. The closure temperature of apatite grains depends on grain size, with grain width significantly more influential than length. Smaller/thinner grains will have lower closure temperatures than larger/wider grains. Effective sphere radii (ESR) of collected grains ranges from 13-36 μm . Ages of apatite grains in the western Idaho shear zone range from ~ 113 -74 Ma with closure temperatures between 414-453 °C. Ages of apatite grains in the Salmon River suture zone range from ~ 116 -90 Ma with closure temperatures between 413-466 °C.

Plutonic Rocks. Samples containing apatite were found in the Hazard Creek and Little Goose Creek complexes. 47 apatite grains were collected from samples 101, 103B, 104A, 104B, and 106.

Sample 101 (Fig. 8A, 8A, 12A, 14A) contained four grains with one outlier. three apatite grains yielded a weighted mean age of 77.84 ± 3.06 Ma (MSWD=5.4). Average closure temperature for this sample was 432.5 ± 2 °C. This sample was split into two age groups with

population one consisting of one grain at 79.74 ± 3.28 Ma with a closure temperature of $439.62 \pm 3^\circ\text{C}$ and population two consisting of two grains at 64.84 ± 8.49 Ma with a closure temperature of $425.3 \pm 3^\circ\text{C}$

Sample 103B (Fig. 8B, 10B, 12B, 14B) contained four grains with one outlier. Three apatite grains produced a ^{207}Pb corrected weighted mean age of 96.93 ± 6.85 Ma (MSWD=13). Average closure temperature for this sample was $432.0 \pm 1.7^\circ\text{C}$. This sample was split into two populations with population one consisting of two grains at 115.7 ± 10.1 Ma with a closure temperature of $435.3 \pm 2.12^\circ\text{C}$ and population two consisting of one grain at 80.74 ± 9.31 Ma with a closure temperature of $425.5 \pm 3^\circ\text{C}$.

Sample 104A (Fig. 8C, 10C, 12C, 14C) contained 12 apatite grains with a weighted mean age of 74.05 ± 3.12 Ma (MSWD 5.5). Average closure temperature for this sample was $436.6 \pm 0.9^\circ\text{C}$. This sample was split into two populations with population one consisting of five grains at 94.83 ± 6.61 Ma (MSWD=0.3) with a closure temperature of $441.3 \pm 1.3^\circ\text{C}$ and population two consisting of seven grains at 68.11 ± 3.53 Ma (MSWD=1.4) with a closure temperature of $433.3 \pm 1.1^\circ\text{C}$.

Sample 104B (Fig. 8D, 10D, 12D, 14D) contained 12 apatite grains with two outliers. Ten grains yielded a weighted mean age of 117.95 ± 4.43 Ma (MSWD=3.3). Average closure temperature for this sample was $432.8 \pm 0.9^\circ\text{C}$. This sample was split into two populations with population one consisting of seven grains at 128.68 ± 6.11 Ma (MSWD=0.38) with a closure temperature of $437.4 \pm 1.1^\circ\text{C}$ and population two consisting of three grains at 106.11 ± 6.42 Ma (MSWD=0.56) with a closure temperature of $422.1 \pm 1.8^\circ\text{C}$.

Sample 106 (Fig. 8E, 10E, 12E, 14E) contained 26 apatite grains with 12 outliers. Fourteen grains yielded a weighted mean age of 73.10 ± 1.88 Ma (MSWD=12). Average closure

temperature for this sample was 430.0 ± 0.8 °C. This sample was split into two populations with population one consisting of eight grains at 90.02 ± 3.39 Ma (MSWD=0.43) with a closure temperature of 431.1 ± 1.1 °C and population two consisting of six grains at 64.30 ± 2.38 Ma (MSWD=5) with a closure temperature of 429.5 ± 1.2 °C.

Below Pollock Mountain Thrust Fault. Samples from below the Pollock Mountain fault were collected from the Squaw Creek schist. Apatite was found in one sample, 21.

Sample 21 (Fig. 9E, 11E, 13E, 14F) contained five apatite grains with one outlier that was excluded. The sample had a ^{207}Pb corrected weighted mean age of 96.49 ± 6.44 Ma (MSWD=1.6) Average closure temperature for this sample was 413.3 ± 1.5 °C.

Above Pollock Mountain Thrust Fault. Samples from above the Pollock Mountain fault were collected from the Pollock Mountain amphibolite. 68 apatite grains were collected from four samples: 18, 19, 114, and 116.

Sample 18 (Fig. 9A, 11A, 13A, 14G) contained five apatite grains with a ^{207}Pb corrected weighted mean age of 98.31 ± 2.89 Ma (MSWD=21). Average closure temperature for this sample was 438.1 ± 1.3 °C. This sample consists of two age populations, with population one consisting of two grains at 123.5 ± 6.36 Ma with a closure temperature of 465.4 ± 2.1 °C and population two consisting of three grains at 91.78 ± 3.24 Ma (MSWD=1.8) with a closure temperature of 420.5 ± 1.7 °C.

Sample 19 (Fig. 9B, 11B, 13B, 14H) contained six grains with one outlier. Five apatite grains yielded a ^{207}Pb corrected weighted mean age of 92.79 ± 6.44 Ma (MSWD=4.5). Average closure temperature for this sample was 421.3 ± 1.3 °C.

Sample 114 (Fig. 9C, 11C, 13C, 14I) contained 37 apatite grains with 19 outliers. Eighteen grains yielded a mean age of 94.01 ± 2.78 Ma (MSWD=8.6). Average closure

temperature for this sample was 430.1 ± 0.7 °C. This sample was split into three populations of grains. Population one consists of five grains with an age of 123.29 ± 4.63 Ma (MSWD=0.14) with a closure temperature of 436.6 ± 1.3 °C, population two consists of seven grains with an age of 102.68 ± 4.63 Ma (MSWD=0.24) and a closure temperature of 430.4 ± 1.1 °C, and population three consists of five grains with an age of 79.45 ± 3.90 Ma (MSWD=0.47) with a closure temperature of 424.6 ± 1.3 °C.

Sample 116 (Fig. 9D, 11D, 13D, 14J) contained 20 grains with ten outliers. Ten grains yielded a mean age of 90.78 ± 4.51 Ma (MSWD=5.1). Average closure temperature for this sample was 426.0 ± 0.9 °C.

Table 1. Mean zircon ages, MSWD, and grain counts for samples from this study. Samples with elevated MSWD (>3) had multiple age populations created.

Sample Number	Mean Zircon Age (Ma)	MSWD	Number of Grains
101	141.90 ± 10.4	1.4	3
103B	144.74 ± 2.14	1.7	8
104A	121.19 ± 1.25	6.1	37
104B	131.78 ± 2.20	1.3	19
106	105.52 ± 1.27 Ma	0.88	3
107	104.47 ± 0.59 Ma	14	26
18	138.07 ± 3.29	0.71	5
19	114.91 ± 3.70	0.29	3
114	120.69 ± 1.41	3	15
116	114.15 ± 1.13	7	23
21	121.71 ± 4.01	7.9	3
22	115.19 ± 7.10	0.2	3

Table 2. Mean apatite ages, MSWD, and grain counts for samples from this study. Samples with elevated MSWD (>3) had multiple age populations created.

Sample Number	Mean Apatite Age (Ma)	MSWD	Number of Grains
101	77.84 ± 3.06	5.4	3
103B	96.93 ± 6.85	13	3
104A	74.05 ± 3.12	5.5	12
104B	117.95 ± 4.43	3.3	10
106	73.10 ± 1.88	12	14
18	98.31 ± 2.89	21	5
19	92.79 ± 6.44	4.5	5
114	94.01 ± 2.78	8.6	18
116	90.78 ± 4.51	5.1	10
21	96.49 ± 6.44	1.6	4

Table 3. Mean rutile ages, MSWD, and grain counts for samples from this study.

Sample Number	Mean Rutile Age (Ma)	MSWD	Number of Grains
104B	116.44 ± 7.23	1.0	14

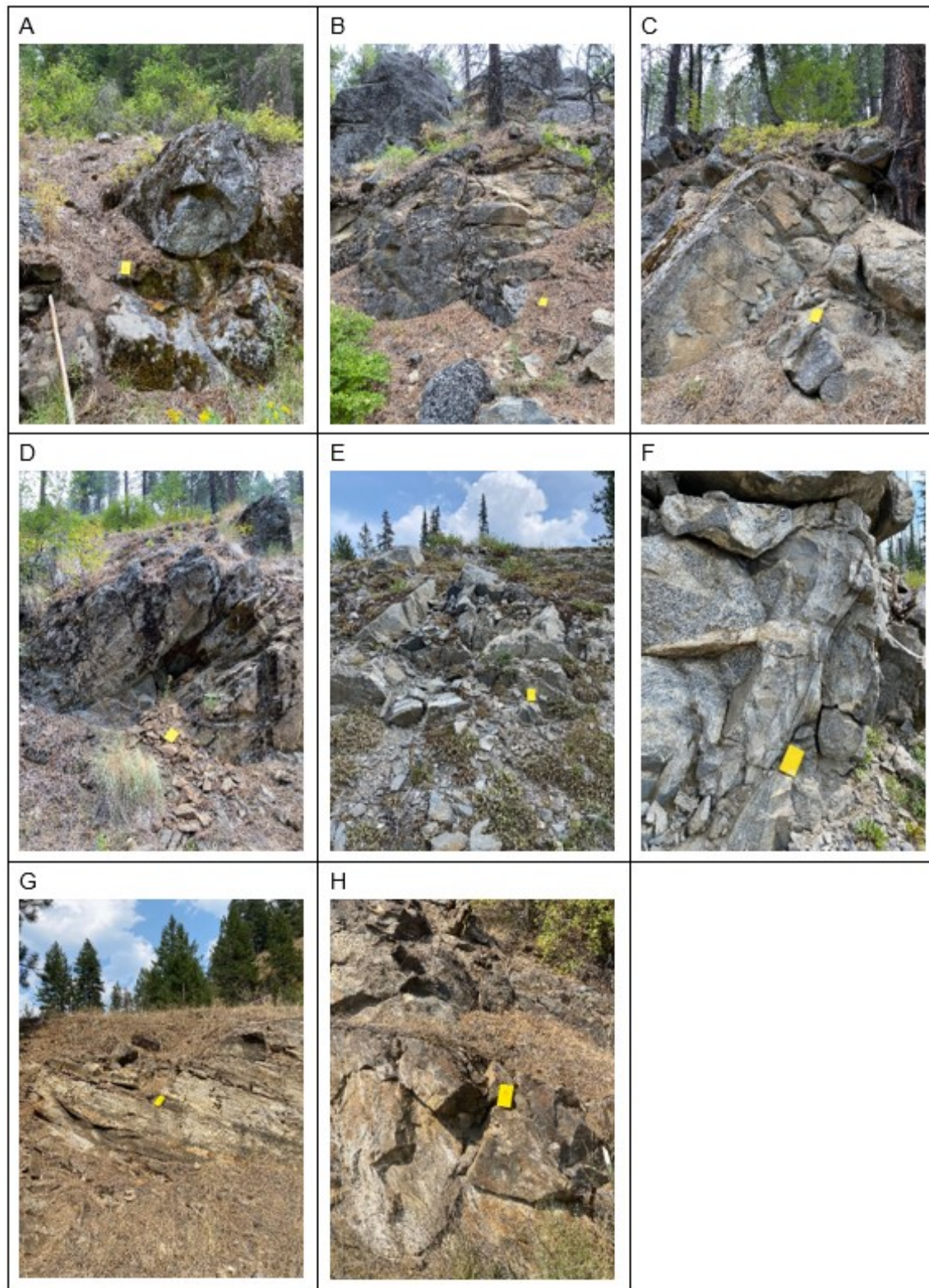


Figure 3. Sample location photos for samples 101 (A), 103B (B), 104A (C), 104B (D), 106 (E), 107 (F), 114 (G), and 116 (H).

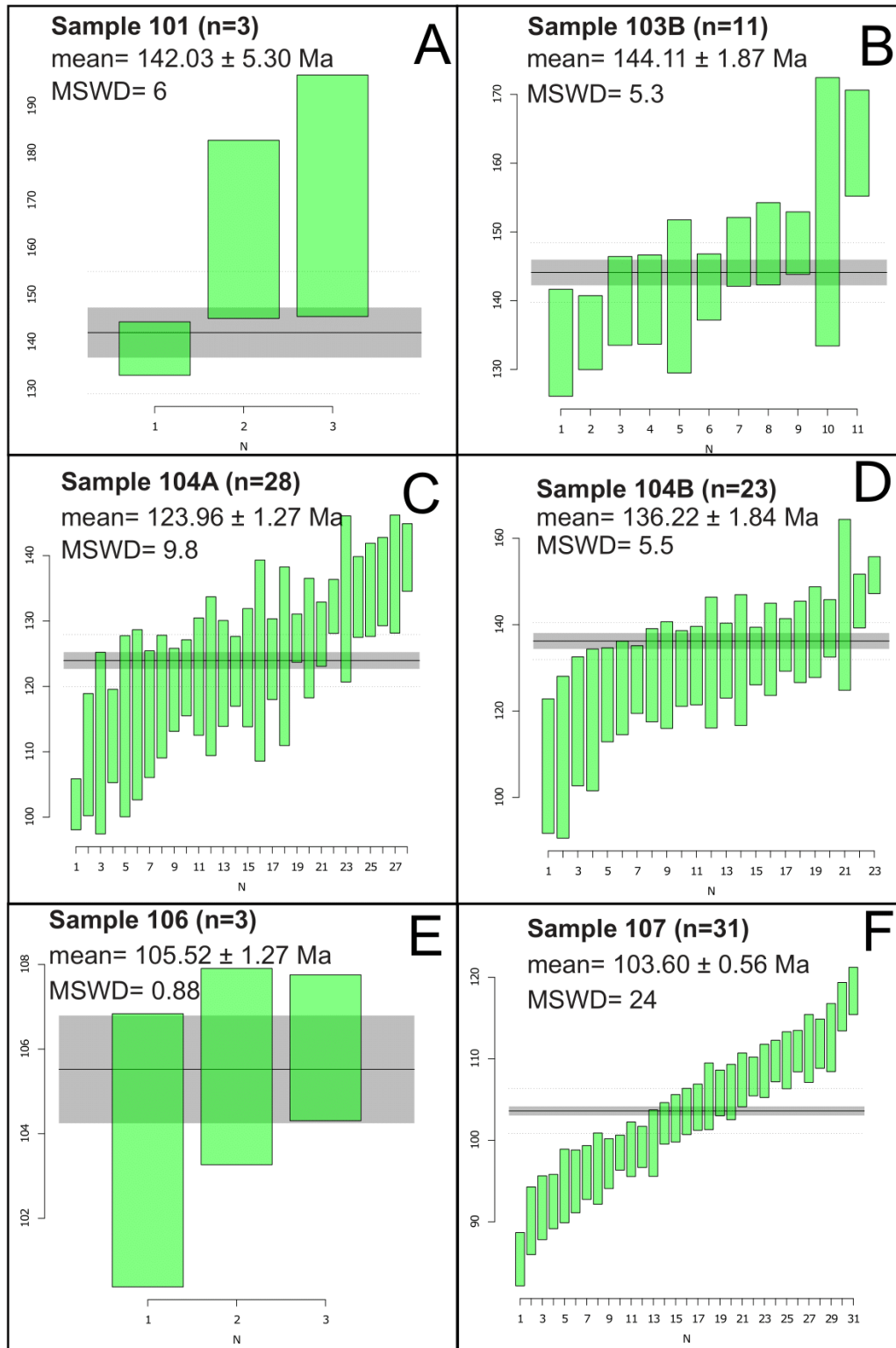


Figure 4. Weighted mean plots for zircon samples from the Hazard Creek and Little Goose Creek complexes.

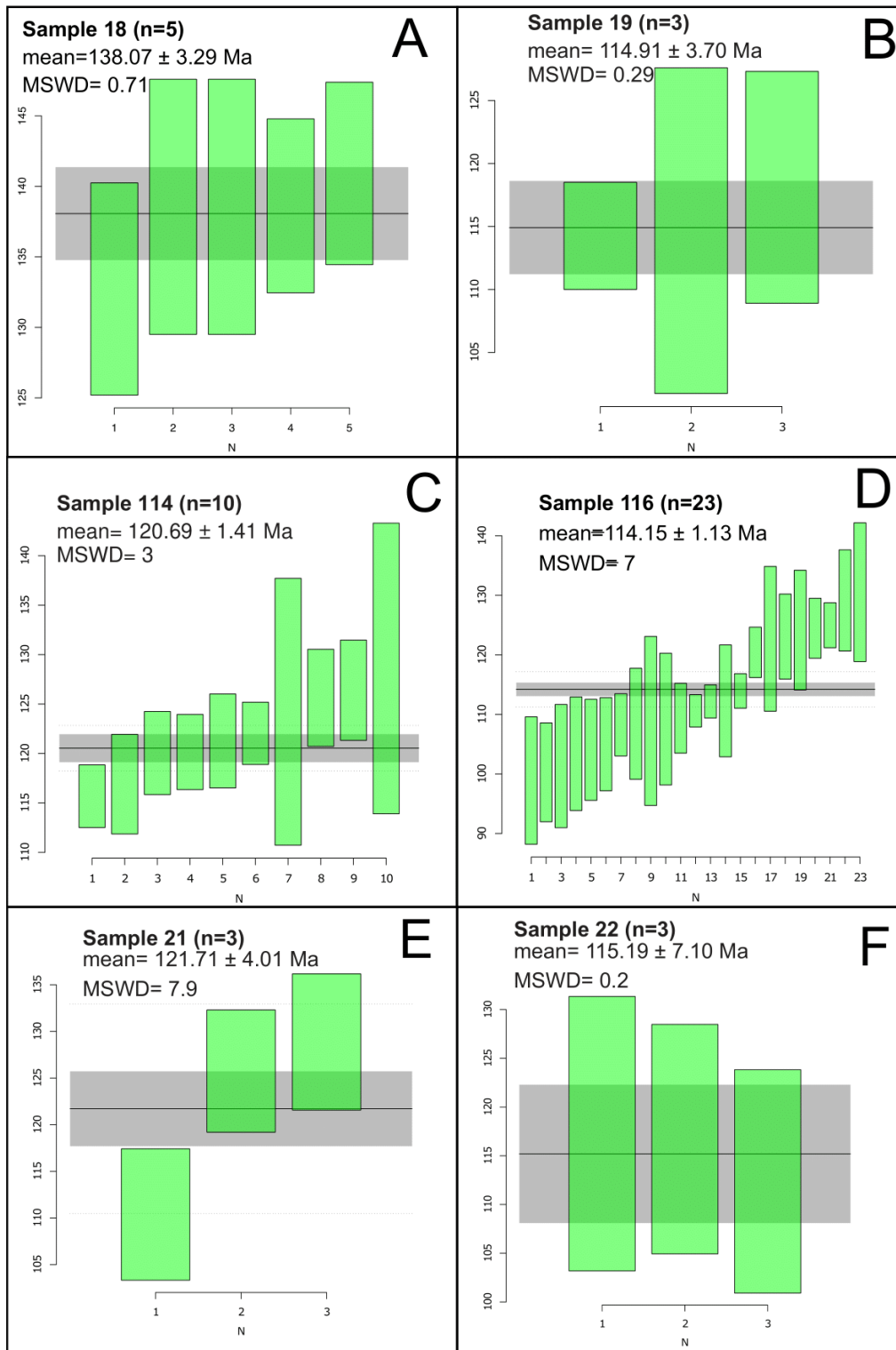


Figure 5. Weighted mean plots for zircon samples from the Pollock Mountain and Rapid River plates.

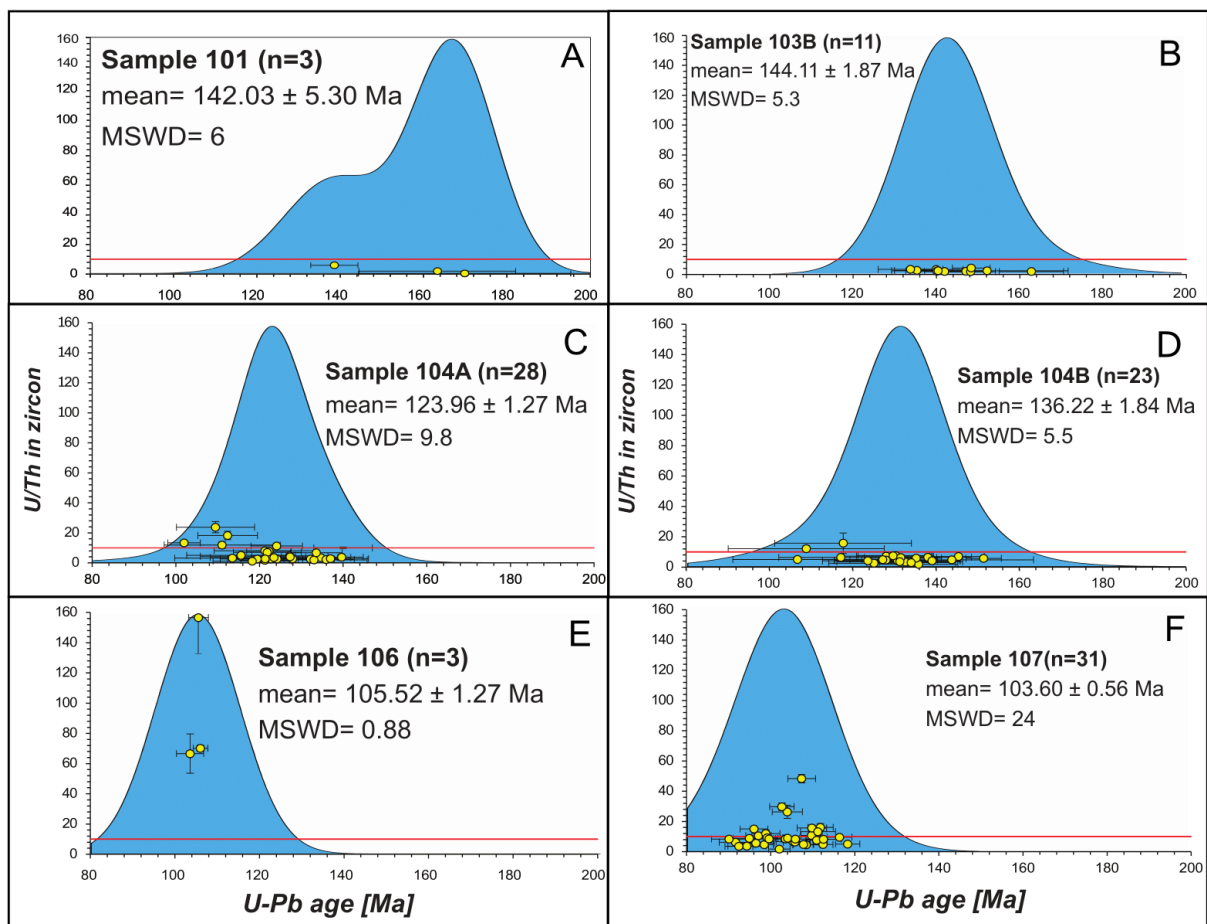


Figure 6. Zircon crystallization age vs. U/Th ratio with kernel density estimate (KDE) for U-Pb zircon samples from the Hazard Creek and Little Goose Creek complexes. Error is recorded to σ_2 .

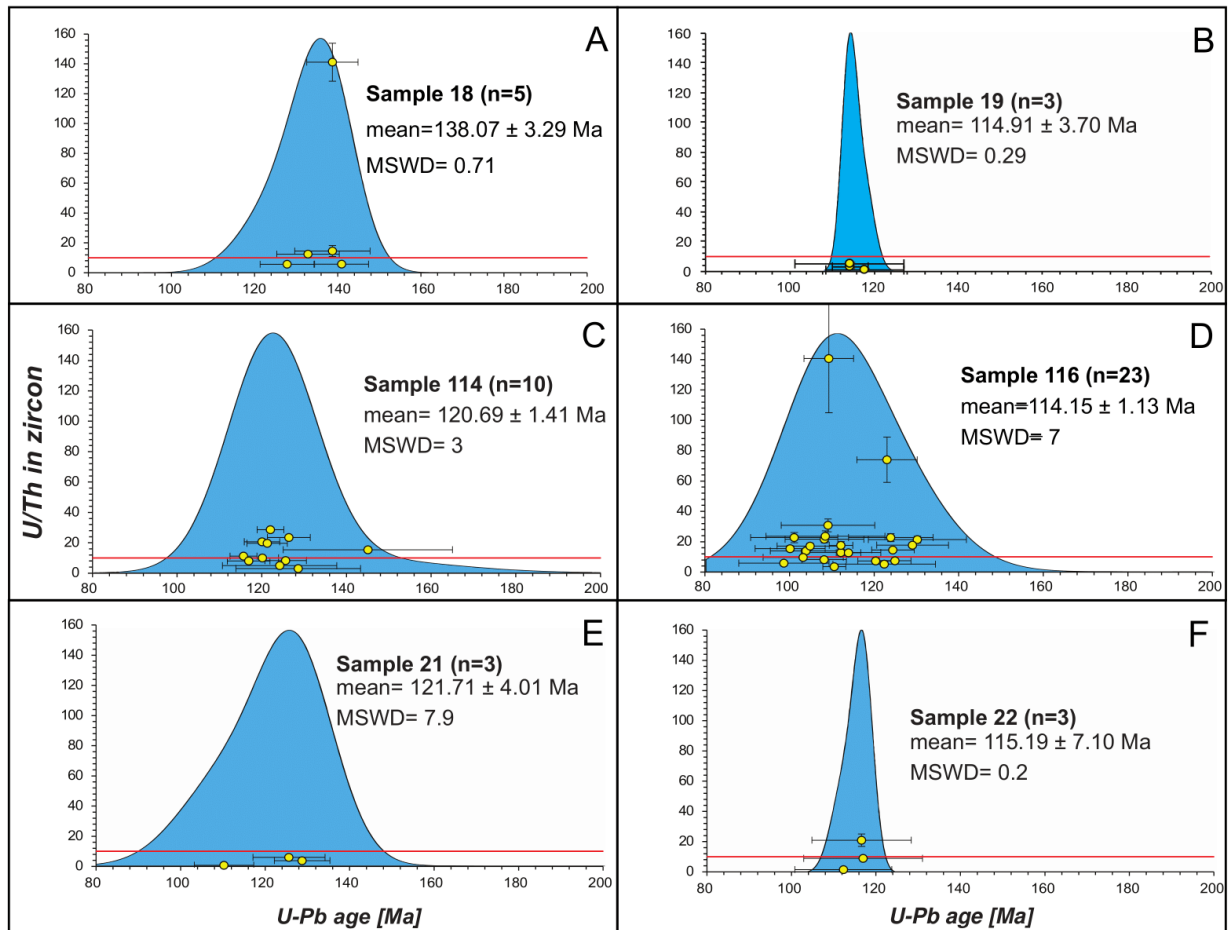


Figure 7. Zircon crystallization age vs. U/Th ratio with kernel density estimate (KDE) for U-Pb zircon samples from the Pollock Mountain and Rapid River plates. Error is recorded to σ_2 .

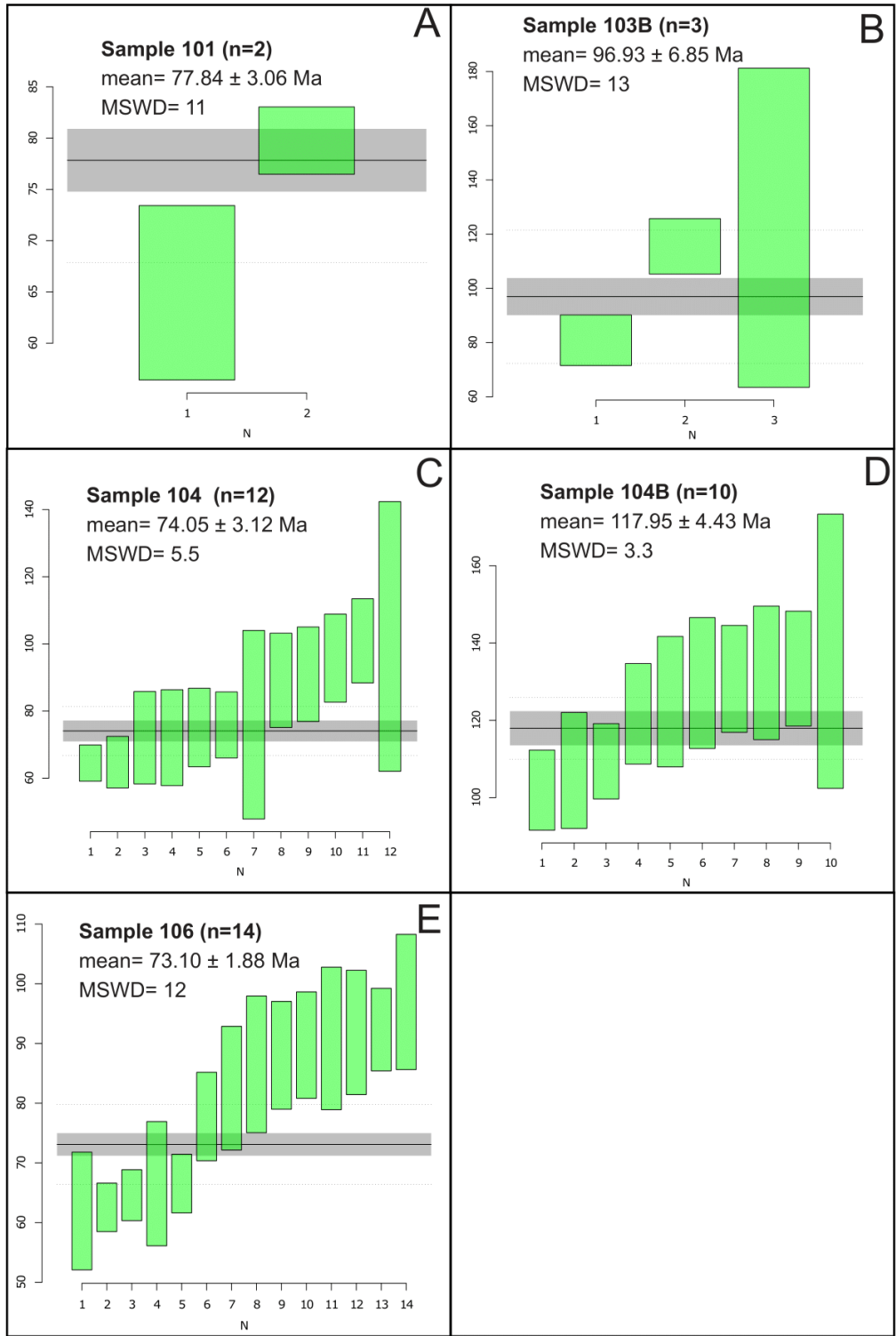


Figure 8. Weighted mean plots for apatite samples from the Hazard Creek and Little Goose Creek complexes.

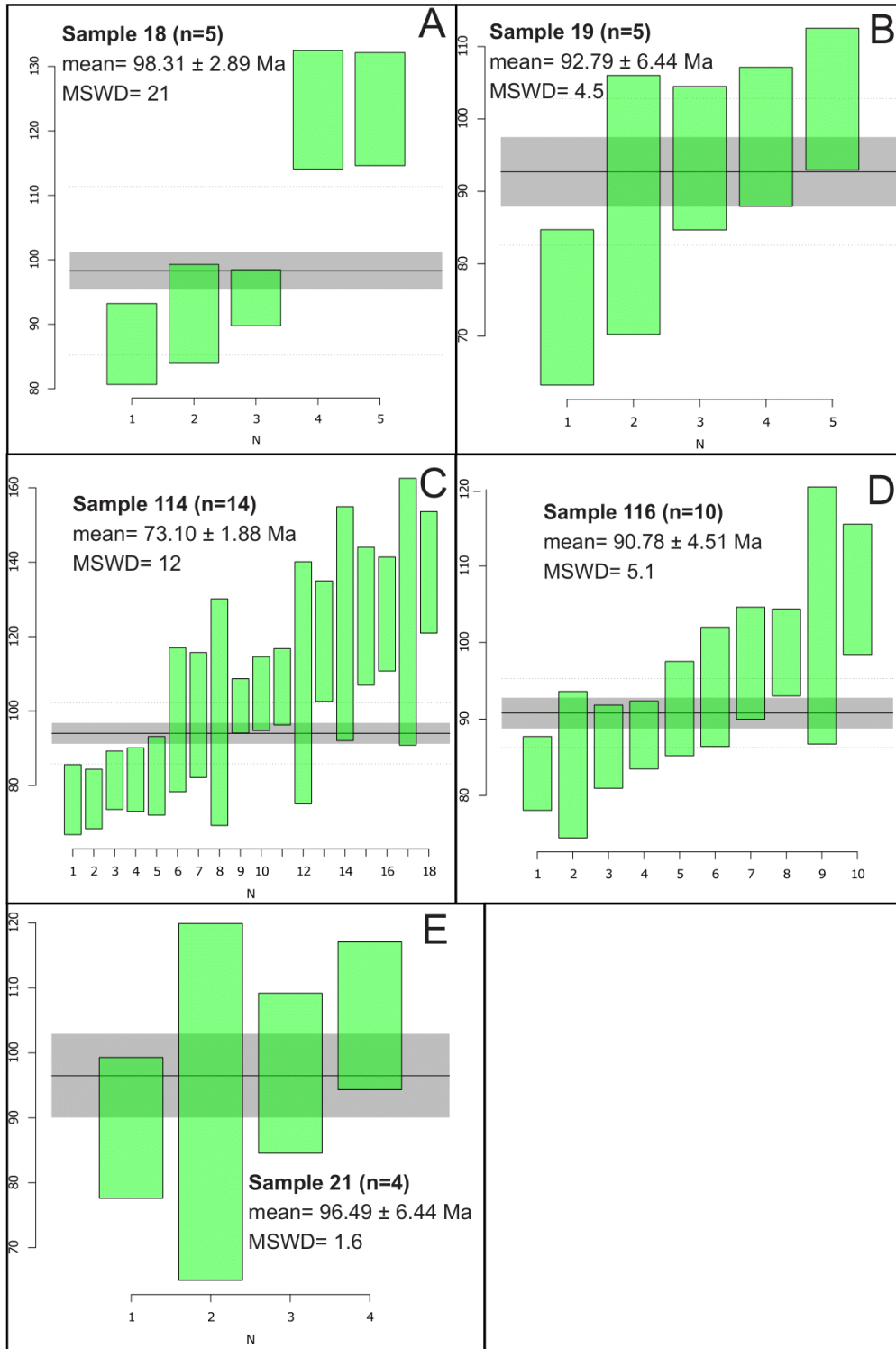


Figure 9. Weighted mean plots for apatite samples from the Pollock Mountain and Rapid River plates.

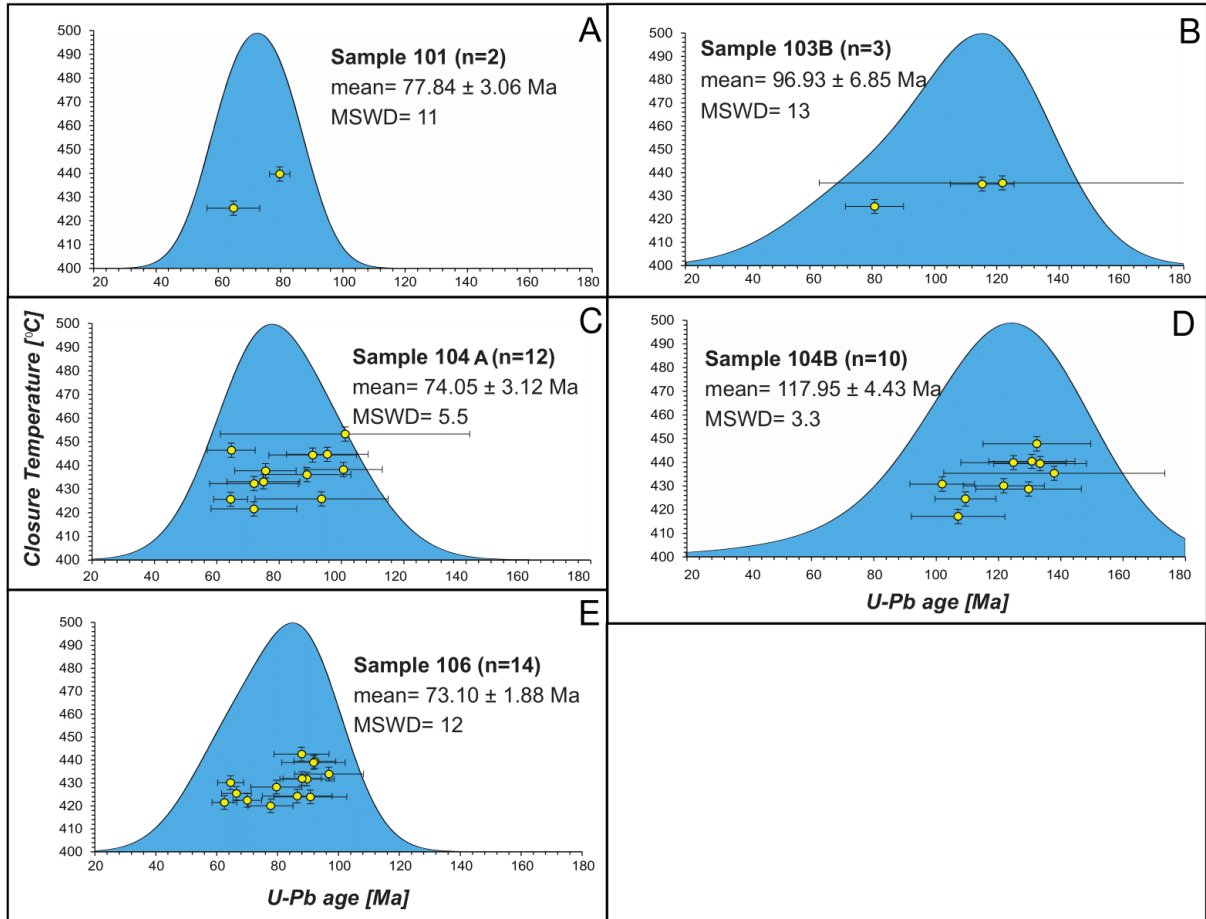


Figure 10. Apatite closure temperatures vs. U-Pb age with kernel density estimate (KDE) for age of apatite grains from the Hazard Creek and Little Goose Creek complexes. Error is recorded to σ_2 .

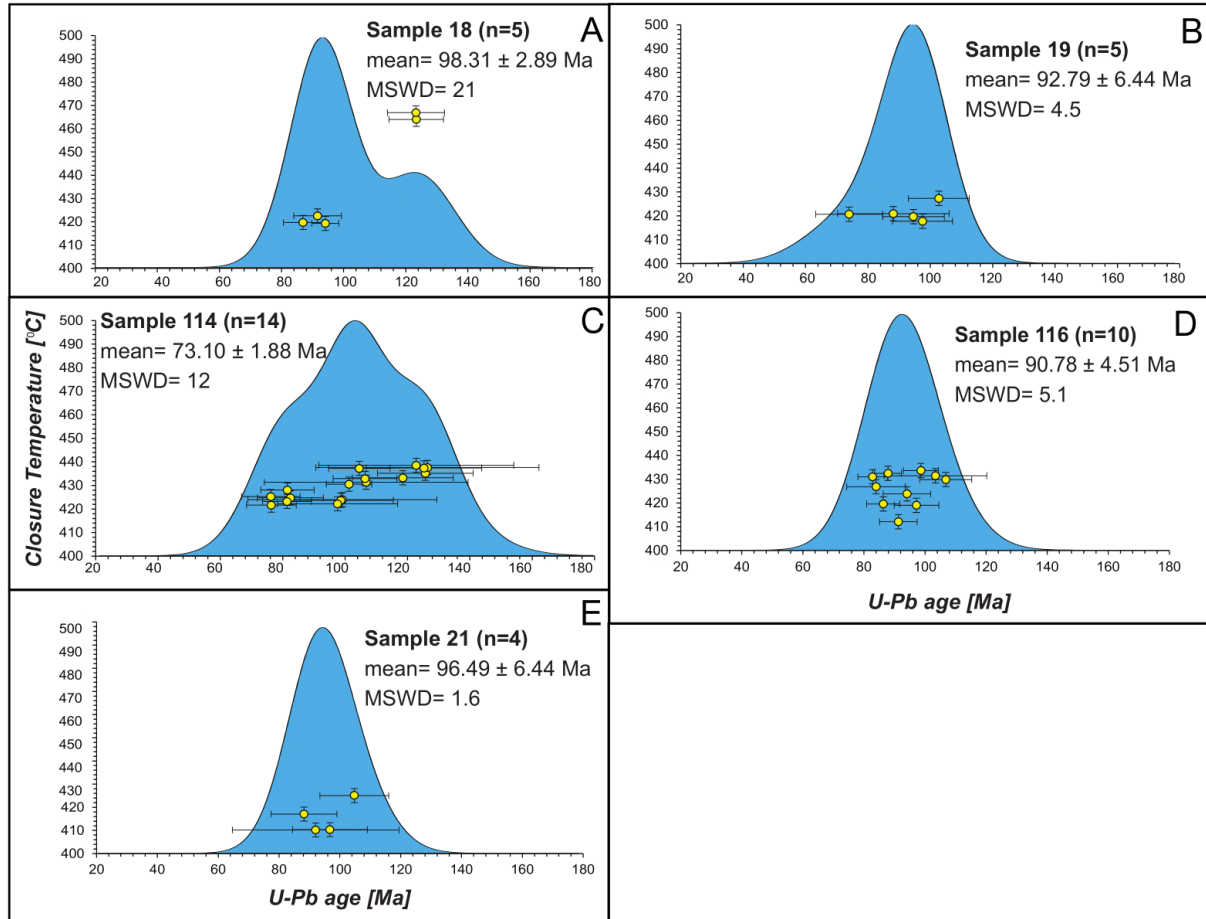


Figure 11. Apatite closure temperatures vs. U-Pb age with kernel density estimate (KDE) for age of apatite grains from Pollock Mountain and Rapid River plates. Error is recorded to σ_2 .

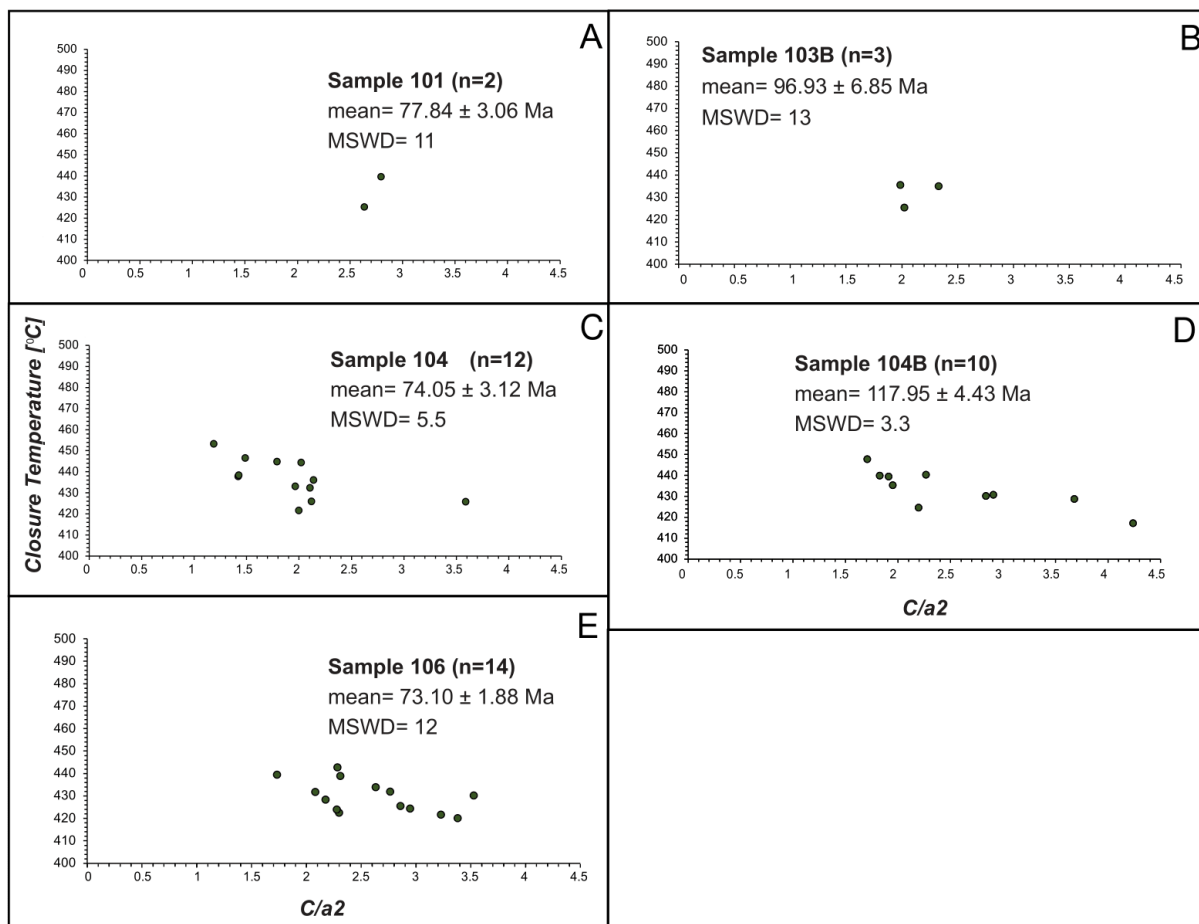


Figure 12. C (long)/a2 (short) axis values vs. U-Pb age for apatite grains from the Hazard Creek and Little Goose Creek complexes.

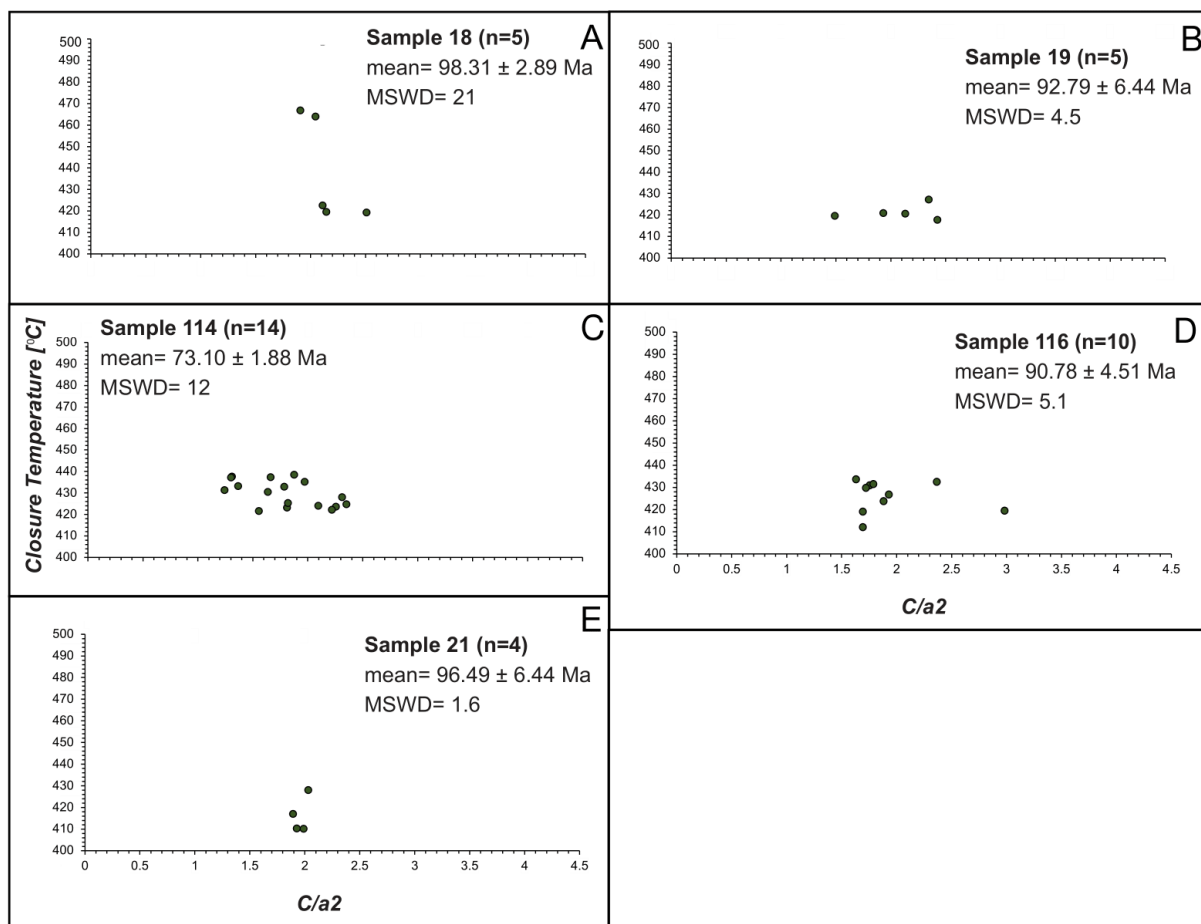


Figure 13. C (long)/a2 (short) axis values vs. U-Pb age for apatite grains from the Pollock Mountain and Rapid River plates.

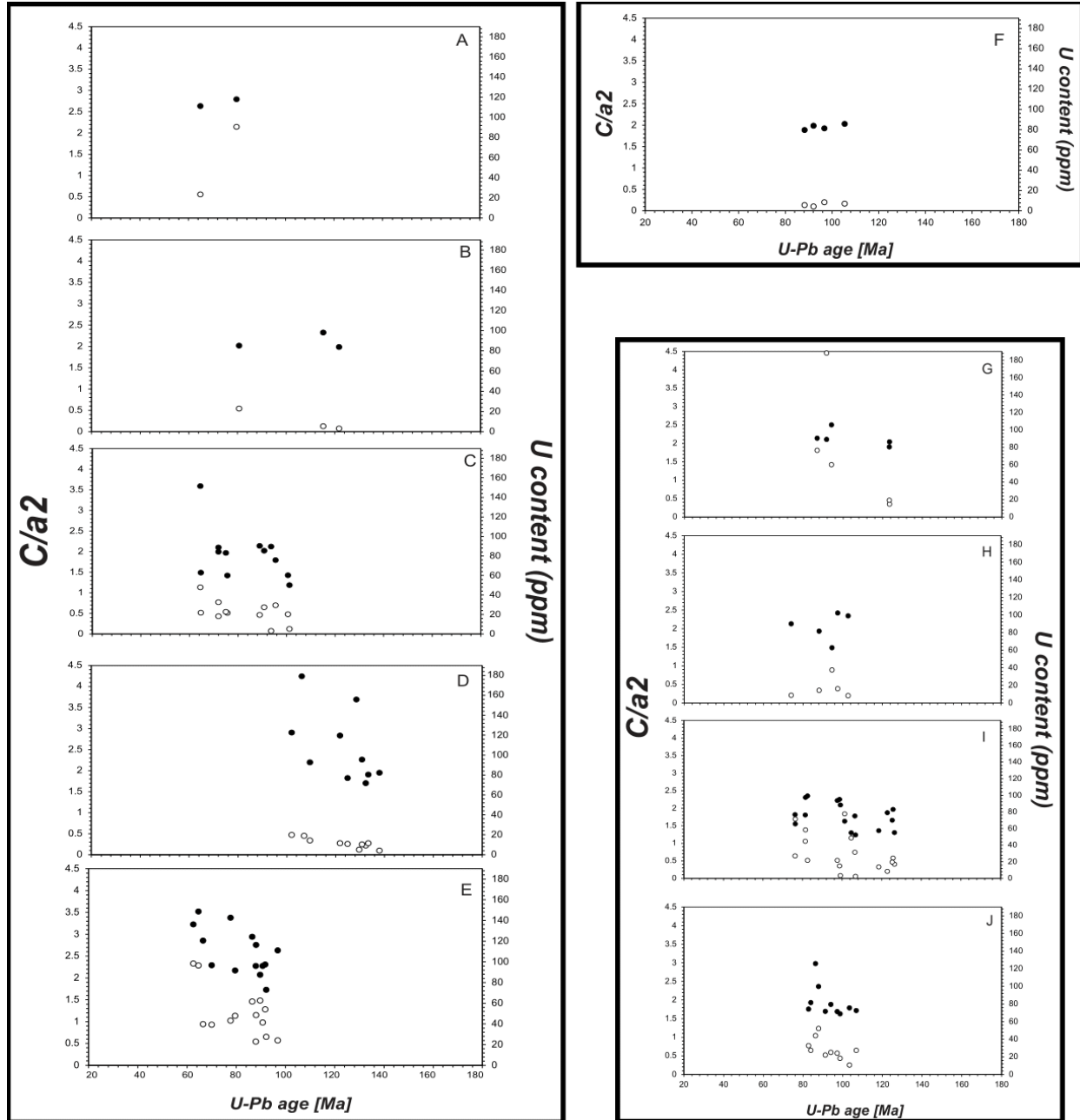


Figure 14. C/a2 (black) and U content (white) vs. U-Pb age for apatite from the Hazard Creek and Little Goose Creek complexes (left), below the Pollock Mountain fault (upper right), and above the Pollock Mountain fault (lower right).

DISCUSSION

Igneous and Metamorphic Zircon History

Zircon U-Pb ages and U/Th ratios record the crystallization and metamorphic history of the Salmon River suture zone and western Idaho shear zone. Zircons analyzed in this study have ages ranging from 169-114 Ma in the Salmon River suture zone and 112-103 Ma in the western Idaho shear zone. In the Salmon River suture zone, the temporal distribution of zircon ages shows the youngest grains occurring to the west, with ages becoming progressively older moving east towards the Sr isopleth line. In the western Idaho shear zone, grain ages in the Little Goose Creek complex overlap with shear zone deformation which occurred between 105 Ma and 90 Ma (Giorgis et al., 2008; Braudy et al., 2016). Zircon U/Th of rocks in the Salmon River suture zone and western Idaho shear zone record both igneous and metamorphic conditions. Metamorphic zircons in the suture zone had ages ranging from 130-100 Ma, reflecting previous studies which propose metamorphism spanning from 141 to ~112 Ma (McKay, 2011; Wilford and Vervoort, 2012; McKay et al., 2017). The oldest metamorphic ages from this study are recorded in the Pollock Mountain plate. Metamorphism in the western Idaho shear zone occurred from approximately 118-101 Ma (Manduca et al., 1993; Giorgis et al., 2008). Zircons from this study record metamorphism between 112-103 Ma. For the plutonic rocks of the Hazard Creek and Little Goose Creek complexes, with U-Pb zircon data from this study (Fig. 4, 6), emplacement of the Hazard Creek complex could be expanded to 145-115 Ma with metamorphism at 125-101 Ma. Emplacement and metamorphism of the Little Goose Creek complex could be expanded to 111-95 Ma.

Below Pollock Mountain Thrust Fault. Zircon grains from the Rapid River plate record magmatism and metamorphism from 128-110 Ma. Zircon grains with U/Th less than 10 range in age from 128-110 Ma, while grains with elevated ratios occur at ~116 Ma. Published Sm-Nd garnet ages from McKay et al. (2017) interpret metamorphism in the Rapid River plate to have occurred from 124-113 Ma. High and low U/Th zircon ages from this study overlap with accepted crystallization ages, therefore the Rapid River plate is interpreted to have undergone isothermal loading of 9kbar at 650 °C between 124-113 Ma (McKay et al., 2017), with coeval igneous activity occurring from around 118-113 Ma during intrusion of the Hazard Creek complex (U-Pb zircon; Manduca et al., 1993).

Above Pollock Mountain Thrust Fault. Zircons in the Pollock Mountain plate record magmatism and metamorphism from 138-98 Ma. Grains with U/Th ratios under 10 form a 138-98 Ma population, while grains with elevated U/Th ratios form a 138-100 Ma population. The zircon age ranges partially coincide with zoned garnet Sm-Nd ages from McKay et al. (2017), which were interpreted to show metamorphism beginning with a prolonged tectonothermal event spanning from ~141-124 Ma.

Plutonic Rocks. U/Th ratios of zircon in the plutonic rocks of the Salmon River suture zone and western Idaho shear zone indicate igneous activity spanning from ~169-90 Ma with metamorphism occurring between 124-96 Ma. Rocks from the Hazard Creek complex have older ages than rocks from the Little Goose Creek complex.

Hazard Creek complex. Zircon grains from the Hazard Creek record igneous activity and metamorphism from 169-101 Ma. Zircons with U/Th less than 10 have ages from 169-106 Ma, while grains with ratios above 10 occur between 124-101 Ma. The Hazard Creek complex is made up of multiple orthogneiss, trondhjemite, tonalite, and potassium feldspar bearing intrusive

rocks, with the oldest crystalloblastic orthogneiss units recording crystallization and metamorphism between 160 and 125 Ma (Manduca et al., 1993). All samples collected in this study from the Hazard Creek complex are orthogneisses. Zircon grains with low U/Th agree with accepted crystallization ages and grains with elevated U/Th ratios agree with proposed metamorphic ages, therefore it is interpreted that initial intrusion of the Hazard Creek complex occurred prior to suture zone metamorphism and continued through peak metamorphic conditions. Later intrusions underwent amphibolite-grade metamorphism during and after intrusion. Age estimates for metamorphism also overlap with proposed shear zone deformation post 118 Ma, therefore later elevated U/Th ages could reflect continued shear zone-related metamorphism (Gray, 2013; McKay et al., 2017).

Little Goose Creek complex. The Little Goose Creek complex records magmatism and metamorphism that post-dates the Hazard Creek complex. Zircon grains with U/Th less than 10 range in age from 116-90 Ma, while grains with elevated U/Th range from 111-98 Ma. Crystallization of the Little Goose Creek complex is proposed to have occurred at 110 ± 5 Ma (Manduca et al., 1993; Giorgis et al., 2008; McKay et al., 2011). Because high and low U/Th zircon ages overlap with accepted crystallization ages, the Little Goose Creek complex is interpreted to have intruded during peak to near-peak metamorphic conditions, experiencing amphibolite-grade metamorphism during and post-crystallization, resulting in elevated U/Th ratios in 14 grains. Age estimates for metamorphism occurring 111-98 Ma also overlap with accepted timing of shear zone deformation from 105-90 Ma (Giorgis et al., 2008; Braudy et al., 2016), therefore it is interpreted that post-emplacement metamorphism is the result of coeval transpressional deformation in the western Idaho shear zone.

Zr-in-Rutile Thermometry

Rutile grains were found in sample 104B from the Hazard Creek complex. U-Pb age for this sample is 116.44 ± 7.23 Ma. The age of these grains coincides with accepted emplacement and deformation ages in the Hazard Creek complex ~ 118 Ma (Manduca et al., 1993; Gray, 2013; McKay et al., 2017). Grains from sample 104B occurred as small, needle-like crystals, which is consistent with the morphology of rutile in low to medium-grade metamorphic conditions (Meinhold, 2010). Zr content was also consistent with metamorphism, ranging from 190-445 ppm with an average of 258.6 ppm (Tomkins et al., 2007; Meinhold et al., 2008). As a result, the rutile grains are interpreted to be metamorphic in origin. The rutile closure temperatures found in this study are near the proposed peak-metamorphic conditions found in the Pollock Mountain plate (McKay et al., 2017), therefore this study proposes that the Hazard Creek complex was emplaced at the time of peak metamorphism in the Pollock Mountain plate.

Apatite Thermochronology

Apatite ages and closure temperatures record the post-peak metamorphic conditions in the Salmon River suture zone and western Idaho shear zone. U-Pb ages of apatite reflect the time when the mineral cooled below the closure temperature for the U-Pb system. Closure temperature varies by grain and was calculated using equation (2).

Suture Zone. Apatite grains from above and below the Pollock Mountain fault span roughly the same ages. Below the Pollock Mountain fault, sample 21 has an average age of 96.5 Ma, while grains from above (18, 19, 114, 116) have ages ranging from 98-90 Ma. U-Pb closure temperature is lower below the fault than above, with closure temperature of 413 ± 1.5 °C below the fault, and between 465 ± 2.1 °C and 420.5 ± 1.7 °C above.

Plutonic Rocks. Apatite grains from the Hazard Creek complex are older than grains from the Little Goose Creek complex. Apatite populations in the Hazard Creek complex (101, 103B, 104A, 104B) range from 128-68 Ma, while populations from the Little Goose Creek complex (106) range from 90-64 Ma. U-Pb closure temperature is slightly higher in the Hazard Creek complex (441-422 °C), than the Little Goose Creek complex (429-431 °C).

Multi-Mineral Cooling Paths

In the Salmon River suture zone, past studies have focused on areas near the Salmon River and Pollock Mountain (Lund and Snee, 1988; McKay et al., 2017; Rankin, 2022), resulting in a gap in data for rocks in between. Previous studies by McKay et al. (2017) and Rankin (2022) concluded that exhumation in the Pollock Mountain region initiated prior to exhumation in the Salmon River. Multi-mineral cooling paths were created to determine if exhumation timing was concurrent with published estimates to the north or south, or if exhumation occurred intermediately.

To create a complete picture of cooling history in the Salmon River suture zone and western Idaho shear zones, published hornblende, biotite, and garnet ages from Lund and Snee ($^{40}\text{Ar}/^{39}\text{Ar}$ hornblende and biotite, 1988), McKay et al. (Sm-Nd garnet, 2017), Giorgis et al. ($^{40}\text{Ar}/^{39}\text{Ar}$ hornblende and biotite, 2008), and Manduca (1988) were used. The closure temperature of argon is ~580-490 °C in hornblende (Harrison, 1982) and ~345-280 for biotite (Harrison et al., 1985), making them useful for estimating post-metamorphic temperatures during cooling and exhumation. For cooling paths, a closure temperature of 550 °C was used for hornblende, and 300 °C was used for biotite.

Five locations from Lund and Snee (1988) to provide $^{40}\text{Ar}/^{39}\text{Ar}$ ages for hornblende and biotite. Multiple types of ages are reported in this study due to the behavior of argon in complex metamorphic environments. For samples with relatively simple thermal histories, argon is preserved in mineral grains and releases at the same age (Lund and Snee, 1988). These samples are reported as plateau ages. In samples with more complex thermal histories, argon can be lost at multiple stages, resulting in a spectrum of ages for one sample (Lund and Snee, 1988). These samples are reported as Ar loss ages. Samples R30 and R29 were collected from above the Pollock Mountain amphibolite fault in middle to upper amphibolite facies rocks. R30 yielded a preferred $^{40}\text{Ar}/^{39}\text{Ar}$ hornblende age of 118.0 ± 0.6 Ma, while R29 produced a plateau $^{40}\text{Ar}/^{39}\text{Ar}$ hornblende age of 108.1 ± 0.5 Ma. Samples R18, R17, and R16 were collected below the Pollock Mountain fault in the Riggins Group along the Salmon River. R18 produced a preferred $^{40}\text{Ar}/^{39}\text{Ar}$ hornblende age of 106.5 ± 1.4 Ma. R17 yielded an Ar loss age for hornblende of 107-105 Ma. R16 yielded an Ar loss age for hornblende of 100.5-93 Ma, and a plateau $^{40}\text{Ar}/^{39}\text{Ar}$ biotite age of 88.2 ± 0.5 Ma (Lund and Snee, 1988).

Three locations from McKay et al. (2017) were used to obtain Sm-Nd Garnet rim ages to constrain initiation of cooling in the Salmon River suture zone. Sample ID23 was collected from a garnet schist above the Pollock Mountain amphibolite, yielding a four-point isochron age of 125.9 ± 1.3 Ma with peak metamorphic conditions of 625-675 °C. Sample ID26 was collected from the Squaw Creek schist below the Pollock Mountain fault, producing a nine-point isochron age of 124.3 ± 5.8 Ma with peak metamorphic conditions of 600-675 °C. Sample ID48 was collected from a chlorite-biotite schist on the eastern limb of the Lake Creek antiform, producing a six-point isochron age of 112.5 ± 1.5 Ma with metamorphic conditions of 600-700 °C (McKay et al., 2017).

In the western Idaho shear zone and Hazard Creek complex, hornblende and biotite $^{40}\text{Ar}/^{39}\text{Ar}$ from Giorgis et al. (2008) and Manduca (1988) were used to create paths for the Hazard Creek and Little Goose Creek complexes. Four sample locations were chosen from Giorgis et al. (2008) for hornblende and biotite data. Sample I99-E1 was chosen from the Hazard Creek complex, and samples I96-23b, I00-245e1, and I01-5c were selected from the Little Goose Creek complex. All selections were sampled from mylonitic granodiorite gneisses except for I01-5c, which was sampled from a mesoscale shear zone mylonite. Sample I99-E1 yielded a plateau $^{40}\text{Ar}/^{39}\text{Ar}$ age of 80.4 ± 0.6 Ma for biotite. Sample I96-23b yielded an $^{40}\text{Ar}/^{39}\text{Ar}$ plateau age of 80.0 ± 0.4 Ma for hornblende. Sample I00-245e1 yielded $^{40}\text{Ar}/^{39}\text{Ar}$ plateau ages of 81.5 ± 0.3 Ma for biotite and 81.0 ± 0.4 Ma for hornblende. Sample I01-5c yielded $^{40}\text{Ar}/^{39}\text{Ar}$ plateau ages of 81.8 ± 0.6 Ma for biotite and 77.7 ± 0.5 Ma for hornblende (Giorgis et al., 2008). One sample was chosen from Manduca (1988) for $^{40}\text{Ar}/^{39}\text{Ar}$ hornblende ages of the Hazard Creek complex. The sample was collected from the Jack's Creek pluton and had a reported age of 95.1 ± 3 Ma (Manduca, 1988).

All minerals from Lund and Snee (1988), McKay et al. (2017), Giorgis et al. (2008), and Manduca (1988) were plotted along with rutile and apatite samples from this study to create a complete temperature-time path of cooling in the Salmon River suture zone and western Idaho shear zone. Cooling age estimates for apatite and rutile are based on closure temperature and Zr-in-rutile calculations.

Below Pollock Mountain Thrust Fault. Minerals in the footwall of the Pollock Mountain fault show a more prolonged initial cooling history than rocks above (Fig. 15). Cooling rate from peak metamorphism at 640 °C to 550 °C occurs at 4.4 °C/m.y., before accelerating to

17.9 °C/m.y. between 550 °C and 415 °C and 92.3 °C/m.y. between 415 °C and 300 °C. Overall cooling from 640 °C to 300 °C occurs at 9.2 °C/m.y. (Fig. 15).

Above Pollock Mountain Thrust Fault. Minerals in the hanging wall of the Pollock Mountain fault show more rapid cooling compared to rocks below (Fig. 15). Cooling rate from peak metamorphism at 650 °C to 500 °C is 5.6 °C/m.y., accelerating to 16.1 °C/m.y. between 500 °C and 425 °C. Biotite samples were not available in the area, however estimated cooling rates of 50 °C/m.y. would exist between 425 °C and 300 °C. Overall cooling from peak metamorphism to 425 °C is 9 °C/m.y. with estimated cooling from 650 °C to 300 °C of 13.4 °C/m.y. Rapid exhumation (50 °C /m.y.) of the Pollock Mountain plate is indicated to initiate around 108 Ma (Fig. 15). Initiation of rapid cooling falls in between published data from McKay et al. (2017) and Rankin (2022) of the Salmon River suture zone in the Riggins and Pollock Mountain area, supporting their theory that cooling of the Pollock Mountain plate occurred earlier to the south.

Overall trends show that the Pollock Mountain plate cooled at a faster rate than the Rapid River plate. Cooling of the Pollock Mountain plate began at ~118 Ma (Fig. 15) and is interpreted to be the date where exhumation of the plate began. The date of initial exhumation of the Pollock Mountain plate is around the same time as proposed intrusion by the Hazard Creek complex (Manduca et al., 1993; Gray, 2013; McKay et al., 2017). Cooling rates for the Rapid River plate show prolonged cooling between 650-550 °C, with accelerated rates beginning at ~95 Ma (Fig. 15). This may reflect prolonged metamorphism upon burial from movement on the Pollock Mountain thrust fault. McKay et al. (2017) proposes movement on the Rapid River fault to initiate after 113 Ma. This study agrees with exhumation likely beginning between 113 and 97 Ma. Once past the closure temperature for hornblende at 500 °C, the cooling rates for both plates

are rapid, indicating quick transport to the surface post 108 Ma in the Pollock Mountain plate and post 97 Ma in the Rapid River plate.

Plutonic Rocks. Temperature-time paths in the plutonic samples show prolonged cooling in the Hazard Creek complex and rapid cooling in the Little Goose Creek complex.

Hazard Creek complex. Minerals in the Hazard Creek complex record more prolonged cooling than the Little Goose Creek complex (Fig. 15). Cooling rates from 650 °C to 500 °C are 2.9 °C/m.y., accelerating to 10.4 °C/m.y. from 500 °C to 430 °C and 41.6 °C/m.y. between 430°C and 300 °C. Overall cooling from 650 °C to 300 °C is 6.4 °C/m.y. Rapid cooling (>40 °C/m.y.) begins at ~95 Ma, coinciding with accelerated exhumation of the Pollock Mountain plate.

Little Goose Creek complex. Minerals in the Little Goose Creek complex record rapid cooling from the onset of their emplacement ~110 Ma (Fig. 15). Cooling rate from 500 °C to 425 °C is 56.8 °C/m.y, accelerating to 178.5 °C/m.y. from 425 °C to 300 °C. Overall cooling from 500 °C to 300 °C is 62.5 °C/m.y. The rapid cooling in the Little Goose Creek complex aligns with the estimated cessation of transpressional deformation in the western Idaho shear zone at ~90 Ma (Giorgis et al., 2008).

Exhumation Model of the Salmon River Suture Zone

Using U-Pb ages and thermochronology data from apatite in this study as well as pressure-temperature data from McKay et al. (2017), a model was created to show approximate burial depths of the Pollock Mountain and Rapid River plates over time (Fig. 16). Burial depth was calculated by using equation (3) for lithostatic pressure using pressure values in garnets from McKay et al. (2017) and crustal density estimates for the Pollock Mountain amphibolite and Lightning Creek schist by Nandi (2018):

$$P = \rho gh \quad (3)$$

where P represents pressure, ρ represents the density of the material, g represents the gravitational constant, and h represents the burial depth of the material. Temperature values from the same garnets from McKay et al. (2017) were divided by obtained depth values to obtain average geothermal gradients for both units. Apatite closure temperatures from this study were divided by calculated geothermal gradients to determine their approximate burial depths at the age they passed through their closure temperature.

Metamorphism of the Pollock Mountain plate was occurring at 145-140 Ma at depths of ~24 km (Fig. 16). Zircon ages from the Hazard Creek complex indicate initial crystallization began concurrently. At 130-125 Ma, the Pollock Mountain plate was experiencing peak metamorphism at depths of ~26-27 km while the onset of Rapid River plate metamorphism had begun at depths of ~24 km (Fig. 16). Simultaneously in the western Idaho shear zone, magmatism migrates eastward (Giorgis et al., 2005). The Pollock Mountain fault began movement at ~125 Ma with the Rapid River fault at around ~113 Ma (McKay et al., 2017). At 100-90 Ma, The Pollock Mountain and Rapid River plates are passing through the closure temperature of apatite (~425 °C in this study). Currently exposed areas of the Pollock Mountain plate are still structurally higher at this point, reflecting the younger cooling path of rocks above the Pollock Mountain fault (Fig. 16). At that time, the western Idaho shear zone undergoes the last stages of transpressional deformation and shortening, with the Hazard Creek and Little Goose Creek complexes entering the phase of rapid cooling.

Lithospheric Delamination Hypothesis

Lithospheric delamination occurs during orogenesis when dense lithospheric material at depth detaches and founders into less dense asthenosphere (Kay and Mahlburg-Kay, 1993). This process is used to explain the absence of lithospheric mantle material under orogens when the processes that thicken upper crustal material should also have thickened lower crustal material as well (Li et al., 2016). Upon delamination, rapid regional isostatic uplift (100-500 °C/m.y.), erosion, thinning of crustal material, and increased magmatism occurs (Bird, 1979; Molnar et al., 1993; Garzzone et al., 2008). Lithospheric delamination has been proposed to be involved in numerous cordilleran orogens, including the Sierra Nevada (Manley et al., 200; Lang Farmer et al., 2002), the Tibetan Plateau (Molnar et al., 1993; Zhang et al., 2007), and the Andes range (Kay and Mahlburg-Kay, 1991; Garzzone et al., 2008).

Lithospheric delamination is proposed as an exhumation model in the Salmon River suture zone by Selverstone et al. (1992). They performed analysis on minerals from the Rapid River and Pollock Mountain plates, interpreting that they underwent distinct metamorphic histories. Since these units are proposed to originate from the same island arc protolith (Hamilton, 1963a; Alberti et al., 1988), any model must account for their separate burial and heating paths as well as their subsequent juxtaposition (Selverstone et al., 1992). Due to the subvertical nature of the $^{87}\text{Sr}/^{86}\text{Sr}$ isotope boundary in the area (Manduca, 1988), constraints were put in place that disallow underthrusting of arc material (Selverstone et al., 1992). The highest-grade metamorphosed parts of the Pollock Mountain plate were buried to a depth of at least ~30km, four times their current stratigraphic thickness and twice the current distance to the Sr boundary (Selverstone et al., 1992). Early studies propose the most efficient burial mechanism is the thickening and bending downward of the crust (Selverstone et al., 1992; Getty et al., 1993).

This results in a large protrusion of dense lithospheric material into the mantle at depths of over 100km (Selverstone et al., 1992). This mantle drip detached $\sim 120 \pm 5$ Ma, resulting in a period of rapid uplift in the order of >3 km/m.y. (Selverstone et al., 1992). This rapid rate of uplift is proposed due to the presence of preserved two-stage rimmed garnets in the Salmon River suture zone. Selverstone et al., (1992) argue that, based on models from Crank (1975) and Cygan and Lasaga (1985), uplift at any lesser rate would cause the zones in the garnet to assimilate and not be preserved after exhumation. Studies that infer lithospheric delamination suggest that currently exposed levels of the Rapid River and Pollock Mountain plates were juxtaposed during this period at a depth of 15-20km (Selverstone et al., 1992; Getty et al., 1993). Rapid uplift continued until $\sim 105 \pm 5$ Ma, at which point a process of slow ‘hinged’ uplift began (Selverstone et al., 1992). This process continued for ~ 50 m.y. at minimum uplift rates of 0.36km/m.y. (Selverstone et al., 1992).

In lithospheric delamination scenarios, metamorphic cooling rates range between 100 and 500 °C/m.y. (Zeck et al., 1992; Monié et al., 1994; Sánchez-Rodríguez and Gebauer, 2000). These rates are orders of magnitude higher than cooling rates that this study recorded in the Salmon River suture zone. In a lithospheric delamination environment, there would not be a significant difference in cooling rates between units above and below the Pollock Mountain fault, however cooling rates differ between these units, with cooling rates between garnet and apatite of 6.2 °C/m.y. below the Pollock Mountain fault and 9 °C/m.y. above for the same minerals (Fig. 15). Selverstone et al. (1992) argues that units in the Salmon River suture zone had to cool ~ 600 °C in less than 4 m.y. to preserve zoning in two-stage garnets, however evidence in this study suggests that cooling to ~ 600 °C lasted ~ 14 m.y. above the Pollock Mountain fault and ~ 18 m.y. below (Fig. 15). Periods of rapid exhumation in both units of the Salmon River suture zone

coincide with transpressional deformation in the western Idaho shear zone, which spanned from ~104-90 Ma (Giorgis et al., 2008).

Thrust Propagation Hypothesis

Nappe stacking in orogenic wedges is a widely studied phenomenon in accretionary orogenesis (Platt, 1986; Ratschbacher et al., 1989; Van Gool et al., 1999). Subduction-accretion complexes can be generalized as wedge-shaped complexes that alternate between compression (crustal thickening) and extension (crustal thinning) over the duration of convergence (Ratschbacher et al., 1989). If accretion grows the front of the wedge past a stable equilibrium point, internal shortening through thrusting and folding will occur to maintain a stable geometry (Platt, 1986). Nappe stacking has been proposed to occur in several accretionary orogens such as the Northern Californian Coast Ranges (Suppe, 1973), the Nagssugtoqidian Orogen in west Greenland (Van Gool et al., 1999), and the Appalachians (Benoit et al., 2014). In the central Appalachian Piedmont, Bosbyshell et al. (2016) observed a nappe stack where the highest structural nappe records the most intense metamorphic conditions, with metamorphic grade decreasing with each successive nappe.

McKay et al. (2017) propose that the observed decrease in metamorphic grade in thrust sheets from east to west as well as younging of cooling ages reflects separate uplift events as the result of a series of forward-breaking fold-thrust belts. Juxtaposition of the Rapid River and Pollock Mountain plates coincides with exhumation of the hanging wall of the Pollock Mountain fault burying and inducing metamorphism in the footwall (McKay et al., 2017). Pressure-temperature-time (P-T-t) studies of the area provide evidence for a westward younging of burial, with ~140-125 Ma peak metamorphism in the eastern packages of the Salmon River suture zone

and subsequent burial of western packages at ~125-115 Ma, coinciding with cooling to the east (McKay et al., 2017). Coupled with recent mapping of thrust sheets (Blake et al., 2009; Gray et al., 2012), they propose that metamorphism in the area was driven by forward-breaking thrust sheets progressively exhuming higher-grade terrane, heating, and burying western sheets in the process. (McKay et al., 2017).

Multi-mineral temperature-time paths of units on either side of the Pollock Mountain fault show that units in the Salmon River suture zone cooled from peak metamorphism at separate times. Temperatures in the Rapid River plate are above 550 °C at the time the Pollock Mountain plate is interpreted to cool below the closure temperature of apatite (~425 °C) (Fig. 15). This provides evidence that movement of higher-grade rocks along the Pollock Mountain fault buried units in the Rapid River plate, allowing a more prolonged period of heating. Faster exhumation in the hanging wall (9 °C/m.y.) than the footwall (6.2 °C/m.y.) from peak metamorphism to 425 °C provides evidence for thrust faulting conjoining units from different crustal depths. At sub-500 °C at around 90 Ma, the cooling rates from the Pollock Mountain and Rapid River plates seem to merge at 50 °C/m.y. and are nearly identical afterwards. This is interpreted as the time that the rocks exposed at the surface were juxtaposed via movement from the Pollock Mountain Fault. The final phases of cooling in the Salmon River suture zone conclude at around 90 Ma, which coincides with the cessation of transpressional movement in the western Idaho shear zone (Giorgis et al., 2008). In the western Idaho shear zone, cooling in the Hazard Creek complex is prolonged, while cooling does not initiate in the Little Goose Creek complex until post 90 Ma. At ~80 Ma and around 40 °C, the cooling rates of the Hazard Creek and Little Goose Creek complexes merge at ~ 150 °C/m.y., which is interpreted as the two units being transported to the surface together post-shear zone deformation.

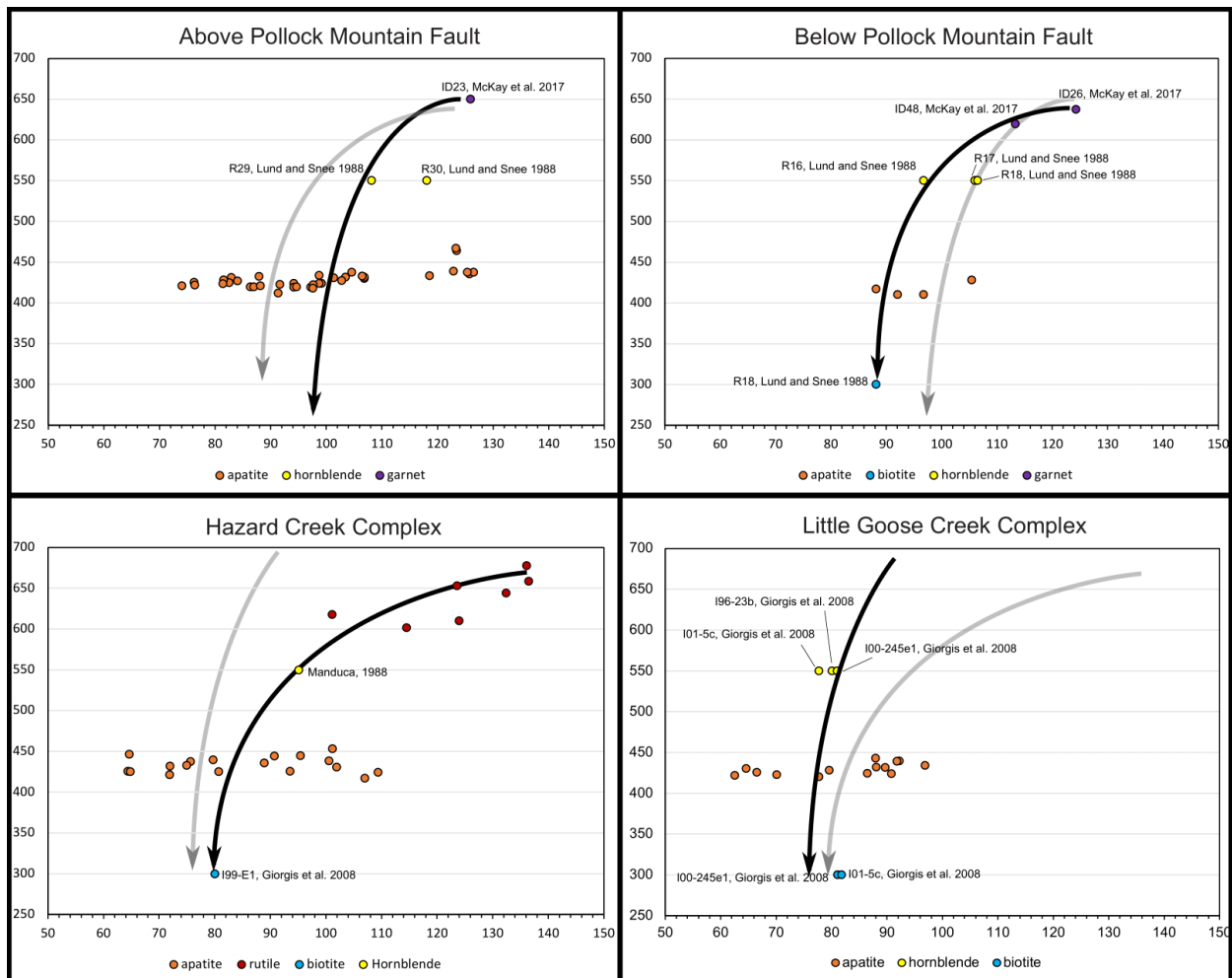


Figure 15. Temperature-time paths using: U-Pb apatite closure temperature, U-Pb rutile closure temperature, Sm-Nd garnet, $^{39}\text{Ar}/^{40}\text{Ar}$ hornblende, and $^{39}\text{Ar}/^{40}\text{Ar}$ biotite. Horizontal axis represents age in Ma and vertical axis represents closure temperature in °C. Black arrows show cooling path of the listed unit, with gray arrow showing cooling path of adjacent unit.

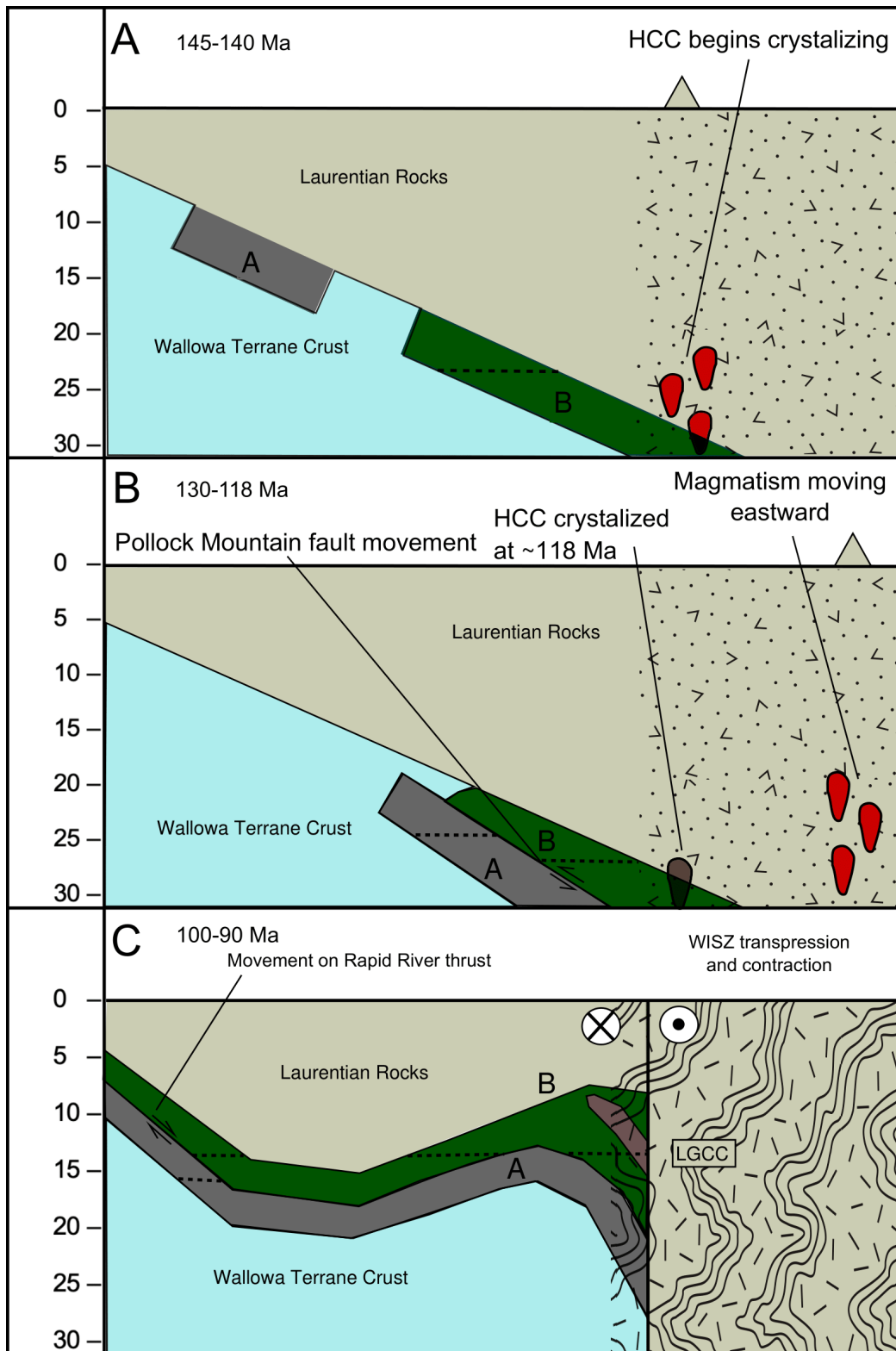


Figure 16. Generalized exhumation model of the Salmon River suture zone. Dashed line represents location of currently exposed rock based on garnet data from McKay et al. (2017) and apatite from this study.f

CONCLUSION

The Salmon River suture zone and western Idaho shear zone provide a unique window into the processes that occur during accretionary orogenesis. Oceanic arc terranes amalgamated in the late Triassic-early Jurassic before suturing onto the North American craton in the late Jurassic and early Cretaceous. Rocks exposed at the surface record burial to nearly 30 km and metamorphism ranging from greenschist to upper-amphibolite facies. U-Pb geochronology and thermochronology techniques were used on zircon, rutile, and apatite from the Salmon River suture zone between Pollock Mountain and the Salmon River, and from the Hazard Creek and Little Goose Creek complexes of the western Idaho shear zone. This information was used to create a temperature-time cooling path and estimates of burial depths. For rocks in the Salmon River suture zone, zircons yielded weighted mean ages of 138-98 Ma and apatites yielded ages of 98-90 Ma. In plutonic rocks, zircons yielded ages of 144-103 Ma, apatites yielded ages of 117-73 Ma, and rutiles yielded ages of 116 Ma. Differences in apatite ages are not distinct enough to distinguish if they decrease in a certain direction. Apatite closure temperature was calculated using the formula from Dodson (1973) and constrains temperatures to between ~410-445 °C, providing valuable information in mid-grade metamorphic conditions. Previous mineralogic studies by Lund and Snee (1988), Manduca (1988), Giorgis et al. (2008), and McKay et al. (2017) were used alongside data from this study to create a complete cooling history of the Salmon River suture zone and western Idaho shear zone. Rocks above and below the Pollock Mountain fault record different cooling histories, with rocks above cooling earlier than rocks below. Rapid cooling in all samples correlates with the cessation of transpressional deformation in the western Idaho shear zone ~90 Ma. Cooling rates are significantly less in the

Salmon River suture zone than is required to fit the lithospheric delamination model, while temperature-time models are compatible with the thrust propagation model. Whole rock exhumation from garnet to apatite is faster in the Pollock Mountain plate (9 °C/m.y.) than the Rapid River plate (6.2 °C/m.y.). Slower cooling occurs in the Hazard Creek complex (6.4 °C/m.y.) compared to more rapid cooling in the Little Goose Creek complex (18 °C/m.y.). Overall trends show the cooling histories of the Pollock Mountain and Rapid River plates merging at ~90 Ma once rocks are below 500 °C, indicating their juxtaposition and simultaneous transport to the surface. In the western Idaho shear zone, cooling histories for the Hazard Creek and Little Goose Creek complexes merge at ~80 Ma below 400 °C, reflecting their uplift and exhumation after deformation in the shear zone ceases.

REFERENCES

- Aliberti, E. A., 1988, A structural, petrographic, and isotopic study of the Rapid River area and selected mafic complexes in the northwestern United States: Implications for the evolution of an abrupt island arc-continent boundary [Ph.D. thesis], 194 pp., Harvard University.
- Armstrong, R.L., Taubeneck, W.H., and Hales, P.O., 1977, Rb-Sr and K-Ar geochronometry of Mesozoic granitic rocks and their Sr isotopic composition, Oregon, Washington, and Idaho: Geological Society of America Bulletin, v. 88, p. 397.
- Avé Lallemant, H.G., Phelps, D.W., and Sutter, J.F., 1980, ^{40}Ar - ^{39}Ar ages of some pre-Tertiary plutonic and metamorphic rocks of eastern Oregon and their geologic relationships: Geology, v. 8, p. 371.
- Axelsson, E., Pape, J., Berndt, J., Corfu, F., Mezger, K., and Raith, M.M., 2018, Rutile R632 - a new natural reference material for U-Pb and zirconium determination: Geostandards and Geoanalytical Research, v. 42, p. 319–338, doi: 10.1111/ggr.12213.
- Benoit, M.H., Ebinger, C., and Crampton, M., 2014, Orogenic bending around a rigid Proterozoic magmatic rift beneath the Central Appalachian Mountains: Earth and Planetary Science Letters, v. 402, p. 197–208, doi: 10.1016/j.epsl.2014.03.064.
- Bird, P., 1979, Continental delamination and the Colorado Plateau: Journal of Geophysical Research: Solid Earth, v. 84, p. 7561–7571, doi: 10.1029/jb084ib13p07561.
- Bishop, E.M., 1995, High-pressure, low-temperature schistose rocks of the Baker terrane, northeastern Oregon, in Vallier, T.L., and Brooks, H.C., eds., Geology of the Blue Mountains region of Oregon, Idaho, and Washington: U.S. Geological Survey Professional Paper 1438, p. 211-219.
- Blake, D.E., Gray, K.D., Giorgis, S., and Tikoff, B., 2009, A tectonic transect through the Salmon River suture zone along the Salmon River Canyon in the Riggins region of west-central Idaho, *in* Volcanoes to Vineyards: Geologic Field Trips through the Dynamic Landscape of the Pacific Northwest, Geological Society of America, p. 345–372.
- Blake, D.E., Bruce, M.L., and Reed, D.N., 2016, Geologic Map of the Riggins Hot Springs Quadrangle and Adjacent Areas, Idaho County, Idaho: Idaho Geological Survey, scale 1:24,000.
- Bollen, E.M., 2015, Explaining discontinuous garnet zoning using reaction history P-T models: An example from the Salmon River Suture Zone, west-central Idaho [M.S.thesis]: p. 35-55. University of Alabama.

- Bracciali, L., Parrish, R.R., Horstwood, M.S.A., Condon, D.J., and Najman, Y., 2013, UPB La-(MC)-ICP-MS dating of rutile: New reference materials and applications to sedimentary provenance: *Chemical Geology*, v. 347, p. 82–101, doi: 10.1016/j.chemgeo.2013.03.013.
- Braudy, N., Gaschnig, R.M., Wilford, D., Vervoort, J.D., Nelson, C.L., Davidson, C., Kahn, M.J., and Tikoff, B., 2016, Timing and deformation conditions of the western Idaho Shear Zone, West Mountain, west-central Idaho: *Lithosphere*, v. 9, p. 157–183, doi: 10.1130/1519.1.
- Brooks, H.C., and Vallier, T.L., 1978, Mesozoic rocks and tectonic evolution of eastern Oregon and western Idaho: *Pacific Coast Paleogeography Symposium*, p. 133- 145.
- Burke, K., Ashwal, L.D., and Webb, S.J., 2003, New way to map old sutures using deformed alkaline rocks and carbonatites: *Geology*, v. 31, p. 391, doi: 10.1130/0091-7613(2003)031<0391:nwtmos>2.0.co;2.
- Cherniak, D.J., 1991, Lead diffusion in apatite and zircon using ion implantation and Rutherford backscattering techniques: *Geochemica et Cosmochimica Acta*, v. 55, p. 1663-1673.
- Chew, D.M., Petrus, J.A., and Kamber, B.S., 2014. U–Pb LA–ICPMS dating using accessory mineral standards with variable common Pb: *Chemical Geology*, v. 363, p. 185-199.
- Chew, D.M., Babechuk, M.G., Cogné, N., Mark, C., O'Sullivan, G.J., Henrichs, I.A., Doepke, D., and McKenna, C.A., 2016, (La,Q)-ICPMS trace-element analyses of Durango and McClure mountain apatite and implications for making natural La-ICPMS mineral standards: *Chemical Geology*, v. 435, p. 35–48, doi: 10.1016/j.chemgeo.2016.03.028.
- Chew, D.M., and Spikings, R.A., 2021, Apatite U-PB thermochronology: A Review: *Minerals*, v. 11, p. 1095, doi: 10.3390/min11101095.
- Cochrane, R., Spikings, R.A., Chew, D., Wotzlaw, J.-F., Chiaradia, M., Tyrrell, S., Schaltegger, U., and Van der Lelij, R., 2014, High temperature (>350°C) thermochronology and mechanisms of Pb loss in apatite: *Geochimica et Cosmochimica Acta*, v. 127, p. 39–56, doi: 10.1016/j.gca.2013.11.028.
- Cowan, D.S., 1985, Structural styles in Mesozoic and Cenozoic mélanges in the western Cordillera of North America: *Geological Society of America Bulletin*, v. 96, p. 451–462, doi: 10.1130/0016-7606(1985)96<451:SSIMAC>2.0.CO;2.
- Crank, J., 1975, *The Mathematics of Diffusion*: Oxford University Press, New York.
- Criss, R.E., and Fleck, R.J., 1987, Petrogenesis, geochronology and hydrothermal systems of the northern Idaho batholith and adjacent areas based on $^{18}\text{O}/^{16}\text{O}$, D/H, $^{87}\text{Sr}/^{86}\text{Sr}$, K-Ar and $^{40}\text{Ar}/^{39}\text{Ar}$ studies: *U.S Geological Survey Professional Paper*, 1436, p. 95-137.
- Cygan, R.T., and Lasaga, A.C., 1985, Self-diffusion of magnesium in garnet at 750 degrees to 900 degrees C: *American Journal of Science*, v. 285, p. 328–350, doi: 10.2475/ajs.285.4.328.

- Davis, G.A., Monger, J.W.H., and Burchfiel, B.C., 1978, Mesozoic construction of Cordilleran “collage”, central British Columbia to Central California: AAPG Bulletin, v. 62, doi: 10.1306/c1ea5431-16c9-11d7-8645000102c1865d.
- DeCelles, P.G., Ducea, M.N., Kapp, P., and Zandt, G., 2009, Cyclicity in Cordilleran Orogenic Systems: Nature Geoscience, v. 2, p. 251–257, doi: 10.1038/ngeo469.
- DeYoung, S.G., 2019, Geologic mapping and geochronology of the Heavens Gate 7.5-minute quadrangle: How long does it take to accrete an island arc to a continent? [M.S. thesis]: p. 16-18. Missouri State University.
- Dickinson, W. R., Helmold, K. P., and Stein, J. A., 1979, Mesozoic lithic sandstones in central Oregon: Journal of Sedimentary Petrology, v. 49, p. 501–516.
- Dickinson, W.R., 2004, Evolution of the North American cordillera: Annual Review of Earth and Planetary Sciences, v. 32, p. 13–45.
- DiPietro, J.A., 2013, Keys to the interpretation of geological history: Landscape Evolution in the United States, p. 327–344, doi: 10.1016/b978-0-12-397799-1.00020-8.
- Dodson, M.H., 1973, Closure temperature in cooling geochronological and Petrological Systems: Contributions to Mineralogy and Petrology, v. 40, p. 259–274, doi: 10.1007/bf00373790.
- Dorsey, R.J., and LaMaskin, T.A., 2007, Stratigraphic record of Triassic-Jurassic collisional tectonics in the Blue Mountains Province, Northeastern Oregon: American Journal of Science, v. 307, p. 1167–1193, doi: 10.2475/10.2007.03.
- Fleck, R.J., and Criss, R.E., 1985, Strontium and oxygen isotopic variations in Mesozoic and Tertiary plutons of central Idaho: Contributions to Mineralogy and Petrology, v. 90, p. 291-308.
- Fleck, R.J., and Criss, R.E., 2004, Location, age, and tectonic significance of the western Idaho Suture Zone (WISZ): U.S. Geological Survey Professional Paper 1738, p. 15-50.
- Gärtner, A., Linnemann, U., Sagawe, A., Hofmann, M., Ullrich, B., and Kleber, A., 2015, Morphology of zircon crystal grains in sediments – characteristics, classifications, definitions: Journal of Central European Geology, v. 59, p. 65–73.
- Garzzone, C.N., Hoke, G.D., Libarkin, J.C., Withers, S., MacFadden, B., Eiler, J., Ghosh, P., and Mulch, A., 2008, Rise of the Andes: Science, v. 320, p. 1304–1307, doi: 10.1126/science.1148615.
- Getty, S.R., Selverstone, J., Wernicke, B.P., Jacobsen, S.B., Aliberti, E., and Lux, D.R., 1993, Sm-Nd dating of multiple garnet growth events in an arc-continent collision zone, northwestern U.S. Cordillera: Contributions to Mineralogy and Petrology. Beitrage zur Mineralogie und Petrologie, v. 115, p. 45–57.

- Giorgis, S., Tikoff, B., and McClelland, W., 2005, Missing Idaho arc: Transpressional modification of the $87\text{Sr}/86\text{Sr}$ transition on the western edge of the Idaho Batholith: *Geology*, v. 33, p. 469, doi: 10.1130/g20911.1.
- Giorgis, S., McClelland, W., Fayon, A., Singer, B.S., and Tikoff, B., 2008, Timing of deformation and exhumation in the western Idaho shear zone, McCall, Idaho: *Geological Society of America bulletin*, v. 120, p. 1119–1133.
- Gray, K.D., and Oldow, J.S., 2005, Contrasting structural histories of the Salmon River Belt and Wallowa Terrane: Implications for terrane accretion in northeastern Oregon and west-central Idaho: *Geological Society of America Bulletin*, v. 117, p. 687, doi: 10.1130/b25411.1.
- Gray, K.D., Watkinson, A.J., Gaschnig, R.M., and Isakson, V.H., 2012, Age and structure of the crevice pluton: Overlapping orogens in west-central Idaho?: *Canadian Journal of Earth Sciences*, v. 49, p. 709–731, doi: 10.1139/e2012-016.
- Gray, K.D., 2013, Structure of the arc-continent transition in the Riggins region of west-central Idaho [Ph.D. Thesis]: p. 18-102, Washington State University, Pullman.
- Goldstrand, P.M., 1994, The Mesozoic geologic evolution of the northern Wallowa Terrane, Northeastern Oregon and Western Idaho: US Geological Survey professional paper, 1439.
- Hamilton, W., 1963a, Overlapping of late Mesozoic orogens in Western Idaho: *Geological Society of America Bulletin*, v. 74, p. 779, doi: 10.1130/0016-7606(1963)74[779:oolmoi]2.0.co;2.
- Hamilton, W., 1963b, Metamorphism in the Riggins region Western Idaho: *Geological Survey Professional Paper* 436.
- Hamilton, W., 1969, Reconnaissance geologic map of the Riggins quadrangle, west-central Idaho: U.S. Geological Survey Miscellaneous Geologic Investigations Map I-579, scale 1:125,000.
- Harrison, J.E., and Jobin, D.A., 1963, Geology of the Clark Fork Quadrangle, Idaho-Montana: *Geological Survey Bulletin* 1141-k, p. K26, doi: 10.3133/b1141k.
- Harrison, T.M., 1982, Diffusion of 40Ar in hornblende: *Contributions to Mineralogy and Petrology*, v. 78, p. 324–331, doi: 10.1007/bf00398927.
- Harrison, T.M., Duncan, I., and McDougall, I., 1985, Diffusion of 40Ar in biotite: Temperature, pressure and compositional effects: *Geochimica et Cosmochimica Acta*, v. 49, p. 2461–2468, doi: 10.1016/0016-7037(85)90246-7.
- Hillhouse, J.W., Grommé, C.S., and Vallier, T.L., 1982, Paleomagnetism and Mesozoic tectonics of the Seven Devils Volcanic Arc in northeastern Oregon: *Journal of Geophysical Research*, v. 87, p. 3777, doi: 10.1029/jb087ib05p03777.

- Kay, R.W., and Mahlburg-Kay, S., 1991, Creation and destruction of lower continental crust: *Geologische Rundschau*, v. 80, p. 259–278, doi: 10.1007/bf01829365.
- Kay, R.W., and Mahlburg Kay, S., 1993, Delamination and delamination magmatism: *Tectonophysics*, v. 219, p. 177–189, doi: 10.1016/0040-1951(93)90295-u.
- Kirkland, C.L., Smithies, R.H., Taylor, R.J.M., Evans, N., and McDonald, B., 2015, Zircon U/Th ratios in magmatic environs: *Lithos*, v. 212-215, p. 397–414, doi: 10.1016/j.lithos.2014.11.021.
- Kirkland, C.L., Yakymchuk, C., Szilas, K., Evans, N., Hollis, J., McDonald, B., and Gardiner, N.J., 2018, Apatite: A U-Pb thermochronometer or geochronometer?: *Lithos*, v. 318-319, p. 143–157, doi: 10.1016/j.lithos.2018.08.007.
- Kooijman, E., Mezger, K., and Berndt, J., 2010, Constraints on the U–Pb systematics of metamorphic rutile from in situ *la*-ICP-MS analysis: *Earth and Planetary Science Letters*, v. 293, p. 321–330, doi: 10.1016/j.epsl.2010.02.047.
- Kotowski, J., Nejbert, K., and Olszewska-Nejbert, D., 2021, Rutile mineral chemistry and zircon-in-rutile thermometry in provenance study of Albian (uppermost Lower cretaceous) terrigenous quartz sands and sandstones in southern Extra-Carpathian Poland: *Minerals*, v. 11, p. 553, doi: 10.3390/min11060553.
- Kuntz, M.A., 2007, The Idaho Batholith near McCall, Idaho—Field Relations, Petrology, Major-Element Chemistry, Emplacement History, and Magma Genesis: USGS Professional Paper 1738.
- Kuntz, M.A., and Snee, L.W., 2007, Introduction to Geological Studies of the Salmon River Suture Zone and Adjoining Areas, West-Central Idaho and Eastern Oregon: U.S. Geological Survey Professional Paper 1738, p. 1-14.
- Kurz, G.A., Schmitz, M.D., Northrup, C.J., and Vallier, T.L., 2012, U-Pb geochronology and geochemistry of intrusive rocks from the Cougar Creek Complex, Wallowa arc terrane, Blue Mountains Province, Oregon-Idaho: *Geological Society of America Bulletin*, v. 124, p. 578–595, doi:10.1130/B30452.1.
- LaMaskin, T.A., Vervoort, J.D., Dorsey, R.J., and Wright, J.E., 2011, Early Mesozoic paleogeography and tectonic evolution of the Western United States: Insights from detrital zircon U-Pb geochronology, Blue Mountains Province, Northeastern Oregon: *Geological Society of America Bulletin*, v. 123, p. 1939–1965, doi: 10.1130/b30260.1.
- Lang Farmer, G., Glazner, A.F., and Manley, C.R., 2002, Did lithospheric delamination trigger late cenozoic potassic volcanism in the Southern Sierra Nevada, California?: *Geological Society of America Bulletin*, v. 114, p. 754–768, doi: 10.1130/0016-7606(2002)114<0754:dldtlc>2.0.co;2.

- Li, Z., Liu, M., and Gerya, T., 2016, Lithosphere delamination in continental collisional orogens: A systematic numerical study: *Journal of Geophysical Research: Solid Earth*, v. 121, p.5186-5211.
- Li, Q.-li, Lin, W., Su, W., Li, X.-hua, Shi, Y.-hong, Liu, Y., and Tang, G.-qiang, 2011, Sm-U-Pb rutile age of low-temperature eclogites from southwestern Chinese Tianshan, NW China: *Lithos*, v. 122, p. 76–86, doi: 10.1016/j.lithos.2010.11.007.
- Long, S.P., Barba, W.K., McKay, M.P., and Soignard, E., 2023, Thermal architecture of the Salmon River Suture Zone, Idaho, USA: Implications for the structural evolution of a ductile accretionary complex during arc-continent collision: *Geosphere*, v. 19, p. 1103–1127, doi: 10.1130/ges02621.1.
- Lund, K., 2004, Geology of the Payette National Forest and vicinity, west-central Idaho (ver. 1.1, April 2021): U.S. Geological Survey Professional Paper 1666–A, 89 p., doi: 10.3133/pp1666.
- Lund, K., and Snee, L.W. 1988. Metamorphism, structural development, and age of the continent — island arc juncture in west-central Idaho. *In* *Metamorphism and crustal evolution of the western United States. Edited by G. Ernst.* Prentice Hall, Englewood Cliffs, N.J., Rubey, pp. 296–331
- Lund, K., Aleinikoff, J.N., Yacob, E.Y., Unruh, D.M., and Fanning, C.M., 2008, Coolwater culmination: Sensitive high-resolution ion microprobe (SHRIMP) U-Pb and isotopic evidence for continental delamination in the Syringa Embayment, Salmon River suture, Idaho: *Tectonics*, v. 27, doi:10.1029/2006tc002071.
- Manduca, C.A., 1988, Geology and geochemistry of the Oceanic Arc-continent boundary in the western Idaho Batholith near McCall [PhD thesis]: p. 106-132, California Institute of Technology.
- Manduca, C.A., Kuntz, M.A., and Silver, L.T., 1993, Emplacement and deformation history of the western margin of the Idaho batholith near McCall, Idaho: Influence of a major terrane boundary: *Geological Society of America Bulletin*, v. 105, p. 749.
- Manley, C.R., Glazner, A.F., and Farmer, G.L., 2000, Timing of volcanism in the Sierra Nevada of California: Evidence for Pliocene delamination of the Batholithic Root?: *Geology*, v. 28, p. 811–814, doi: 10.1130/0091-7613(2000)028<0811:tovits>2.3.co;2.
- McClelland, W.C., Tikoff, B., and Manduca, C.A., 2000, Two-phase evolution of accretionary margins: examples from the North American Cordillera: *Tectonophysics*, v. 326, p. 37–55.
- McKay, M.P., 2011, Pressure-temperature-time paths, prograde garnet growth, and protolith of Tectonites from a polydeformational, polymetamorphic terrane: Salmon River Suture Zone, west-central Idaho [M.S. thesis]: p. 1-106, University of Alabama.

- McKay, M.P., Bollen, E.M., Gray, K.D., Stowell, H.H., and Schwartz, J.J., 2017, Prolonged metamorphism during long-lived terrane accretion: Sm-Nd garnet and U-Pb zircon geochronology and pressure-temperature paths from the Salmon River suture zone, west-central Idaho, USA: *Lithosphere*, v. 9, p. 683–701.
- McKay, M. P., Jackson, W.T., and Hessler, A.M., 2018, Tectonic stress regime recorded by zircon U/Th: *Gondwana Research*, v. 7, p. 1-9.
- Meinhold, G., 2010, Rutile and its applications in Earth sciences: *Earth-Science Reviews*, v. 102, p. 1–28, doi: 10.1016/j.earscirev.2010.06.001.
- Meinhold, G., Anders, B., Kostopoulos, D., and Reischmann, T., 2008, Rutile chemistry and thermometry as provenance indicator: An example from Chios Island, Greece: *Sedimentary Geology*, v. 203, p. 98–111, doi: 10.1016/j.sedgeo.2007.11.004.
- Molnar, P., England, P., and Martinod, J., 1993, Mantle dynamics, uplift of the Tibetan Plateau, and the Indian Monsoon: *Reviews of Geophysics*, v. 31, p. 357, doi: 10.1029/93rg02030.
- Monié, P., Torres-Roldán, R.L., and García-Casco, A., 1994, Cooling and exhumation of the western Betic Cordilleras, 40Ar/39AR thermochronological constraints on a collapsed terrane: *Tectonophysics*, v. 238, p. 353–379, doi: 10.1016/0040-1951(94)90064-7.
- Nandi, S.K., 2018, Geology of the purgatory saddle 7.5 minute quadrangle, and gravity and magnetic analysis of accreted terrane boundary, Western Idaho [M.S. thesis]: p. 42-72. Missouri State Univesity.
- Northrup, C.J., Schmitz, M., Kurz, G., and Tumpane, K., 2011, Geologic Field Trips to the Basin and Range, Rocky Mountains, Snake River Plain, and Terranes of the U.S. Cordillera, p. 67–88, doi: 10.1130/2011.0021(03).
- Paton, C., Woodhead, J., Hellstrom, J., Hergt, J., Greig, A. and Maas, R. 2010, Improved laser ablation U-Pb zircon geochronology through robust down-hole fractionation correction. *G Cubed*, v. 11, doi:10.1029/2009GC002618.
- Paton, C., Hellstrom, J., Paul, B., Woodhead, J. and Hergt, J., 2011. Iolite: Freeware for the visualisation and processing of mass spectrometric data. *Journal of Analytical Atomic Spectrometry*. doi:10.1039/c1ja10172b.
- Petrus, J.A. and Kamber, B.S. (2012) VizualAge: A novel approach to laser ablation ICP-MS U-Pb geochronology data reduction: *Geostandards and Geoanalytical Research*, v. 36(3), p. 247-270.
- Platt, J.P., 1986, Dynamics of orogenic wedges and the uplift of high-pressure metamorphic rocks: *Geological Society of America Bulletin*, v. 97, p. 1037, doi: 10.1130/0016-7606(1986)97<1037:doowat>2.0.co;2.
- Press, F., and Siever, R., 1998, *in Earth*, New York, NY, Freeman, p. 534–535.

- Rankin, C.G., 2022, U-Pb Apatite Chronometry of Intrusions in an Accretionary Metamorphic Belt in Western Idaho, USA [M.S. thesis]: p. 3-71, Missouri State University.
- Ratschbacher, L., Frisch, W., Neubauer, F., Schmid, S.M., and Neugebauer, J., 1989, Extension in compressional orogenic belts: The eastern Alps: *Geology*, v. 17, p. 404, doi: 10.1130/0091-7613(1989)017<0404:eicobt>2.3.co;2.
- Sánchez-Rodríguez Lourdes, and Gebauer, D., 2000, Mesozoic formation of pyroxenites and Gabbros in the Ronda area (southern Spain), followed by early miocene subduction metamorphism and emplacement into the middle crust: U–PB sensitive high-resolution ion microprobe dating of Zircon: *Tectonophysics*, v. 316, p. 19–44, doi: 10.1016/s0040-1951(99)00256-5.
- Schmidt, K.L., Schwartz, D.M., Lewis, R.S., Vervoort, J.D., LaMaskin, T.A., and Wilford, D.E., 2013, New detrital zircon ages constrain the origin and evolution of the Riggins Group assemblage along the Salmon River suture zone, western Idaho: Presented to GSA cordilleran section - 109th annual meeting.
- Schmidt, K.L., Gray, K.D., Lewis, R.S., Steven, C.J., and Isakson, V.H., 2016, Mesozoic tectonics west of the accretionary boundary in west-central Idaho: *Exploring the Geology of the Inland Northwest*, p. 175–209, doi: 10.1130/2016.0041(06).
- Schwartz, J.J., Snoke, A.W., Frost, C.D., Barnes, C.G., Gromet, L.P., and Johnson, K., 2009, Analysis of the Wallowa-Baker terrane boundary: Implications for tectonic accretion in the Blue Mountains Province, Northeastern Oregon: *Geological Society of America Bulletin*, v. 122, p. 517–536, doi: 10.1130/b26493.1.
- Schwartz, J.J., Snoke, A.W., Cordley, F., Johnson, K., Frost, C.D., Barnes, C.G., LaMaskin, T.A., and Wooden, J.L., 2011, Late Jurassic magmatism, metamorphism, and deformation in the Blue Mountains Province, northeastern Oregon: *Geological Society of America Bulletin*, v. 123, p. 2083–2111, doi:10.1130/B30327.1.
- Schwartz, T.M., Surpless, K.D., Colgan, J.P., Johnstone, S.A., and Holm-Denoma, C.S., 2021, Detrital zircon record of magmatism and sediment dispersal across the North American Cordilleran Arc System (28–48°N): *Earth-Science Reviews*, v. 220, p. 103734, doi: 10.1016/j.earscirev.2021.103734.
- Selverstone, J., Wernicke, B.P., and Aliberti, E.A., 1992, Intracontinental subduction and hinged unroofing along the Salmon River Suture Zone, west central Idaho: *Tectonics*, v. 11, p. 124–144.
- Sláma, J., Košler, J., Condon, D.J., Crowley, J.L., Gerdes, A., Hanchar, J.M., Horstwood, M.S.A., Morris, G.A., Nasdala, L., Norberg, N., Schaltegger, U., Schoene, B., Tubrett, M.N., and Whitehouse, M.J., 2008, Plešovice zircon — a new natural reference material for U–Pb and HF isotopic microanalysis: *Chemical Geology*, v. 249, p. 1–35, doi: 10.1016/j.chemgeo.2007.11.005.

- Smye, A.J., Marsh, J.H., Vermeesch, P., Garber, J.M., and Stockli, D.F., 2018, Applications and limitations of U-Pb thermochronology to middle and lower crustal thermal histories: *Chemical geology*, v. 494, p. 1–18.
- Soreghan, M.J., Gehrels, G.E., and Dickinson, W.R., 2000, Geodynamic interpretation of Paleozoic tectonic trends oriented oblique to the Mesozoic Klamath-Sierran continental margin in California: Paleozoic and Triassic paleogeography and tectonics of western Nevada and Northern California, *in* Paleozoic and Triassic paleogeography and tectonics of Western Nevada and Northern California, Boulder, Colorado, Geological Society of America, p. 209–246, doi: 10.1130/0-8137-2347-7.209.
- Strong, T.R., and Driscoll, R.L., 2016, A process for reducing rocks and concentrating heavy minerals: U.S. Geological Survey Open-file Report 2016-1022, p. 1-16.
- Suppe, J., 1973, Geology of the leech lake mountain--ball mountain region, California: A cross section of the northeastern Franciscan Belt and its tectonic implications: Berkeley, California, University of California Press.
- Tikoff, B., Kelso, P., Manduca, C., Markley, M.J., and Gillaspy, J., 2001, Lithospheric and crustal reactivation of an ancient plate boundary: the assembly and disassembly of the Salmon River suture zone, Idaho, USA, *in* Holdsworth, R.E., Strachan, R.A., Magloughin, J.F., and Knipe, R.J., eds., *The Nature and Tectonic Significance of Fault Zone Weakening*: Geological Society of London, Special Publications, no. 186, p. 213- 231.
- Tomkins, H.S., Powell, R., and Ellis, D.J., 2007, The pressure dependence of the zirconium-in-rutile thermometer: *Journal of Metamorphic Geology*, v. 25, p. 703–713, doi: 10.1111/j.1525-1314.2007.00724.x.
- Trop, J.M., Benowitz, J., Cole, R.B., and O’Sullivan, P., 2019, Cretaceous to Miocene magmatism, sedimentation, and exhumation within the Alaska Range Suture Zone: A polyphase reactivated terrane boundary: *Geosphere*, v. 15, p. 1066–1101, doi: 10.1130/ges02014.1.
- Usuki, T., Iizuka, Y., Hirajima, T., Svojtka, M., Lee, H.-Y., and Jahn, B.-M., 2017, Significance of zr-in-rutile thermometry for deducing the decompression P–T path of a garnet–clinopyroxene granulite in the Moldanubian Zone of the Bohemian Massif: *Journal of Petrology*, v. 58, p. 1173–1198, doi: 10.1093/petrology/egx050.
- Vallier, T.L., 1977, The Permian and Triassic Seven Devils Group, western Idaho and northeastern Oregon: U.S., Geological Survey Bulletin 1437, p. 1-58.
- Vallier, T.L., and Batiza, R., 1978, Petrogenesis of spilite and keratophyre from a Permian and Triassic volcanic arc terrane, eastern Oregon and western Idaho, U.S.: *Canadian Journal of Earth Sciences*, v. 15, p. 1356–1369.
- Vallier, T.L., and Brooks, H.C., 1986, Geology of the Blue Mountains region of Oregon, Idaho, and Washington: Geologic implications of Paleozoic and Mesozoic paleontology and

- biostratigraphy, Blue Mountains Province, Oregon and Idaho: U.S. Geological Survey Professional Paper 1435.
- Vallier, T.L., 1995, Petrology of pre-Tertiary igneous rocks in the Blue Mountains region of Oregon, Idaho, and Washington: Implications for the geologic evolution of a complex island arc, in Vallier, T.L., and Brooks, H.C., eds., *Geology of the Blue Mountains region of Oregon, Idaho, and Washington*: U.S. Geological Survey Professional Paper 1438, p. 125-209.
- Vallier, T.L., 1998, *Islands & rapids: A geologic story of Hells Canyon*: Lewiston, Idaho, Confluence Press, 168 p.
- Van Gool, J.A.M., Kriegsman, L.M., Marker, M., and Nichols, G.T., 1999, Thrust stacking in the inner Nordre Strømfjord area, West Greenland significance for the tectonic evolution of the Palaeoproterozoic Nagssugtoqidian Orogen: *Precambrian Research*, v. 93, p. 71–86, doi: 10.1016/s0301-9268(98)00098-9.
- Vermeesch, P., 2018, IsoplotR: a free and open toolbox for geochronology. *Geoscience Frontiers*, v. 9, p.1479-1493, doi:10.1016/j.gsf.2018.04.001.
- Ware, B., Tumpane, K.P., Kurz, G.A., Schmitz, M.D., and Northrup, C.J., 2022, Geochronology and geochemistry of the Huntington Formation, Olds Ferry Terrane, Blue Mountains Province, northern U.S. cordillera: Implications for accreted Terrane Correlation and assembly: *Geological Society of America Bulletin*, doi: 10.1130/b36036.1.
- Watson, E.B., Wark, D.A., and Thomas, J.B., 2006, Crystallization thermometers for zircon and rutile: Contributions to mineralogy and petrology. *Beitrage zur Mineralogie und Petrologie*, v. 151, p. 413–433.
- Wilford, D.E., and Vervoort, J.D., 2012, Lu-Hf garnet geochronology of the Salmon River Suture Zone, west-central Idaho [M.S. thesis]: p 66-77, Washington State University.
- Willett, S.D., and Brandon, M.T., 2002, On steady states in mountain belts: *Geology*, v. 30, p. 175.
- Yakymchuk, C., Kirkland, C., and Clark, C., 2018, U/Th ratios in metamorphic zircon: *Journal of Metamorphic Geology*, v. 36, p. 715-737, doi:10.1111/jmg.12307.
- Yonkee, W.A., and Weil, A.B., 2015, Tectonic evolution of the Sevier and Laramide belts within the North American Cordillera Orogenic System: *Earth-Science Reviews*, v. 150, p. 531–593, doi: 10.1016/j.earscirev.2015.08.001.
- Zack, T., Moraes, R., and Kronz, A., 2004, Temperature dependence of Zr in rutile: Empirical calibration of a rutile thermometer: *Contributions to Mineralogy and Petrology*, v. 148, p. 471–488, doi: 10.1007/s00410-004-0617-8.

- Žák, J., Verner, K., Johnson, K., and Schwartz, J.J., 2012, Magma emplacement process zone preserved in the roof of a large Cordilleran batholith, Wallowa Mountains, northeastern Oregon: *Journal of Volcanology and Geothermal Research*, v. 227-228, p. 61–75, doi: 10.1016/j.jvolgeores.2012.03.001.
- Zak, J., Verner, K., Tomek, F., Holub, F.V., Johnson, K., and Schwartz, J.J., 2015, Simultaneous batholith emplacement, terrane/continent collision, and oroclinal bending in the Blue Mountains Province, North American Cordillera: *Tectonics*, v. 34, p. 1107-1128.
- Zeck, H.P., Monié, P., Villa, I.M., and Hansen, B.T., 1992, Very high rates of cooling and uplift in the Alpine Belt of the Betic Cordilleras, Southern Spain: *Geology*, v. 20, p. 79, doi: 10.1130/0091-7613(1992)020<0079:vhroca>2.3.co;2.
- Zen, E.-an, 1985, Implications of magmatic epidote-bearing plutons on crystal evolution in the accreted terranes of Northwestern North America: *Geology*, v. 13, p. 266, doi: 10.1130/0091-7613(1985)13<266:iomepo>2.0.co;2.
- Zen, E.-an, and Hammarstrom, J.M., 1984, Magmatic epidote and its petrologic significance: *Geology*, v. 12, p. 515, doi: 10.1130/0091-7613(1984)12<515:meaips>2.0.co;2.
- Zhang, H.-F., Parrish, R., Zhang, L., Xu, W.-C., Yuan, H.-L., Gao, S., and Crowley, Q.G., 2007, A-type granite and Adakitic Magmatism Association in Songpan–Garze Fold Belt, eastern Tibetan Plateau: Implication for lithospheric delamination: *Lithos*, v. 97, p. 323–335, doi: 10.1016/j.lithos.2007.01.002.

APPENDICES

Appendix A. UTM coordinates (Zone 11T) of samples used in this study. Datum used is WGS 84.

Sample ID	Easting	Northing
SPJCOR18	550149	5014928
SP19	549920	5015249
21	548469	5016290
22	548466	5016443
101	556513	5003728
103B	556450	5003204
104A	556771	5002628
104B	557045	5002369
106	565165	4996464
107	567069	5004435
114	551671	5012819
116	551353	5014493
ID23	546401	5008963
ID26	551980	5028503
ID48	562366	5028290
R16	557366	5029728
R17	556402	5030010
R18	555667	5030056

Appendix A Continued: UTM Coordinates of Samples

Sample ID	Easting	Northing
R29	555614	5000227
R30	551620	5014258
I99-E1	562523	4978723
I96-23b	565401	4998812
I01-5c	567305	4996870
I00-245e1	567127	5004428

Appendix B. U-Pb Zircon Ages

Sample Name	Source File	Final Pb206/U238 age (Ma)	± (Ma)	Final Pb206/U238 age (207Pb corr) (Ma)	± (Ma)	U/Th ratio	±
104A	21IDJC104A.ZR.03	121.29	12.14	-	-	8.14	1.02
	21IDJC104A.ZR.04	134.67	7.13	-	-	3.54	1.02
	21IDJC104A.ZR.05	122.67	9.05	-	-	2.54	0.67
	21IDJC104A.ZR.06	132.20	4.13	-	-	2.59	0.57
	21IDJC104A.ZR.07	124.10	6.18	-	-	11.21	1.94
	21IDJC104A.ZR.08	112.37	7.14	-	-	18.24	2.85
	21IDJC104A.ZR.09	157.80	32.55	-	-	2.22	0.21
	21IDJC104A.ZR.10	122.26	5.33	-	-	7.69	0.46
	21IDJC104A.56	124.22	13.64	-	-	2.63	0.45

Appendix B Continued: U-Pb Zircon Ages

Sample Name	Source File	Final Pb206/U238 age (Ma)	± (Ma)	Final Pb206/U238 age (207Pb corr) (Ma)	± (Ma)	U/Th ratio	±
	21IDJC104A.66	115.55	9.69	-	-	4.39	0.52
	21IDJC104A.69	133.04	12.70	-	-	1.94	0.43
	21IDJC104A.70	124.10	45.65	-	-	4.53	0.59
	21IDJC104A.71	121.86	8.10	-	-	6.98	1.33
	21IDJC104A.72	146.33	11.76	-	-	4.12	1.58
	21IDJC104A.73	121.31	5.81	-	-	1.73	0.25
	21IDJC104A.74	127.24	9.13	-	-	4.70	1.65
	21IDJC104A.75	127.94	4.91	-	-	2.75	1.03
	21IDJC104A.76	135.93	6.72	-	-	2.19	0.80
	21IDJC104A.77	165.53	74.67	-	-	3.90	0.91

Appendix B Continued. U-Pb Zircon Ages

21IDJC104A.78	158.46	15.34	-	-	2.39	0.31
21IDJC104A.79	139.67	5.17	-	-	3.83	0.91
21IDJC104A.80	111.07	13.88	-	-	11.92	2.31
21IDJC104A.82	115.58	13.01	-	-	5.05	0.53
21IDJC104A.83	101.96	3.90	-	-	13.29	1.14
21IDJC104A.84	188.50	7.39	-	-	3.07	0.64
21IDJC104A.85	121.34	8.98	-	-	2.72	0.61
21IDJC104A.86	113.53	13.80	-	-	3.20	0.40
21IDJC104A.87	96.52	17.09	-	-	1.53	0.10
21IDJC104A.88	133.60	6.18	-	-	6.78	0.87
21IDJC104A.89	148.44	21.11	-	-	2.51	0.14
21IDJC104A.90	142.05	6.10	-	-	5.46	1.05

Appendix B Continued. U-Pb Zircon Ages

	21IDJC104A.92	119.45	6.35	-	-	2.60	0.43
	21IDJC104A.93	127.35	3.70	-	-	4.08	0.74
	21IDJC104A.94	109.49	9.33	-	-	23.77	3.71
	21IDJC104A.95	137.01	9.04	-	-	2.77	0.61
	21IDJC104A.96	158.62	15.78	-	-	3.65	0.46
	21IDJC104A.97	123.46	15.29	-	-	3.58	0.17
	21IDJC104A.98	118.26	9.36	-	-	1.15	0.49
	21IDJC104A.100	139.16	7.36	-	-	4.44	0.80
104B	21IDJC104B.22	132.64	6.66	-	-	3.23	0.27
	21IDJC104B.53	151.44	4.27	-	-	5.71	0.91
	21IDJC104B.60	125.11	10.82	-	-	2.50	0.40
	21IDJC104B.62	135.83	9.44	-	-	1.75	0.48

Appendix B Continued. U-Pb Zircon Ages

21IDJC104B.64	128.05	10.80	-	-	7.17	1.90
21IDJC104B.65	138.02	10.50	-	-	6.47	1.27
21IDJC104B.66	135.24	6.09	-	-	5.85	0.64
21IDJC104B.69	145.38	6.22	-	-	6.91	0.69
21IDJC104B.70	130.35	9.08	-	-	7.58	1.85
21IDJC104B.72	130.74	15.11	-	-	4.16	1.15
21IDJC104B.73	108.85	18.72	-	-	12.09	2.09
21IDJC104B.74	129.69	8.77	-	-	7.43	0.78
21IDJC104B.76	134.05	10.64	-	-	2.87	0.21
21IDJC104B.77	131.53	8.68	-	-	6.18	1.54
21IDJC104B.78	139.05	6.68	-	-	4.14	1.40
21IDJC104B.79	131.31	15.10	-	-	3.49	0.82

Appendix B Continued. U-Pb Zircon Ages

	21IDJC104B.81	117.73	16.41	-	-	15.68	6.74
	21IDJC104B.82	123.61	10.86	-	-	4.05	0.96
	21IDJC104B.83	128.01	12.36	-	-	4.54	0.81
	21IDJC104B.84	143.78	19.66	-	-	4.78	0.44
	21IDJC104B.85	117.15	14.88	-	-	6.32	1.02
	21IDJC104B.86	127.21	7.85	-	-	4.86	0.73
	21IDJC104B.88	224.37	58.55	-	-	8.49	1.67
	21IDJC104B.89	106.74	15.50	-	-	4.91	0.59
106	21IDJC106.AP.05	103.59	3.23	-	-	66.62	13.02
	21IDJC106.55B	152.93	19.62	-	-	54.91	12.11
	21IDJC106.60B	205.31	22.27	-	-	7.01	1.35
	21IDJC106.65B	255.10	33.29	-	-	7.87	0.92

Appendix B Continued. U-Pb Zircon Ages

	21IDJC106.68	105.58	2.32	-	-	156.64	23.81
	21IDJC106.82	106.02	1.72	-	-	70.10	2.06
107	21IDJC107.AP.02	105.36	4.09	-	-	6.63	1.17
	21IDJC107.B.AP.02	98.47	2.15	-	-	4.67	1.13
	21IDJC107.B.AP.08	97.11	3.05	-	-	10.54	1.21
	21IDJC107.ZR.04	103.96	3.59	-	-	26.35	4.35
	21IDJC107.ZR.05	112.45	2.38	-	-	4.76	0.48
	21IDJC107.04	109.71	2.55	-	-	10.80	0.73
	21IDJC107.58	105.79	2.80	-	-	6.37	0.41
	21IDJC107.59	139.73	13.67	-	-	2.66	0.69
	21IDJC107.60	109.80	3.50	-	-	15.64	1.91
	21IDJC107.67	103.52	2.84	-	-	8.50	2.48

Appendix B Continued. U-Pb Zircon Ages

21IDJC107.68	98.87	3.34	-	-	12.03	2.26
21IDJC107.69	116.38	2.97	-	-	9.56	0.85
21IDJC107.71	94.35	4.51	-	-	3.69	0.44
21IDJC107.73	96.48	4.37	-	-	5.58	0.77
21IDJC107.74	104.04	2.83	-	-	8.89	1.00
21IDJC107.75	118.31	2.90	-	-	5.07	0.33
21IDJC107.76	91.68	3.92	-	-	6.26	0.27
21IDJC107.77	99.17	2.53	-	-	9.13	1.66
21IDJC107.78	90.09	4.15	-	-	8.36	1.10
21IDJC107.81	108.49	3.26	-	-	4.57	0.71
21IDJC107.82	111.84	3.02	-	-	16.09	2.46
21IDJC107.84	110.93	2.54	-	-	7.54	1.35

Appendix B Continued. U-Pb Zircon Ages

21IDJC107.85	102.06	2.55	-	-	1.75	0.42
21IDJC107.86	94.92	3.85	-	-	8.88	1.22
21IDJC107.87	96.02	3.30	-	-	15.01	1.07
21IDJC107.88	92.46	3.33	-	-	3.52	0.26
21IDJC107.89	111.24	4.17	-	-	13.23	1.47
21IDJC107.90	102.68	2.91	-	-	29.75	2.48
21IDJC107.91	112.57	4.17	-	-	8.21	1.73
21IDJC107.92	85.39	3.27	-	-	7.64	1.26
21IDJC107.93	99.61	4.08	-	-	8.50	0.79
21IDJC107.94	107.39	3.30	-	-	48.29	2.77
21IDJC107.95	107.82	2.38	-	-	4.74	0.45
21IDJC107.98	105.90	3.39	-	-	8.35	1.41

Appendix B Continued. U-Pb Zircon Ages

103B	21IDJC103B.AP.01	139.89	6.46	-	-	3.28	0.19
	21IDJC103B.31	106.89	2.95	-	-	5.86	0.42
	21IDJC103B.39	147.05	5.00	-	-	2.01	0.14
	21IDJC103B.47	135.29	5.38	-	-	2.66	0.49
	21IDJC103B.54	141.94	4.81	-	-	1.95	0.28
	21IDJC103B.59	148.20	5.98	-	-	1.83	0.30
	21IDJC103B.60	148.33	4.54	-	-	4.27	0.38
	21IDJC103B.61	133.76	7.76	-	-	3.39	0.29
	21IDJC103B.66	140.07	6.49	-	-	2.16	0.45
	21IDJC103B.67	152.13	19.47	-	-	2.35	0.51
	21IDJC103B.68	162.79	7.71	-	-	1.87	0.23
	21IDJC103B.69	140.37	11.13	-	-	2.43	0.11

Appendix B Continued. U-Pb Zircon Ages

101	21IDJC101.02	169.85	25.46	-	-	0.35	0.01
	21IDJC101.17	163.33	18.79	-	-	2.02	0.14
	21IDJC101.37	138.58	5.66	-	-	5.88	0.53
116	21IDJC116.03	171.01	4.55	174.35	4.64	2.40	0.10
	21IDJC116.20	269.69	21.75	112.17	9.39	12.88	1.93
	21IDJC116.21	258.18	22.20	130.23	11.60	21.40	2.18
	21IDJC116.22	379.64	30.02	108.25	9.32	21.62	2.25
	21IDJC116.23	285.68	34.37	108.49	14.07	23.56	3.65
	21IDJC116.24	615.35	101.37	105.54	27.03	4.71	1.03
	21IDJC116.26	273.16	26.08	101.10	10.30	22.72	3.39
	21IDJC116.27	247.27	19.34	103.90	8.47	13.95	1.14
	21IDJC116.32	190.59	18.96	109.09	11.05	30.79	4.19

Appendix B Continued. U-Pb Zircon Ages

21IDJC116.34	440.17	31.32	123.95	10.01	22.74	2.62
21IDJC116.35	134.82	13.35	122.39	12.14	5.22	0.61
21IDJC116.36	357.57	24.59	104.87	7.82	17.19	1.77
21IDJC116.37	363.39	27.15	100.13	8.28	15.48	1.73
21IDJC116.38	280.17	23.98	103.23	9.48	9.71	1.21
21IDJC116.42	123.50	7.16	123.05	7.13	74.00	14.92
21IDJC116.45	121.02	4.26	120.39	4.24	7.41	1.87
21IDJC116.46	111.38	2.74	110.59	2.72	3.60	0.69
21IDJC116.47	124.57	5.04	124.46	5.03	14.61	1.34
21IDJC116.48	112.26	2.78	112.17	2.78	17.66	2.42
21IDJC116.51	111.27	5.96	109.29	5.86	140.69	35.73
21IDJC116.52	141.59	5.96	141.47	5.95	9.19	1.41

Appendix B Continued. U-Pb Zircon Ages

	21IDJC116.53	124.95	3.78	124.95	3.78	7.43	1.20
	21IDJC116.60	131.33	8.63	129.10	8.49	17.78	1.46
	21IDJC116.61	113.89	2.90	113.93	2.90	12.71	1.40
	21IDJC116.62	148.96	7.15	108.20	5.23	8.23	0.39
	21IDJC116.63	472.29	44.34	98.66	10.66	5.88	1.14
114	21IDJC114.AP.03	106.13	11.14	-	-	7.92	1.11
	21IDJC114.03B	120.05	4.20	-	-	20.68	1.68
	21IDJC114.04	126.40	5.07	-	-	23.47	0.89
	21IDJC114.07	122.04	3.15	-	-	28.58	1.32
	21IDJC114.18	125.63	4.91	-	-	8.32	0.36
	21IDJC114.19	121.27	4.75	-	-	19.67	0.75
	21IDJC114.21	115.68	3.17	-	-	11.20	1.00

Appendix B Continued. U-Pb Zircon Ages

	21IDJC114.26B	196.75	25.01	-	-	27.44	5.55
	21IDJC114.49	168.52	14.47	-	-	4.95	0.27
	21IDJC114.85	116.90	5.04	-	-	8.03	0.72
	21IDJC114.89	128.60	14.70	-	-	3.04	0.27
	21IDJC114.91	120.15	3.80	-	-	9.98	0.72
	21IDJC114.93	145.07	19.99	-	-	15.44	1.44
	21IDJC114.95	136.04	5.59	-	-	5.72	0.31
	21IDJC114.96	124.22	13.50	-	-	4.95	0.56
18	21IDSPJCOR18.03	277.44	17.02	-	-	15.21	1.32
	21IDSPJCOR18.05	346.62	30.60	-	-	22.64	3.34
	21IDSPJCOR18.06	138.55	9.05	-	-	7.49	0.42
	21IDSPJCOR18.08	300.17	19.45	-	-	14.65	1.28

Appendix B Continued. U-Pb Zircon Ages

	21IDSPJCOR18.14	124.37	3.21	-	-	93.96	19.70
	21IDSPJCOR18.17	138.62	6.17	-	-	141.14	12.67
	21IDSPJCOR18.18	248.14	24.56	-	-	20.48	2.30
	21IDSPJCOR18.24	140.92	6.47	-	-	5.67	0.19
	21IDSPJCOR18.25	132.72	7.53	-	-	12.47	1.10
	21IDSPJCOR18.06.B	138.55	9.05	-	-	7.49	0.42
	21IDSPJCOR18.14.B	124.37	3.21	-	-	93.96	19.70
19	21IDSP19.03	210.16	16.03	117.94	9.18	1.03	0.16
	21IDSP19.15	122.23	4.55	114.22	4.25	2.14	0.18
	21IDSP19.24	716.86	59.86	114.32	12.88	4.95	1.16
21	21IDJC21.30	110.27	7.04	101.59	6.50	0.72	0.03
	21IDJC21.41	167.79	8.53	94.28	4.87	1.65	0.10

Appendix B Continued. U-Pb Zircon Ages

	21IDJC21.43	125.65	6.57	125.31	6.55	5.99	1.10
	21IDJC21.46	159.72	3.13	116.24	2.29	0.47	0.02
	21IDJC21.47	167.28	12.41	107.52	8.07	2.97	0.18
	21IDJC21.53	128.76	7.30	131.25	7.44	3.86	0.89
22	21IDJC22.05	180.68	21.50	116.97	14.07	8.92	0.83
	21IDJC22.06	284.72	27.50	116.60	11.76	20.96	4.05
	21IDJC22.11	313.62	30.32	112.28	11.46	1.50	0.15

Appendix C. U-Pb Rutile Ages

Sample Name	Source File	Final Pb206/U238 age (Ma)	± (Ma)	Zr90 (ppm)	Temperature (°C) (+)	Temperature (°C) (-)
104B	21IDJC104B.B.RT. 01	145.21	64.00	190.49	613.08	600.47
	21IDJC104B.B.RT. 02	95.51	49.73	218.00	623.21	610.87
	21IDJC104B.B.RT. 04	651.69	123.12	191.33	613.41	600.81
	21IDJC104B.B.RT. 06	184.21	17.76	177.88	608.02	595.29
	21IDJC104B.B.RT. 07	135.63	31.58	307.23	650.07	638.46
	21IDJC104B.B.RT. 11	99.65	48.69	173.22	606.08	593.29
	21IDJC104B.B.RT. 12	145.74	41.59	184.71	610.80	598.13
	21IDJC104B.B.RT. 13	164.49	45.69	455.77	683.00	672.39
	21IDJC104B.B.RT. 14	92.77	24.95	342.58	658.93	647.59
	21IDJC104B.B.RT. 15	202.99	51.87	213.15	621.51	609.12

Appendix C Continued. U-Pb Rutile Ages

Sample Name	Source File	Final Pb206/U238 age (Ma)	± (Ma)	Zr90 (ppm)	Temperature (°C) (+)	Temperature (°C) (-)
	21IDJC104B.B.RT. 16	106.66	25.28	220.91	624.22	611.91
	21IDJC104B.B.RT. 20	105.67	49.38	219.74	623.82	611.49
	21IDJC104B.B.RT. 22	129.71	87.47	196.36	615.34	602.79
	21IDJC104B.B.RT. 24	113.36	29.40	287.28	644.69	632.93
	21IDJC104B.B.RT. 25	152.17	41.15	373.91	666.18	655.05
	21IDJC104B.B.RT. 26	82.90	49.83	199.70	616.60	604.08
	21IDJC104B.B.RT. 27	133.23	28.23	364.87	664.14	652.95
	21IDJC104B.B.RT. 29	164.83	60.46	340.65	658.47	647.11
	21IDJC104B.B.RT. 30	253.47	58.65	301.33	648.51	636.86
	21IDJC104B.B.RT. 31	118.76	53.61	212.31	621.21	608.81

Appendix D: U-Pb Apatite Ages and Closure Temperatures

Sample Name	Source File	Final Pb206/U238 age (Ma)	± (Ma)	Final Pb206/U238 age (207Pb corr) (Ma)	± (Ma)	U content (ppm)	± (ppm)	C long (um)	a2 short (um)	ESR (um)	Closure Temperature (°C)
104A	21IDJC104A.01	75.64	9.83	-	-	21.50	1.20	56.88	40.04	19.93	437.76
	21IDJC104A.03	74.96	11.69	-	-	22.71	1.00	91.83	46.71	24.86	433.08
	21IDJC104A.04	101.18	40.00	-	-	5.21	0.51	76.84	64.68	30.79	453.28
	21IDJC104A.14	64.66	7.67	-	-	21.76	0.68	107.49	72.27	36.36	446.44
	21IDJC104A.17	71.90	13.76	-	-	18.22	0.67	66.40	33.25	17.75	421.63
	21IDJC104A.27	71.94	14.23	-	-	32.63	1.45	94.96	45.15	24.32	432.32
	21IDJC104A.36	100.59	12.52	-	-	20.22	1.03	82.67	57.95	28.87	438.28
	21IDJC104A.45	90.75	14.05	-	-	27.35	1.53	129.72	64.22	34.35	444.41
	21IDJC104A.52	95.45	13.09	-	-	29.53	1.52	118.64	66.24	34.65	444.72
	21IDJC104A.67	88.93	14.06	-	-	19.50	0.67	107.37	50.23	27.13	436.11
	21IDJC104A.68	64.42	5.41	-	-	47.94	2.33	124.09	34.59	20.04	425.72
	21IDJC104A.81	93.59	21.36	-	-	3.26	0.21	79.05	37.29	20.11	425.84
104B	21IDJC104B.B.ZR.03	107.04	15.01	-	-	18.85	2.80	111.36	26.29	15.49	417.12

Appendix D Continued. U-Pb Apatite Ages and Closure Temperatures

Sample Name	Source File	Final Pb206/U238 age (Ma)	± (Ma)	Final Pb206/U238 age (207Pb corr) (Ma)	± (Ma)	U content (ppm)	± (ppm)	C long (um)	a2 short (um)	ESR (um)	Closure Temperature (°C)
	21IDJC104B.13	132.29	17.28	-	-	9.19	0.43	124.23	72.91	37.76	447.79
	21IDJC104B.14	124.83	16.89	-	-	10.88	0.77	105.01	57.57	30.22	439.88
	21IDJC104B.15	133.38	14.87	-	-	11.57	0.85	107.51	56.36	29.83	439.43
	21IDJC104B.18	101.94	10.37	-	-	19.95	0.84	95.23	32.78	18.53	424.55
	21IDJC104B.21	109.41	9.75	-	-	14.39	1.14	78.30	35.69	19.36	424.55
	21IDJC104B.34	130.72	13.84	-	-	10.37	0.72	127.38	56.25	30.67	440.40
	21IDJC104B.35	121.69	13.01	-	-	11.61	0.52	114.76	40.47	22.80	430.11
	21IDJC104B.40	79.26	11.46	-	-	12.95	0.53	93.53	50.54	26.60	435.42
	21IDJC104B.45	137.88	35.48	-	-	4.09	0.43	97.25	49.95	26.54	435.34
	21IDJC104B.46	148.33	19.50	-	-	4.43	0.29	109.00	49.37	26.81	435.69
	21IDJC104B.52	129.66	16.94	-	-	5.10	0.21	138.60	37.69	21.90	428.73
106	21IDJC106.08	101.81	6.93	-	-	119.23	3.92	58.25	19.70	11.16	406.46
	21IDJC106.10	104.88	10.25	-	-	64.27	2.53	100.68	35.26	19.89	425.45
	21IDJC106.12	120.37	8.50	-	-	36.09	0.84	93.84	56.02	28.91	438.33

Appendix D Continued. U-Pb Apatite Ages and Closure Temperatures

Sample Name	Source File	Final Pb206/U238 age (Ma)	± (Ma)	Final Pb206/U238 age (207Pb corr) (Ma)	± (Ma)	U content (ppm)	± (ppm)	C long (um)	a2 short (um)	ESR (um)	Closure Temperature (°C)
	21IDJC106.15	66.49	4.91	-	-	39.85	0.83	76.37	33.27	18.18	422.44
	21IDJC106.16	33.42	3.23	-	-	155.96	3.29	86.36	29.98	16.93	420.05
	21IDJC106.18	70.06	4.65	-	-	39.50	1.13	136.49	59.86	32.68	442.63
	21IDJC106.20	87.90	9.03	-	-	23.00	0.61	69.61	40.26	20.91	439.44
	21IDJC106.21	92.22	6.90	-	-	27.54	0.86	120.12	45.66	25.47	433.91
	21IDJC106.22	96.86	11.31	-	-	24.06	1.52	99.41	29.42	16.94	420.07
	21IDJC106.27	77.71	7.40	-	-	43.24	1.43	79.21	34.79	18.99	423.89
	21IDJC106.29	90.75	11.94	-	-	41.44	2.05	99.79	33.91	19.20	424.27
	21IDJC106.33	86.44	11.44	-	-	61.86	2.19	92.25	44.40	23.86	431.67
	21IDJC106.49	89.66	8.91	-	-	62.68	1.72	124.02	53.73	29.39	438.90
	21IDJC106.53	91.79	10.41	-	-	54.15	1.74	86.67	39.88	21.60	428.26
	21IDJC106.56	79.58	8.33	-	-	47.98	5.09	118.11	42.78	24.02	431.89
	21IDJC106.58	88.06	6.31	-	-	48.61	1.43	82.48	36.58	19.93	425.53
	21IDJC106.61	113.03	7.23	-	-	37.39	1.32	119.46	39.20	22.29	429.34

Appendix D Continued. U-Pb Apatite Ages and Closure Temperatures

Sample Name	Source File	Final Pb206/U238 age (Ma)	± (Ma)	Final Pb206/U238 age (207Pb corr) (Ma)	± (Ma)	U content (ppm)	± (ppm)	C long (um)	a2 short (um)	ESR (um)	Closure Temperature (°C)
	21IDJC106.64	111.45	7.12	-	-	37.82	1.53	139.20	39.49	22.84	430.17
	21IDJC106.69	64.58	4.27	-	-	96.55	2.18	99.83	30.94	17.72	421.58
	21IDJC106.72	62.54	4.06	-	-	98.45	2.15	117.03	47.33	26.16	434.84
	21IDJC106.76	115.35	10.61	-	-	31.64	0.97	59.80	35.17	18.21	434.61
	21IDJC106.80	125.67	10.70	-	-	33.26	1.23	119.49	49.24	27.14	436.12
	21IDJC106.81	103.33	9.79	-	-	50.72	1.11	86.28	39.03	21.20	427.62
	21IDJC106.83	47.42	2.80	-	-	206.75	8.87	104.15	52.33	27.92	437.10
	21IDJC106.84	104.94	8.39	-	-	46.35	0.96	125.06	20.75	12.57	410.30
	21IDJC106.AP.08	112.29	6.83	-	-	119.53	3.01	115.83	50.04	27.38	436.42
103B	21IDJC103B.AP.03	307.84	25.93	115.30	10.22	5.33	0.17	111.93	48.07	26.33	435.06
	21IDJC103B.AP.04	1539.44	377.46	121.81	58.82	3.08	0.14	99.60	50.16	26.75	435.61
	21IDJC103B.18	413.14	40.09	80.74	9.31	22.90	1.46	75.20	37.19	19.90	425.47
	21IDJC103B.51	106.62	11.79	263.52	28.04	18.09	0.82	119.21	65.49	34.36	444.42
101	21IDJC101.23	64.84	8.49	-	-	23.55	2.84	93.50	35.46	19.78	425.28

Appendix D Continued. U-Pb Apatite Ages and Closure Temperatures

Sample Name	Source File	Final Pb206/U238 age (Ma)	± (Ma)	Final Pb206/U238 age (207Pb corr) (Ma)	± (Ma)	U content (ppm)	± (ppm)	C long (um)	a2 short (um)	ESR (um)	Closure Temperature (°C)
	21IDJC101.25	184.68	49.13	-	-	1.54	0.11	135.33	45.62	25.86	434.44
	21IDJC101.37	79.74	3.28	-	-	90.76	5.82	149.10	53.35	30.00	439.62
	21IDJC101.39	61.40	452.84	-	-	0.11	0.03	138.33	40.98	23.59	431.27
116	21IDJC116.ZR.06	186.63	12.82	-	-	48.05	2.43	118.68	25.78	15.31	416.72
	21IDJC116.ZR.08	154.09	11.16	-	-	62.57	1.42	102.99	30.70	17.66	421.47
	21IDJC116.ZR.10	148.99	12.88	-	-	48.59	2.44	100.22	22.77	13.46	412.52
	21IDJC116.B.AP.03	116.73	8.03	-	-	44.61	1.92	78.76	28.60	16.05	418.29
	21IDJC116.02	86.33	5.44	-	-	44.06	2.89	87.69	29.42	16.68	419.57
	21IDJC116.05	82.84	4.82	-	-	32.72	1.01	78.76	44.90	23.39	430.98
	21IDJC116.06	115.92	8.67	-	-	15.78	0.57	69.04	27.77	15.36	416.84
	21IDJC116.07	44.73	3.62	-	-	84.70	4.95	81.12	42.07	22.31	429.37
	21IDJC116.08	103.40	16.81	-	-	10.60	0.70	56.84	31.80	16.63	431.48
	21IDJC116.09	91.28	6.15	-	-	22.09	1.73	43.49	25.68	13.28	412.08
	21IDJC116.10	70.71	5.23	-	-	34.99	2.85	74.77	29.75	16.48	419.17

Appendix D Continued. U-Pb Apatite Ages and Closure Temperatures

Sample Name	Source File	Final Pb206/U238 age (Ma)	± (Ma)	Final Pb206/U238 age (207Pb corr) (Ma)	± (Ma)	U content (ppm)	± (ppm)	C long (um)	a2 short (um)	ESR (um)	Closure Temperature (°C)
	21IDJC116.11	49.71	4.31	-	-	61.62	6.34	60.16	50.54	24.07	431.97
	21IDJC116.12	83.97	9.57	-	-	27.45	0.89	75.33	39.04	20.71	426.83
	21IDJC116.14	98.63	5.68	-	-	18.28	1.12	80.24	49.24	25.27	433.64
	21IDJC116.18	64.17	4.60	-	-	73.29	2.43	74.14	38.63	20.47	426.44
	21IDJC116.19	97.19	7.31	-	-	24.21	1.65	53.75	31.75	16.42	419.05
	21IDJC116.39	87.87	4.43	-	-	52.03	2.43	105.24	44.49	24.43	432.47
	21IDJC116.41	63.84	2.10	-	-	184.98	8.48	94.16	39.15	21.55	428.18
	21IDJC116.44	106.80	8.50	-	-	27.43	2.44	75.08	43.64	22.65	429.87
	21IDJC116.49	94.07	7.79	-	-	24.99	1.59	67.42	35.86	18.93	423.80
114	21IDJC114.ZR.01	126.08	10.52	-	-	27.10	0.73	85.82	32.13	17.96	434.13
	21IDJC114.ZR.03	162.99	16.44	-	-	15.50	0.59	91.21	45.73	24.40	432.44
	21IDJC114.ZR.07	149.77	20.35	-	-	28.71	1.23	136.15	49.76	27.90	437.09
	21IDJC114.ZR.08	195.36	34.03	-	-	12.83	1.41	208.48	48.60	28.67	438.03
	21IDJC114.01	41.10	4.47	-	-	12.70	0.38	51.86	41.01	19.84	425.38

Appendix D Continued. U-Pb Apatite Ages and Closure Temperatures

Sample Name	Source File	Final Pb206/U238 age (Ma)	± (Ma)	Final Pb206/U238 age (207Pb corr) (Ma)	± (Ma)	U content (ppm)	± (ppm)	C long (um)	a2 short (um)	ESR (um)	Closure Temperature (°C)
	21IDJC114.02	57.52	9.27	-	-	6.25	0.28	38.72	22.82	11.81	408.27
	21IDJC114.03	34.99	5.36	-	-	13.89	1.00	57.91	37.75	19.12	424.13
	21IDJC114.11	58.46	7.16	-	-	8.94	0.46	68.12	52.58	25.60	434.09
	21IDJC114.13	72.02	12.77	-	-	6.53	0.31	48.70	37.69	18.34	422.72
	21IDJC114.14	106.77	32.69	-	-	2.49	0.38	42.75	34.42	16.58	431.37
	21IDJC114.16	29.95	4.01	-	-	35.20	1.30	50.29	34.44	17.25	420.69
	21IDJC114.17	99.13	30.33	-	-	21.71	0.91	74.11	35.40	19.05	424.01
	21IDJC114.22	46.51	4.42	-	-	22.09	1.19	62.93	32.47	17.24	420.66
	21IDJC114.23	40.11	4.53	-	-	27.36	0.73	47.96	27.14	14.16	414.16
	21IDJC114.27	82.46	10.56	-	-	21.71	0.91	83.54	35.53	19.49	424.77
	21IDJC114.29	122.81	31.29	-	-	8.46	0.63	103.39	55.20	29.12	438.58
	21IDJC114.43	125.73	15.30	-	-	24.65	0.64	97.73	49.64	26.43	435.20
	21IDJC114.46	106.40	10.25	-	-	31.58	1.27	84.49	47.39	24.77	432.95
	21IDJC114.48	73.03	9.30	-	-	67.55	2.18	85.03	40.71	21.90	428.73

Appendix D Continued. U-Pb Apatite Ages and Closure Temperatures

Sample Name	Source File	Final Pb206/U238 age (Ma)	± (Ma)	Final Pb206/U238 age (207Pb corr) (Ma)	± (Ma)	U content (ppm)	± (ppm)	C long (um)	a2 short (um)	ESR (um)	Closure Temperature (°C)
	21IDJC114.53	136.81	16.26	-	-	14.07	0.37	55.43	35.01	17.86	433.94
	21IDJC114.54	54.25	8.61	-	-	46.49	2.79	62.13	42.97	21.48	428.07
	21IDJC114.59	81.52	8.56	-	-	58.34	1.66	90.74	39.29	21.49	428.09
	21IDJC114.62	98.65	16.83	-	-	15.07	1.47	78.07	34.63	18.87	423.68
	21IDJC114.63	81.36	7.84	-	-	44.76	2.25	64.23	35.52	18.61	423.23
	21IDJC114.65	97.58	19.30	-	-	21.68	1.67	73.77	33.25	18.07	422.23
	21IDJC114.66	72.18	5.03	-	-	53.73	2.27	68.09	37.18	19.53	424.85
	21IDJC114.69	118.52	16.17	-	-	13.96	0.44	48.46	35.52	17.51	433.26
	21IDJC114.71	60.72	3.75	-	-	74.37	2.73	66.25	34.38	18.23	422.53
	21IDJC114.72	67.84	5.21	-	-	55.52	2.46	88.63	29.28	16.64	419.48
	21IDJC114.74	53.91	6.77	-	-	69.63	2.35	121.31	36.96	21.21	427.64
	21IDJC114.75	76.17	9.41	-	-	27.22	1.75	68.57	37.75	19.80	425.31
	21IDJC114.76	67.90	4.58	-	-	73.04	2.15	73.04	35.79	19.18	424.23
	21IDJC114.77	126.42	35.78	-	-	17.04	1.69	53.20	40.68	19.85	437.62

Appendix D Continued. U-Pb Apatite Ages and Closure Temperatures

Sample Name	Source File	Final Pb206/U238 age (Ma)	± (Ma)	Final Pb206/U238 age (207Pb corr) (Ma)	± (Ma)	U content (ppm)	± (ppm)	C long (um)	a2 short (um)	ESR (um)	Closure Temperature (°C)
	21IDJC114.78	125.30	18.52	-	-	19.60	1.07	63.62	38.31	19.74	437.42
	21IDJC114.79	76.32	7.99	-	-	71.57	1.98	54.30	34.98	17.76	421.66
	21IDJC114.84	104.55	9.88	-	-	48.74	1.63	52.44	40.33	19.65	437.26
	21IDJC114.93	101.28	7.31	-	-	77.64	2.62	73.45	44.96	23.08	430.53
SPJCOR18	21IDSPJCOR18.16	114.52	8.24	86.93	6.28	76.49	5.30	66.32	30.98	16.74	419.68
	21IDSPJCOR18.23	318.19	22.21	123.37	8.77	14.89	0.83	223.90	109.55	58.72	464.00
	21IDSPJCOR18.24	120.99	5.56	94.10	4.35	60.10	1.16	74.95	29.90	16.56	419.32
	21IDSPJCOR18.26	292.28	20.61	123.27	9.18	19.24	1.10	228.17	119.74	63.37	466.88
	21IDSPJCOR18.38	124.79	10.38	91.61	7.67	188.20	35.20	71.44	33.90	18.27	422.59
SP19	21IDSP19.05	288.30	55.07	88.13	17.88	14.28	1.45	63.40	32.78	17.40	420.96
	21IDSP19.14	146.08	15.17	94.58	9.91	37.47	1.68	49.58	33.25	16.74	419.68
	21IDSP19.16	548.70	103.15	43.64	12.76	4.19	0.20	66.90	44.32	22.37	429.45
	21IDSP19.17	290.95	39.01	73.98	10.73	8.76	0.56	68.15	31.96	17.25	420.69
	21IDSP19.19	178.16	17.25	97.52	9.61	16.28	1.28	69.52	28.66	15.80	417.76

Appendix D Continued. U-Pb Apatite Ages and Closure Temperatures

Sample Name	Source File	Final Pb206/U238 age (Ma)	± (Ma)	Final Pb206/U238 age (207Pb corr) (Ma)	± (Ma)	U content (ppm)	± (ppm)	C long (um)	a2 short (um)	ESR (um)	Closure Temperature (°C)
	21IDSP19.22	247.89	23.40	102.74	9.78	8.25	0.33	89.94	38.31	21.01	427.31
21	21IDJC21.16	197.26	23.61	88.20	10.82	5.70	0.24	55.35	29.28	15.47	417.08
	21IDJC21.18	181.98	53.60	92.05	27.42	4.36	0.49	46.72	23.51	12.54	410.20
	21IDJC21.27	187.83	19.74	105.43	11.32	7.05	0.45	81.34	40.06	21.45	428.02
	21IDJC21.31	388.24	54.82	40.88	6.63	3.48	0.19	51.79	28.14	14.80	415.60
	21IDJC21.34	511.65	54.17	96.74	12.30	8.41	0.46	45.73	23.76	12.60	410.36